ALFRED-WEGENER-INSTITUT
HELMHOLTZ-ZENTRUM FÜR POLAR- UND MEERESFORSCHUNG

792
2025

Berichte
zur Polar- und Meeresforschung
Reports on Polar and Marine Research

Climate Signals from NEUMAYER, Coastal Dronning Maud Land, Antarctica:

A 33-Year Statistical Analysis of Snow Accumulation in a Stake Farm

Valerie Reppert

HELMHOLTZ

Die Berichte zur Polar- und Meeresforschung werden vom Alfred-Wegener-Institut, Helmholtz-Zentrum für Polar- und Meeresforschung (AWI) in Bremerhaven, Deutschland, in Fortsetzung der vormaligen Berichte zur Polarforschung herausgegeben. Sie erscheinen in unregelmäßiger Abfolge.

Die Berichte zur Polar- und Meeresforschung enthalten Darstellungen und Ergebnisse der vom AWI selbst oder mit seiner Unterstützung durchgeführten Forschungsarbeiten in den Polargebieten und in den Meeren.

Die Publikationen umfassen Expeditionsberichte der vom AWI betriebenen Schiffe, Flugzeuge und Stationen, Forschungsergebnisse (inkl. Dissertationen) des Instituts und des Archivs für deutsche Polarforschung, sowie Abstracts und Proceedings von nationalen und internationalen Tagungen und Workshops des AWI.

Die Beiträge geben nicht notwendigerweise die Auffassung des AWI wider.

Herausgeber
Dr. Horst Bornemann

Redaktionelle Bearbeitung und Layout
Susan Amir Sawadkuhi

Alfred-Wegener-Institut
Helmholtz-Zentrum für Polar- und Meeresforschung
Am Handelshafen 12
27570 Bremerhaven
Germany

www.awi.de
www.awi.de/reports

Erstautor:innen bzw. herausgebende Autor:innen eines Bandes der Berichte zur Polar- und Meeresforschung versichern, dass sie über alle Rechte am Werk verfügen und übertragen sämtliche Rechte auch im Namen der Koautor:innen an das AWI. Ein einfaches Nutzungsrecht verbleibt, wenn nicht anders angegeben, bei den Autor:innen. Das AWI beansprucht die Publikation der eingereichten Manuskripte über sein Repositorium ePIC (electronic Publication Information Center, s. Innenseite am Rückdeckel) mit optionalem print-on-demand.

The Reports on Polar and Marine Research are issued by the Alfred Wegener Institute, Helmholtz Centre for Polar and Marine Research (AWI) in Bremerhaven, Germany, succeeding the former Reports on Polar Research. They are published at irregular intervals.

The Reports on Polar and Marine Research contain presentations and results of research activities in polar regions and in the seas either carried out by the AWI or with its support.

Publications comprise expedition reports of the ships, aircrafts, and stations operated by the AWI, research results (incl. dissertations) of the Institute and the Archiv für deutsche Polarforschung, as well as abstracts and proceedings of national and international conferences and workshops of the AWI.

The papers contained in the Reports do not necessarily reflect the opinion of the AWI.

Editor
Dr. Horst Bornemann

Editorial editing and layout
Susan Amir Sawadkuhi

Alfred-Wegener-Institut
Helmholtz-Zentrum für Polar- und Meeresforschung
Am Handelshafen 12
27570 Bremerhaven
Germany

www.awi.de
www.awi.de/en/reports

The first or editing author of an issue of Reports on Polar and Marine Research ensures that he possesses all rights of the opus, and transfers all rights to the AWI, including those associated with the co-authors. The non-exclusive right of use (einfaches Nutzungsrecht) remains with the author unless stated otherwise. The AWI reserves the right to publish the submitted articles in its repository ePIC (electronic Publication Information Center, see inside page of verso) with the option to "print-on-demand".

Titel: Das Pegelfeld Spuso an der Neumayer-Station III für die Ablesung der Schneehöhenveränderung 2021 (Foto: Linda Ort, AWI)

Cover: The Spuso stake farm at Neumayer Station III for reading the change in snow depth in 2021 (Foto: Linda Ort, AWI)

Climate Signals from NEUMAYER, Coastal Dronning Maud Land, Antarctica:

A 33-Year Statistical Analysis of Snow Accumulation in a Stake Farm

---

Valerie Reppert

Please cite or link this publication using the identifiers
https://epic.awi.de/id/eprint/59975/
https://doi.org/10.57738/BzPM_0792_2025
ISSN 1866-3192

Valerie Reppert
Alfred-Wegener-Institut
Helmholtz-Zentrum für Polar- und Meeresforschung
Am Alten Hafen 26
D-27568 Bremerhaven
Email: va.reppert@t-online.de

Die vorliegende Arbeit ist die inhaltlich unveränderte Fassung einer Masterarbeit, die am Alfred-Wegener-Institut, Helmholtz-Zentrum für Polar- und Meeresforschung in der Sektion Glaziologie des Fachbereichs Geowissenschaften angefertigt und 2024 der Fakultät für Geo- und Atmosphärenwissenschaften der Universität Innsbruck vorgelegt wurde.

CONTENTS

ABSTRACT

Changes in snow accumulation on the Antarctic Ice Sheet are of significant relevance to global mean sea level. Measurements taken over a 33-year period near the Neumayer Stations, Dronning Maud Land (DML), Antarctica, were used to statistically analyse both interannual and intraannual trends and variability of snow accumulation. While a significant increases in snow accumulation have been observed at Kohnen Station on the DML plateau in the interior of the continent, the question arises as to whether the coastal measurements near Neumayer show similar trends. This study reveals that two unprecedented accumulation years, 2021 and 2023, were recorded near Neumayer; however, no statistically significant long-term trend could be identified in the time series, which shows several periods of increasing and decreasing mulit-annual means in snow accumulation. Despite this, shifts in certain accumulation characteristics during the study period suggest the possible onset of a positive trend. Specifically, positive annual accumulation anomalies have become more frequent and more intense, the rate of interannual accumulation increase has accelerated, and the current period reflects a prolonged state of above-average accumulation. High interannual variability, however, prevents the identification of a significant trend within the available data period.

Periodicities observed in the time series suggest possible links to larger atmospheric patterns, such as the Antarctic Circumpolar Wave. Further research is required to also investigate the role of the major climate modes such as the Southern Annular Mode (SAM) and El Niño-Southern Oscillation (ENSO) and how these might influence local accumulation trends. This climatological analysis offers valuable data that could be used for future ground-truthing of satellite observations and benchmarking of climate models, especially given the higher temporal resolution of these measurements compared to firn and ice core records.

ZUSAMMENFASSUNG

Veränderungen in der Schneeakkumulation auf dem antarktischen Eisschild sind von erheblicher Bedeutung für den mittleren globalen Meeresspiegel. Messungen, die über einen Zeitraum von 33 Jahren in der Nähe der Neumayer-Stationen im Küstenbereich von Dronning Maud Land (DML), Antarktis, durchgeführt wurden, wurden verwendet, um statistische Analysen der inter- und intraannualen Trends und der Variabilität der Schneeakkumulation zu untersuchen. Während an der Kohnen-Station auf dem DML-Plateau im Inneren des Kontinents signifikante Zunahmen der Schneeakkumulation beobachtet wurden, stellt sich die Frage, ob die Küstenmessungen in der Nähe von Neumayer ähnliche Trends aufweisen.

Diese Studie zeigt, dass in den Jahren 2021 und 2023 zwei beispiellose Akkumulationsjahre in der Nähe von Neumayer aufgezeichnet wurden; jedoch konnte in der Zeitreihe kein statistisch signifikanter langfristiger Trend festgestellt werden. Die Zeitreihe zeigt mehrere Phasen mit zunehmenden und abnehmenden mehrjährigen Mitteln der Schneeakkumulation. Dennoch deuten Veränderungen in bestimmten Akkumulationsmerkmalen während des Untersuchungszeitraums auf einen möglichen Beginn eines positiven Trends hin. Insbesondere treten positive jährliche Akkumulationsanomalien häufiger und intensiver auf, die Rate des interannuellen Akkumulationsanstiegs hat sich beschleunigt, und die aktuelle Periode spiegelt einen verlängerten Zustand überdurchschnittlicher Akkumulation wider. Eine hohe interannuelle Variabilität erschwert jedoch die Identifizierung eines signifikanten Trends innerhalb des verfügbaren Datenzeitraums.

Periodizitäten, die in der Zeitreihe beobachtet wurden, weisen auf mögliche Verbindungen zu größeren atmosphärischen Mustern hin, wie der Antarktischen Zirkumpolarwelle. Weitere Forschungen sind erforderlich, um auch die Rolle der wichtigsten Klimamoden, wie dem Southern Annular Mode (SAM) und der El Niño-Southern Oscillation (ENSO), zu untersuchen und wie diese lokale Akkumulationstrends beeinflussen könnten. Diese klimatologische Analyse bietet wertvolle Daten, die in Zukunft zur Validierung von Satellitenbeobachtungen und als Grundlage für die Kalibrierung von Klimamodellen genutzt werden könnten, insbesondere angesichts der höheren zeitlichen Auflösung dieser Messungen im Vergleich zu Firn- und Eiskernaufzeichnungen.

ACKNOWLEDGMENTS

I am immensely grateful to all those who supported and inspired me along the journey of completing this thesis. My first words of thanks go to my advisors, Olaf Eisen and Rainer Prinz. Olaf, thank you especially for your invaluable time and guidance, which were so essential to this analysis. Rainer, thank you for your thoughtful insights and comments, which brought the necessary finishing touches to my work. I would also like to thank the Alfred-Wegener Institute for the unique opportunity to work with such remarkable and historical data. And a huge acknowledgment to all the dedicated Überwinterer, who have conducted stake measurements in the Antarctic cold.

A big and loving thank you goes to my family, who believe in me when I am my own biggest doubter, and who are always there to support me in every situation. How wonderful it is to have not only one home but three: a huge thanks to the MitterMausWG and the Rumer WG for always putting even the most stressful university days into the background and for the guaranteed fun and relaxation. Finally, I would like to thank Ilga, Loren, Jonathan, and Sebi for not only always being there for me but also for their invaluable feedback on this thesis.

1 INTRODUCTION

1.1 Motivation

Antarctica's total ice mass is equivalent to 58.3 meters of sea-level rise, with East Antarctica alone contributing 53.3 meters (Dufour et al. 2019). Therefore, monitoring snow and ice accumulation and ablation in this region is crucial for understanding future sea-level fluctuations.
As the climate warms, the Clausius-Clapeyron relation states that the atmospheric potential to hold water vapor increases by approximately 7% per degree Kelvin of warming, which enhances moisture transport to polar regions. In combination with other climate dynamics, this is projected to lead to increased precipitation and, consequently, greater snow accumulation in Antarctica (Bengtsson et al. 2011). This thesis examines a 33-year record of snow accumulation at Neumayer Station, Dronning Maud Land (DML), to investigate whether current observations already show evidence of such an increase.
Despite these projections of increased precipitation, assessing trends in Antarctic snowfall remains challenging due to the variability across available observational datasets. Ice core records and reanalysis data suggest minimal changes in precipitation since the 1950s, while altimetry data indicate a recent increase in surface height, potentially linked to enhanced snowfall since the 1990s (Boening et al. 2012). This discrepancy underscores the need for in situ measurements, such as stake farm observations, which provide consistent, long-term data to validate models and reconcile differences between datasets.
Satellite-based studies indicate a positive mass balance in Dronning Maud Land (DML) (Lenaerts et al. 2019), yet satellite data alone cannot fully capture local accumulation processes. Ground-truthing through in situ measurements is essential for accurately estimating accumulation, as satellites may miss regionally specific signals. For instance, Medley et al. (2018) state that in situ measurements reveal no clear trends in temperature or accumulation at Neumayer Station, while significant changes have been observed at Kohnen Station on the plateau, suggesting different patterns between coastal regions and the interior (Medley et al. 2018).
Recent high-accumulation events in DML raise the question of whether they are short-term anomalies or the start of a longer-term trend, similar to Kohnen Station (Wang et al. 2023; Medley et al. 2018). Long-term records from the Neumayer stake farms will assist to determine if these extremes are outliers or signs of broader climatic shifts.
Finally, understanding the seasonal pattern of snow accumulation is crucial for interpreting ice core records, which are key to reconstructing past climate conditions (Schlosser et al. 2010). Any shifts in the seasonality of accumulation due to climate change would directly impact how these records are

interpreted. This study aims to analyze both interannual trends and seasonal accumulation patterns at Neumayer station, focusing on changes over the past three decades.

1.2 Snow Depth, Accumulation and Surface Mass Balance (SMB)

The distribution of snow depth is inherently heterogeneous, with increased variability observed over complex terrain. Even on flat terrain, such as shelf ice, different processes lead to a heterogeneous snow distribution. This is initiated by the precipitation distribution, which is generally more homogeneous than the snow depth itself (Eisen et al. 2008). Spatial variations in snowfall rates are typically governed by the interplay between atmospheric circulation and topography, varying on spatial scales of kilometers or more (Clark et al. 2011).
During and after snowfall, various processes can influence snow depth on more localized scales, often on the order of tens to hundreds of meters (Clark et al. 2011). Following processes contribute to the heterogeneous distribution of snow depth:

- **Wind during Snowfall**: Wind can transport falling snowflakes, leading to inhomogeneities in the snow deposited on the surface. However, given the 40x40 m spatial extent of the stake farm, it is reasonable to assume that snowfall rates are relatively homogeneous across this area.

- **Wind-Driven Snow Redistribution:** Also referred to as drifting snow erosion, snow is generally eroded in regions with high wind speeds and transported to areas of lower wind velocity, resulting in decreased (in erosion areas) or increased (in deposition areas) snow depth (Sundsbø 1998; Voordendag et al. 2024). Creep occurs in the lowest millimeters of the planetary boundary layer, the saltation region extends up to 100 cm, and the suspension region can be several hundred meters thick (Sundsbø 1998). Creep denotes the movement of particles along the surface, whereas saltation describes the trajectory of particles that leap above the surface. Suspension refers to the transport of particles that remain suspended in the airflow. In flat terrain, saltation generally serves as the predominant mode of transport for drifting snow at wind speeds ranging from 10 to 14 m s^{-1}. While drifting snow erosion is considered to be two to three orders of magnitude smaller on a continental scale, it can be locally significant, especially in dry and windy regions (Lenaerts et al. 2010). The resulting snow patterns are heavily influenced by local topography, wind speed, and direction (Voordendag et al. 2024). On average, 30% of the initial accumulation at the stake farm close to Neumayer is removed by wind erosion (Schlosser et al. 2002).

- **Sublimation:** Sublimation can occur either directly from the snow surface or from drifting snow, as the boundary layer atmosphere is undersaturated. The latter describes the sublimation of snow during transport by wind, where snow transitions directly from solid to gaseous phase before redeposition at the surface occurs. Lenaerts et al. (2010) found that drifting snow sublimation removes 16 ± 8% of the annual snowfall at Neumayer Station. In addition, sublimation of drifting snow exceeds surface sublimation at coastal and katabatic wind-controlled Antarctic sites, and this may also apply to the stake farm analysed in this thesis (Lenaerts et al. 2010).

- **Melt:** Melting plays a minor role in snow depth variability in Antarctica, as temperatures only rarely exceed 0°C during the austral summer (Jakobs et al. 2019). Near Neumayer, partial melting can occur near the ice shelf edge during warm days with intense radiation, leading to the occasional formation of denser or even melt layers. However, vertical transport of liquid water does not occur (Lenaerts et al. 2017; van den Broeke et al. 2010).

- **Compaction:** The compaction of the snowpack may be attributed to three primary factors: the overburden of its own weight, pressure exerted by wind, and snow metamorphism processes (Voordendag et al. 2024). Snow metamorphism depends on the temperature during and after snowfall (Schlosser et al. 2002). Frequent fresh snow accumulates at Neumayer implying that the settling of surface snow is limited. Therefore, surface snow density is relatively constant over time (Lenaerts et al. 2010).

Height and density changes at the stakes of a stake farm can be viewed as the cumulative result of the aforementioned processes (van den Broeke et al. 2004).
The Surface Mass Balance (SMB) is typically defined as the *annual* sum of precipitation, surface sublimation, runoff, erosion, and sublimation of drifting snow, integrated over the surface of a glacier, ice sheet, or ice cap (Lenaerts et al. 2010). Solid precipitation is the primary and largest positive contributor to the SMB (Schlosser et al. 2008). Rather than evaluating SMB across the entire surface, it is often measured locally as mass per unit area per unit time. This is referred to as the specific surface mass balance (SSMB), denoted as Σ (van den Broeke and Giesen 2021). The SSMB *during a given period* can be calculated by the change in height Δh over a specified time interval Δt and the average density $\overline{\rho}$ over this change in height (van den Broeke and Giesen 2021; Cuffey and Paterson 2010). The formula is as follows:

$$\Sigma = \frac{\overline{\rho}\Delta h}{\Delta t} \tag{1.1}$$

All methods for determining SMB or SSMB rely on some form of length measurement, such as height change or layer thickness. Converting these length measurements into SMB values necessitates knowledge of the density distribution of the observed sample (Eisen et al. 2008). However, obtaining reliable density profiles poses significant challenges (van den Broeke and Giesen 2021). Traditional methods calculate density by measuring the volume and mass of snow samples; however, accurately determining sample volume under field conditions can be difficult (Eisen et al. 2008). Consequently, SMB or SSMB is often estimated using density estimates that may not align with actual density measurements.
In this context, the term ”snow height change” refers to Δh and includes surface ablation, while the term ”accumulation” strictly pertains to gains; however, in this thesis, ”accumulation” will be used interchangeably with ”snow height changes”, i.e. including ablation, which is considered equivalent to the mass loss from all processes mentioned.
Reliable Density measurements over deep layers are difficult to obtain (van den Broeke and Giesen 2021). To summarise, precipitation, snow depth, accumulation and SMB are closely linked, but represent different concepts.

1.3 Climate

In the following subsections, the climate of Antarctica, DML, and Neumayer Stations across the various spatial scales is examined. Subsection 1.3.1 will look at the broader Antarctic climate system, focusing on the overarching atmospheric and oceanic processes that influence the continent's climate. In subsection 1.3.2, the focus is narrowed to the DML region, analyzing how local topography and geographical features shape precipitation patterns and temperature variations. DML is located in the Atlantic sector of Antarctica extending from approx. 30°W (Coats Land) to 50°E (Enderby Land) (Schlosser et al. 2008). Finally, subsection 1.3.3 will concentrate on the microclimate at the Neumayer Stations.

1.3.1 Antarctica

In this subsection, key aspects of the Antarctic climate will be explored, including radiation, atmospheric circulation, temperature, precipitation, and the influences of the El Niño-Southern Oscillation (ENSO) and the Southern Annular Mode (SAM).
Being completely enclosed by the Southern Ocean, Antarctica is Earth's most isolated continent. 98% of its surface is covered by snow and ice (König-Langlo et al. 1998). Sea ice around Antarctica reaches its maximum extent in September and October, and its minimum in February and March (König-Langlo et al. 1998). Moreover, Antarctica is the continent with the highest average surface elevation.
Radiation: The duration of the polar night (day) varies depending on the location in Antarctica, with the sun remaining below the horizon from approx. May to August and not setting between approx. September and March. Nevertheless, even during the polar day, the combination of low sun elevation angles and the high albedo of snow and ice results in a mostly negative surface radiation balance. When a surface has a negative radiation balance, it loses more energy by radiation than it gains (König-Langlo et al. 1998), which leads to further cooling.
Atmospheric Circulation: The Antarctic atmosphere is surrounded by a zone of sub-polar lows and strong westerlies at approximately 64°S, known as the circumpolar trough or belt. It moves back and forth as sea ice expands and retreats. Westerlies prevail north of this belt, easterlies south. Few depressions and cyclones generated by the circumpolar trough can penetrate into the interior of Antarctica. Cyclonic disturbances can occur throughout the year and introduce a weak meridional wind field, which transports relatively warm and moist air, in an otherwise predominantly zonal flow (König-Langlo et al. 1998; Schlosser et al. 2010). Most of the near-surface circulation on the Antarctic continent is dominated by katabatic effects with katabatic winds blowing perpendicular to terrain contours. Katabatic winds are directional constant and increase in speed with terrain slopes (König-Langlo et al. 1998). During katabatic winds in valleys moisture is transported towards the sea (Dufour et al. 2019).
Temperature: Mean annual temperature decreases with both distance from the coast and increasing surface elevation of the ice sheet (Rotschky 2007). For instance, at the Neumayer stations close to the coast and 43 m a.s.l. the mean annual temperature is -16.1°C (since 1981 until 2021)

(Bagheri Dastgerdi et al. 2021). In contrast, at a site on the Antarctic plateau (75°S, 15°E) at an elevation of 3453 m a.s.l., the annual mean temperature is -48.3°C (Rotschky 2007). The day to day temperature variations are largest during winter in response to the temperature difference between the air masses from the interior and the surrounding ocean (König-Langlo et al. 1998).

Moisture and Precipitation: Katabatic winds transport moisture offshore, while it is transported onshore above the katabatic wind layer (above approx. 950 hPa) (Dufour et al. 2019). Generally, precipitation decreases from the coastal low altitude areas to the inland plateau in Antarctica (Boening et al. 2012; Schlosser et al. 2008). Local minima (maxima) are found in the lee (luv) of topographical ridges (Boening et al. 2012; Schlosser et al. 2008).

There a two common types of precipitation: 1. clear sky precipitation or diamond dust and 2. maritime air intrusions (Turner et al. 2019; Baiman et al. 2023). Clear sky precipitation occurs more frequently (Turner et al. 2019), especially on the Antarctic plateau (interior), as slopes are gentle and orographic lifting negligible. Saturation is maintained by strong radiative cooling of the very cold air masses resulting in the formation of precipitation from clear skies. Precipitation from clear skies is no different from that originating in clouds. However, the low moisture content of very cold air masses makes it optically too thin to be visible as clouds (Wille et al. 2021; Bromwich 1988). Clear sky precipitation occurs in each month but shows some seasonal variations (Schlosser et al. 2010). The second major type of precipitation are maritime air intrusions, often associated with extreme precipitation events (EPEs). Turner et al. (2019) defines an EPE ”to be a daily precipitation total that is within the top 10% of the long-term record of daily precipitation amounts at a location.” EPEs contribute over 40% of the annual total across much of the continent. In coastal areas and on ice shelves, their contribution to the annual total can be even greater (Turner et al. 2019). EPEs can occur when there is a strong meridional flow of amplified planetary waves in the mid-troposphere. Typically, EPEs are observed when the mean sea level pressure in the circumpolar trough to the west of the location drops to a minimum (Turner et al. 2019). They usually last for one to three days, with most lasting only one day (Schlosser et al. 2010). Longer durations occur when atmospheric circulation becomes blocked, most often with a stationary High-Low surface pressure couplet (Turner et al. 2019). They are often linked to one polarity of either the Southern Annular Mode (SAM) or the El-Nino-Southern-Oscillation (ENSO) (Boening et al. 2012; Turner et al. 2019).

Interannual Variability: Two major modes of natural climate variability influencing the Antarctic climate are SAM and ENSO (King et al. 2023b): The ENSO phenomenon is the most significant short-term climate fluctuation, occurring every 3-7 years and lasting 9 months to 2 years. It alters global atmospheric circulation, impacting temperature and precipitation patterns. ENSO comprises three phases: ’El Niño,’ ’La Niña,’ and ’Neutral.’ As a coupled climate phenomenon, ENSO requires simultaneous changes in both the ocean and atmosphere to transition between phases (Wallace and Hobbs 2006). During ’Neutral’ conditions, trade winds blow from east to west across the Pacific, pushing warm equatorial water to the western Pacific. This divergence leads to upwelling of colder bottom water along the South American coast, causing the thermocline to slope across the Pacific. Air pressure is relatively low above the warm West Pacific, in contrast to the high pressure over the colder East Pacific, causing trade winds to seek balance. The less dense, moist air over the West Pacific rises, while the air sinks in the East, resulting in dry and warm subsidence. In La Niña,

sea surface temperatures (SST) in the central and eastern tropical Pacific drop below average, steepening the thermocline and strengthening easterly winds. In contrast, during an El Niño event, SST rises above average in these regions, reducing or reversing the pressure gradient across the Pacific (Wallace and Hobbs 2006; Trenberth 1997). Key impacts of ENSO on the Antarctic climate are reviewed in Li et al. (2021). The tropical-polar connection between ENSO and the Antarctic climate is well-established, with El Niño events generating stationary Rossby wave trains that influence the Amundsen Sea Low (ASL), weakening it by increasing sea level pressure by 2–5 hPa. This weakened ASL alters atmospheric circulation, resulting in regional climate anomalies such as decreased surface air temperatures (SAT) over the Antarctic Peninsula and increased SAT over East Antarctica. El Niño also affects Antarctic sea ice distribution, forming an Antarctic sea ice dipole with increased sea ice concentration in the Bellingshausen and Weddell Seas and decreased concentration in the Amundsen and Ross Seas. Additionally, El Niño events enhance moisture transport to West Antarctica, leading to increased snow accumulation. However, the weakened ASL simultaneously facilitates the onshore flow of Circumpolar Deep Water around West Antarctica, which accelerates sub-ice shelf melting.

The SAM is the dominant pattern of atmospheric variability in the extratropical Southern Hemisphere, characterized by shifts in atmospheric pressure between the mid-latitudes and Antarctica. These shifts influence the strength and position of the westerly winds, with positive phases of SAM leading to stronger, more poleward winds, and negative phases causing the winds to weaken and move equatorward. The SAM index is measured by calculating the difference between the normalized monthly zonal sea level pressure at 40°S and 65°S, using data from six observation stations near these latitudes. SAM significantly influences regional climates, affecting temperature and precipitation patterns across the Southern Hemisphere, including Antarctica. Its recent trend toward a more positive state has been linked to human activities, such as ozone depletion and rising greenhouse gas concentrations (King et al. 2023a).

Marshall et al. (2013) revisits the relationship between SAM and surface air temperature anomalies across Antarctica, focusing particularly on East Antarctica during austral summer and autumn. Traditionally, the SAM's positive phase has been associated with cooling in East Antarctica and warming in the Antarctic Peninsula. However, the authors observe a significant reversal in this SAM-temperature relationship during the first decade of the 21st century. Specifically, they find that positive SAM phases, which were previously linked to cooler temperatures in East Antarctica, are now associated with warmer temperatures in this region.

1.3.2 Dronning Maud Land (DML)

Most precipitation reaching DML is associated with extratropical cyclones reaching the coast, that transport moisture from lower latitudes polewards (Gorodetskaya et al. 2020). These precipitation events fall under the category of maritime air intrusions. Some of the extratropical cyclones are associated with atmospheric rivers (ARs) (Gorodetskaya et al. 2020). According to Gorodetskaya et al. (2020) ARs are long, narrow, and transient corridors, that enhance water vapor transport,

frequently of tropical moisture. These corridors are typically embedded in the warm conveyor belt ahead of the cyclone's cold front. Cyclones that have an AR carry a greater amount of moisture towards the poles than those without an AR. In fact, ARs account for 90% of the annual poleward moisture transport. Although ARs occur only three days per year, they significantly contribute to annual precipitation in DML, accounting for 15 ± 7% according to Baiman et al. (2023), while Simon et al. (2023) report a contribution of 20–40%. Precipitation at the escarpment, which is the transition zone between the coast and the plateau, is significantly topographic and wind-dependent (Schlosser et al. 2008). Coastal DML is susceptible to intermittent and intense EPEs, which often account for more than half (50%) of the total annual precipitation within just a few days each year (Simon et al. 2023; Turner et al. 2019). Local short-term variability in DML is less driven by SAM or ENSO (Turner et al. 2019).

1.3.3 Neumayer (NM)

In this study, the term 'Neumayer Station' is used to collectively refer to the three successive research stations established in Antarctica: the Georg-von-Neumayer Station (operational from 1981 to 1992), Neumayer Station (1992 to 2009), and Neumayer Station III (since 2009). NM, situated on the Ekström Ice Shelf at 70°39'S and 8°15'W, is the German wintering base on the DML coast (see Fig. 1.1). Located about 5 km southwest of Atka Bay and 43 meters above mean sea level, it drifts with the flowing shelf ice 157 meters per year towards the open sea. In summer, the ocean areas east and north of Ekströmisen are often free of sea ice.

Weather Patterns: There are two major regimes dominating the weather at NM. Firstly, clear-sky and dry conditions during southerly katabatic winds are observed frequently. There is only a small moisture transport due to sublimation from the surface and from drifting snow. The moisture is trapped within the stable boundary layer. This regime is often accompanied by a high-pressure ridge over the Weddell Sea (Gorodetskaya et al. 2020). The second common regime involves extratropical cyclones moving eastward from the northern Weddell Sea, advecting humid and warm maritime air masses. As a result, temperatures rise and snowfall intensifies (Gorodetskaya et al. 2020; König-Langlo et al. 1998). Snowfall observations are often classified as 'moderate' to 'heavy' (according to WMO) during the passages of these cyclones (Gorodetskaya et al. 2020). The rare EPEs due to ARs are connected to moderate but very humid northeasterly flow at the surface, turning to northwesterly flow with height (Gorodetskaya et al. 2020). In addition, warm air is advected from the north, so that temperatures are higher than on average during these snowfall events (Schlosser 1999). Occasionally during summer, precipitation can also occur as drizzle or rainfall (Gorodetskaya et al. 2020). **Temperature:** The average annual temperature recorded at NM since 1981 stands at $-16.10°C \pm 1.05°C$. Over this period, observations indicate no significant temporal trend in air temperature (Medley et al. 2018; Bagheri Dastgerdi et al. 2021)

Circulation and Wind: NM lies on the southern boundary of the circumpolar trough and is subject to frequent cyclonic disturbances throughout the year (Gorodetskaya et al. 2020). Straight easterly (90°) winds, varying slightly between 70° and 110°, are predominantly observed at NM primarily

due to the combined effects of (mostly weak) katabatic outflow, which is deflected by the Coriolis force towards the left, and the convergence with coastal easterlies generated by the cyclones of the circumpolar trough. These dynamics result in a prevailing pattern of easterly winds (Schlosser et al. 2010; König-Langlo et al. 1998). Wind speeds are relatively high with an annual mean value of 8.7 m s^{-1} and a standard deviation of $\pm$ 6.1 m s^{-1} (König-Langlo et al. 1998). The katabatic wind alone is characterized by low to moderate wind speeds (about 5 m s^{-1}, rarely more than 10 m s^{-1}) and a predominantly southerly direction (also SW or W directions) (Gorodetskaya et al. 2020). In contrast, wind speeds during cyclonic disturbances can reach 25 m s^{-1} resulting in heavy blowing snow and whiteouts (Gorodetskaya et al. 2020). Drifting and blowing snow can occur at wind speeds of 6-12 m s^{-1} (depending on the condition of the snow surface) and is reported in 40% of all visual observations at NM (Bagheri Dastgerdi et al. 2021). This makes the direct quantification of precipitation very difficult.

1.4 Spatial Variability of Snow Accumulation

Firstly, any analysis of snow accumulation must account for its high spatial variability, meaning that results must be interpreted with respect to their spatial representativeness. Spatial variability refers to the extent to which measurements differ across different locations.

Snow distribution in DML is heavily influenced by the region's topography and the processes of wind-driven sublimation and redistribution (Simon et al. 2023). In general, snow accumulation shows considerable spatial variability, even on scales ranging from meters to kilometers. For instance, wind shadows cast by buildings or terrain features can introduce high spatial variability at the kilometer scale—variability that can be as significant as the temporal variability observed over multidecadal to centennial timescales (Eisen et al. 2008). On a meter scale, sastrugi — elongated ridges formed by wind erosion and deposition — create local spatial variability, which strongly affects the annual variability of accumulation patterns (Eisen et al. 2008). However, because sastrugi are small-scale features, averaging stake measurements within a stake farm typically reduces their influence (McConnell et al. 1997).

In contrast, for individual stake measurements, even 10-year averages are only representative of a few square kilometers (Eisen et al. 2008). As discussed by Frezzotti et al. (2005), slopes and curvatures are the most significant topographic features contributing to spatial variability. Concave depressions, for example, accumulate snow more rapidly than convex ridges. Katabatic winds play a dominant role in snow export and sublimation within the undersaturated wind layer, driving spatial variability on meter scales (Eisen et al. 2008).

Given the high spatial variability in snow accumulation, stake farms serve as essential tools to assess the representativeness of individual measurement points, such as single stakes or ice cores (Frezzotti et al. 2005). If high standard deviations are observed within a stake farm, it is likely due to sastrugi or wind crusts. Additionally, the slope along the prevalent wind direction (SPWD) is a useful measure for assessing spatial variability. When the SPWD is highly variable, the standard deviation also tends to increase. Conversely, when the SPWD is low or accumulation is high, standard de-

viations within the farm tend to decrease (Frezzotti et al. 2005). Spatial variability patterns tend to remain stable over time (Eisen et al. 2008).
Goodwin (1991) conducted a two-year study in Wilkes Land, located east of DML, to examine the seasonality of spatial variability. His results revealed that during autumn, the spatial variability peaked. This was due to the formation of a wind-glazed ice crust during snow-free periods occurring in autumn, which led to the creation of sastrugi and dunes as well as increased surface hardness.

1.5 Temporal Variability of Snow Accumulation

For snow accumulation not only spatial variability but also temporal variability on different time scales needs to be considered. Before reviewing the interannual scale, the intra-annual periods are looked at.

1.5.1 Intra-Annual Variability and Seasonality

In general, information on intra-annual snow accumulation is sparse, as frequent direct measurements of precipitation amount and snow accumulation are difficult to obtain. Particularly, at remote sites in the interior of Antarctica (Dahe et al. 2004). Yet, there are some studies on seasonality of snow accumulation in Antarctica:
Fujii and Ohata (1982) computed monthly means of net accumulation at Mizuho station in eastern DML. Nine stakes were read monthly during a four-year measurement period from 1976–1980. Accordingly, most frequent snowfall occurred in February and March, with a secondary importance of the periods from October to January and August. Fujii and Ohata (1982) found near-zero accumulation from April to July.
At South Pole, McConnell et al. (1997) deployed 50 stakes, which were read monthly for 7.25 years from 1988 onwards. Here, the authors observed a maximal accumulation in spring (September and October) and hardly any accumulation in summer (December and January). However, very large stake-to-stake variability was mentioned. McConnell et al. (1997) showed that the primary source of variability within these short distances of stakes is peak wind velocities that transport snow.
Reijmer and Broeke (2003) installed ten AWSs with sonic altimeters across DML and one on Berkner Island, operating for four and seven years, respectively. The altimeter has a temporal resolution (3 hours) that is much higher than that of stake readings, allowing it to capture the timing of precipitation events. The measurement uncertainty of the instrument is 2 cm, which limits its ability to recognize ablation. Observations show that annual accumulation results from numerous small events and a few large ones, with the latter contributing most to the total. Typically, four to five major events occur annually, characterized by higher temperatures, humidity, wind speeds, and a shift from katabatic to northerly winds, but without clear seasonality. Coastal and escarpment regions in DML experience winter accumulation maxima, while Berkner Island and the plateau peak in summer, though the seasonal cycle at Berkner Island is barely significant at the 5% level (Reijmer and Broeke 2003).

1.5.2 Interannual Variability and Long-Term Trends

Methods and Datasets

Various measurement methods and data sets are used to track long-term trends in snow accumulation or mass balance in Antarctica. Some of the most important methods and data sets are:

- The satellites GRACE and its follow-on mission GRACE-FO (Gravity Recovery and Climate Experiment) measure gravitational field changes providing essential insights into mass balance changes in the polar regions at approx. monthly resolution (Wahr et al. 2000; Velicogna et al. 2020).
- The satellites ICESat, ICESat-2, and CryoSat-2 employ altimetry techniques to measure changes in ice sheet elevation. ICESat was launched in 2003, followed by ICESat-2 and CryoSat-2, which offer improved spatial and temporal resolution (approx. monthly) in capturing ice height variations (Wahr et al. 2000).
- In-situ measurements such as stakes and ultrasonic sensors offer temporal resolutions spanning from hours (ultrasonic sensors) to weeks, months, and years (stakes). These methods have been utilized to sample data over decades in Antarctica (Eisen et al. 2008).
- Ice thickness measurements, such as ground-penetrating radars (GPR), map internal layers of equal age to infer accumulation patterns. Depending on the thickness and properties of the internal layers, GPR profiles can trace back several centuries to even 1000 years with seasonal resolution (Eisen et al. 2008).
- Ice and firn cores provide information on past snow accumulation with seasonal and annual resolution in the layers closer to the surface, while deeper layers offer rough estimates. Ice cores can trace accumulation back up to one million years, depending on the drilling site location (Eisen et al. 2008).
- Regional climate models (RCMs) are employed to analyze the long-term effects of climate change on snow accumulation and the mass balance of the Antarctic. Climate models can simulate long-term trends over centuries or even millennia, although their temporal resolution varies depending on the model and computing capacity. Typically, simulations are performed on time scales of months to decades (Dalaiden et al. 2020).

Stake measurements are locally valuable but are often of limited temporal coverage. In contrast, remote sensing methods offer broader spatial coverage, although they may lack sufficient temporal or spatial resolution and require ground-truthing. Firn and ice cores provide extensive records of snow accumulation and its temporal variability over long periods, but they are spatially sparse and susceptible to post-depositional disturbances like sublimation and snowdrift redistribution. Averaging data from multiple cores, along with high-precision snow density measurement techniques within a region, can help mitigate local noise and enhance our understanding of snow accumulation variability across larger scales (Wang et al. 2017; Weinhart et al. 2020).

Interannual Variability and Trends in Antarctic Ice Sheet Accumulation

Interannual variability in Antarctic snowfall is high being largely influenced by EPEs (Boening et al. 2012; Gorodetskaya et al. 2020). Turner et al. (2019) found that 70% of the annual precipitation variance is explained by the variability in precipitation from EPEs, where the contribution is higher on the ice shelves and lower in the higher parts of the plateau.
As outlined in Dalaiden et al. (2020) and Schlosser and Oerter (2002), three primary mechanisms are responsible for a substantial portion of the observed interannual variability in snow accumulation: thermodynamic processes, large-scale dynamics, and synoptic-scale dynamics.
Thermodynamic processes result in a change in snow accumulation due to a change in air temperature. This is because the maximum moisture content in the atmosphere increases exponentially with air temperature, in accordance with the Clausius-Clapeyron relationship. Consequently, the precipitation of more moisture in the form of snow in Antarctica is possible if air masses become warmer but remain below the freezing point.
The large-scale dynamics transport moisture from lower latitudes to Antarctica. Changes in the atmospheric circulation result in regionally variable trends, with topography exerting the dominant control on precipitation in this case (Dalaiden et al. 2020; Simon et al. 2023). Short-lived synoptic-scale processes, such as ARs and landfalling cyclones, exert a significant influence on interannual variability in the form of EPEs.
It is important to highlight that these three mechanisms are challenging to distinguish due to their mutual dependence. Dalaiden et al. (2020) found that both the large-scale transport and short-lived synoptic scale events control interannual variability in snow accumulation, explaining 49% of the variation across all regions, with the exception of the AIS plateau. In contrast, Turner et al. (2019) asserts that on the ice shelves, EPEs predominantly explain the variance, while this relationship does not hold over the ocean and the higher plateau. The year-to-year variability of EPEs is greater than the interannual variability of annual precipitation itself (Turner et al. 2019).
The high interannual variability of Antarctic snowfall is closely linked to fluctuations in cyclone activity, which are themselves influenced by ENSO and SAM (Boening et al. 2012). According to Turner et al. (2019), the Ross Ice Shelf experiences an increased number of EPEs during an El Niño. Ice core analysis indicates that El Niño reduces precipitation in the EAIS (King et al. 2023b). A slight negative anomaly in mass balance is observed during El Niño events in DML (King et al. 2023b). ENSO affects SMB by modulating heat and moisture transport. This modulation results in lower SST and reduced moisture flux in eastern West Antarctica while increasing SST and moisture flux around the Ross Ice Shelf during an El Niño event (Lenaerts et al. 2019).
SAM influences Antarctic SMB by redistributing precipitation across the continent, with positive SAM phases leading to reduced precipitation in West Antarctica and increased precipitation on the eastern Antarctic Peninsula (Lenaerts et al. 2019). In coastal DML, it is linked to an increase in mass (King et al. 2023b). The combined effect of El Niño and a positive SAM results in a slight increase in the SMB of the EAIS (King et al. 2023b).
Trend: The AIS has experienced an increase in snow accumulation over the past century, which has partially offset the observed ice-dynamic mass loss. This dynamic loss, particularly in the West

Antarctic Ice Sheet (WAIS), has been attributed to ocean warming and grounding line retreat, while the underlying drivers of increased snow accumulation over the AIS remain unclear (Dalaiden et al. 2020; on Climate Change 2023). For the entire Antarctic continent, Dalaiden et al. (2020) calculated a relative increase in modeled snow accumulation of 8% between the periods 1850–1879 and 1985–2014.

Both ice core records and climate models indicate that snow accumulation has risen since the early 19th century, coinciding with a warming of the near-surface atmosphere over the AIS, which is thought to enhance accumulation (Dalaiden et al. 2020; Philippe et al. 2016; Lenaerts et al. 2016). Other suggested drivers include the interaction of orography with the temperature–accumulation relationship and atmospheric circulation patterns (Dalaiden et al. 2020).

On a continental scale, the increase in total accumulation is primarily attributed to short-lived synoptic-scale processes, while the general large-scale circulation contributes minimally. However, there are significant regional differences in these trends. For example, DML has experienced a 30% increase in snow accumulation primarily due to large-scale processes (Dalaiden et al. 2020).

DML

Both large-scale and synoptic-scale transport contribute nearly equally to the interannual variability in DML, with synoptic-scale transport being slightly higher (Dalaiden et al. 2020). Thermodynamic processes, such as the increase in near-surface temperature, are not significantly correlated with SMB (Lenaerts et al. 2013). King and Christoffersen (2024) reveal that periods of persistent positive SAM phases lead to increases in snow surface elevation in coastal DML, whereas sustained El Niño events correlate with decreases in elevation. However, when firn densification models are incorporated into the analysis, the SAM and ENSO signals are significantly reduced. The overall uncertainty increases, indicating that firn processes play a critical role in modulating these observed patterns. Nevertheless, King and Christoffersen (2024) found that two-thirds of the observed variability in ice sheet elevation (as observed by GRACE and satellite altimetry) can be explained by SAM and ENSO processes. These findings are particularly robust for the plateau region of DML, while the coastal areas are associated with greater uncertainty.

Dalaiden et al. (2020) report an increase of 17% in snow accumulation in DML between 1850 and 2014. This is supported by an ice core study by Philippe et al. (2016) conducted on a coastal site (Derwael Ice Rise) of DML. In this study, the average SMB for the period from 1816 to 2011 is 0.47 m water equivalent per year (m w.e. a^{-1}). This value shows an increase for more recent periods, with the mean SMB for the period 1991–2011 rising by 32% to 0.64 m w.e. a^{-1}. However, this ice core was the only source to show increasing SMB in coastal East Antarctica during the last 100 years until 2016 (Philippe et al. 2016). In 2018, however, Medley et al. (2018) reported that the recent increases in snowfall observed in an ice core in western inland DML near Kohnen Station are indicative of a long-term pattern (+5.2 $\pm$ 3.7% per decade) and are unprecedented in the last two millennia. RCMs, however, are unable to reproduce this reconstructed trend, suggesting that not all relevant processes are adequately represented in the models or their initial conditions.

Data from GRACE (Wang et al. 2023; Lenaerts et al. 2013) and modeled data of the regional cli-

mate model RACMO2 suggest that there was an increasing mass anomaly in DML between 2007 and 2013 (Fig. 2b). However, there was no discernible trend in SMB from 1980 based on RACMO2 (as of 2013, Fig 2a) (Lenaerts et al. 2013).
At NM Schlosser and Oerter (2002) analyzed three shallow firn cores that were all drilled either at or close to NM and therefore represent coastal sites. The authors report a decrease in accumulation in the first half of the 20th century and no trend in the second half.
All in all, more recent studies point to an increase of snow accumulation over the last decades. The situation appears to be quite complex, as trends in snow accumulation in DML vary depending on factors such as location (average DML, inland versus coastal) and the method of investigation (modeling, ice/firn core analysis, satellite data). In some cases, trends indicate increasing snow accumulation (modeled data for total DML with high spatial resolution as reported in Dalaiden et al. (2020); inland ice core analysis by Medley et al. (2018); coastal ice core analysis by Philippe et al. (2016)) in eastern DML, while in others, they suggest constant or decreasing accumulation (firn core analysis at coastal stations such as in Schlosser and Oerter (2002)). Trends in accumulation must be interpreted with caution due to the high interannual variability (Schlosser and Oerter 2002). More recent studies agree on increasing (surface) mass balance and can attribute this to increased snowfall (Medley et al. 2018; Boening et al. 2012; Philippe et al. 2016; Wang et al. 2023).

1.6 Goals and Outline

This Master's thesis aims to investigate the various aspects of temporal and spatial trends in the mean and variability of snow accumulation at a stake farm close to NM. For a structured analysis, five major research questions were formulated beforehand, which will be laid out in the following paragraphs, and answers summarized at the end of the thesis in section 4.
Many previous studies (Eisen et al. (2008), Frezzotti et al. (2005),Goodwin (1991), Kuhns et al. (1997), see Section 1.4) found high spatial variability in snow accumulation. Therefore, the first goal (RQ: research question) is:

RQ1: How does the spatial variability of snow accumulation within the stake farm behave?

- Due to challenges in quantifying intra-annual variability, this aspect was not included in the analysis.
- Instead a discussion is included that outlines the challenges of deriving an appropriate metric.
- Long-term stability of snow accumulation patterns and its variability is assessed.

The before-mentioned studies of intra-annual analyses of snow accumulation in Section 1.5.1 all rest upon rather short time series with the longest being 7.25 years. Based on the uniquely long time series of 33 years with comparatively high temporal resolution at NM, we are able to contribute a stable analysis of seasonality in snow accumulation. Thus, the following research question is addressed next:

RQ2: Is there an intra-annual cycle evident in the dataset of accumulation and its temporal variance?

The following aspects are further investigated:

- What does the typical intra-annual cycle of averages and variances look like?
- Is there a shift of seasonal contributions to the annual total?
- How does it compare to the annual cycle computed by model output by Schlosser et al. (2002)?

Considering the complex state of research on long-term trends in snow accumulation (1.5.2), the central goal of this thesis is a profound analysis of the long-term trend at a stake farm close to the coast.

RQ3: What is the temporal evolution of snow accumulation at NM over the past 33 years?

- What is the average accumulation rate per year? Does it remain constant over the 33-year period?
- Does a statistically significant trend exist? In this case, what could be the main driver?
- How high is the interannual variability? Is the variance de-/increasing?

Extrema are analyzed to understand their characteristics and underlying causes. With climate warming, both the mean and variance of the underlying distribution may shift, leading to possible changes in the frequency and intensity of minima and maxima of snow accumulation.

RQ4: What are the extrema observed in the snow accumulation, and what underlying causes are addressed in the literature?

Based on the previous RQs, we want to finally address the following research question:

RQ5: Is there evidence in the time series of snow accumulation that corresponds to global climate warming?

This research question aims to differentiate between natural variability and long-term changes by investigating fluctuations in snow accumulation time series.
The thesis will include a Methods chapter 2 describing stake measurements, data processing, filtering, and computational procedures. The Results chapter 3 will address the findings for RQ1 to RQ3. The discussion 4 of the results will tackle also RQ4 and RQ5 in relation to existing literature. The Conclusion 5 will provide insights into the relevance of the study.

Fig. 1.1: Map of Antarctica indicating ice shelves shaded in grey. Adapted from Abrahamsen (2012). The red star denotes the location of Neumayer III station.

2 METHODOLOGY

Research activities at NM began in 1981 and have continued to this day. However, the station has been rebuilt and relocated three times during this period. First snow accumulation measurements were installed in 1981 close to Georg von Neumayer (GvN) station, which refers to the first location of the research station. With the construction of a new base 'Neumayer', this stake farm was moved and a second stake farm (referred as 'Süd') was established 10 km south of Neumayer (15 km south of GvN) in 1987 (Schlosser and Oerter 2002). The measurements correlate well (r=0.71), although accumulation is higher at 'Süd' than at 'Neumayer' (Schlosser and Oerter 2002). Measurements at the stake farm 'Neumayer' ended 2008. In 2009 the base was rebuilt and relocated again, now called 'Neumayer III'. Measurements at 'Süd' continued, resulting in a uniquely long and consistent time series, which will be analysed in this thesis. Further information on 'Süd' will be provided in the next section.

2.1 Method: Stake Readings

Fig. 2.1: A: Typical bamboo stake. Adapted from Eisen et al. (2008). B: Stake farm Spuso. Photo taken by Linda Ort. https://blogs.helmholtz.de/atkaxpress/2021/12/mein-antarktischer-arbeitsweg/

Stake readings serve as a straightforward method for measuring accumulation and SMB, representing single-point measurements at the surface. These stakes are inserted into the snow or ice, initially with 1 meter protruding from the ground (see Fig. 2.1 subfigure A). Periodically, the length of the stake above the snow surface is measured to track the snow height changes. To minimize disturbances, readings are typically taken from the downwind side, reducing the impact of footprints on the snow surface (Eisen et al. 2008). Observations are preferably made during calm weather condi-

tions. Annually, usually at the end of summer, the stakes are removed and repositioned adjacent to their previous locations (Schlosser et al. 2002). Stake height measurements depend on the stake's bottom remaining still relative to the surrounding snow layer.
A *stake farm* yields individual measurements for a clearly defined small area, typically ranging from tens of meters to kilometers in side length (see Fig. 2.1 subfigure B). These measurements are then averaged to obtain a single accumulation value. Using multiple stakes helps mitigate the effects of small-scale depositional variability. Furthermore, continuously monitoring stake farms provides insight into the gradual build-up of snow cover throughout the year and into seasonality (Eisen et al. 2008).
Uncertainty: There are two primary sources of uncertainty in stake measurements. The first is measurement errors, which can result from incorrectly measuring the length of the protruding stake, submergence of the stake, or surface roughness (e.g. sastrugi). The second source is natural noise introduced by small-scale spatial variability of snow accumulation caused by relief (Eisen et al. 2008). Natural noise, as Eisen et al. (2008) point out, is at least one order of magnitude larger than other sources of uncertainty; however, with an increasing number of stakes, uncertainty is reduced. For example, sastrugi can form within the stake farm, causing significant variations in snow accumulation at each pole. As the number of stakes increases, it becomes less probable that most of them will be impacted by the sastrugi. Thus, the average height change of a stake farm represents the typical accumulation (Schlosser and Oerter 2002).
Stake Farm 'Süd': 'Süd' presents a uniquely long time series dataset. Located 10 kilometers southwest of NM and along the traverse route to the Ritscherflya south of Ekströmisen, this monitoring site comprises 16 aluminum stakes arranged in a 4x4 grid with 10 meters spacing between them (see Figure 2.2). Readings at this stake farm began in December 1990 and have continued to this day. Stake readings at 'Süd' were initially conducted once per month until May 2010, after which they transitioned to a bi-weekly reading. It is important to note that the measurements were dependent on favorable weather conditions, which resulted in irregular intervals between the measurements. These intervals did not usually correspond to the intended 4-week (or 2-week) period.

2.2 Data Processing

2.2.1 Measurement Format

The heights were manually measured and noted on paper, later transfered to a table in Excel format including

- the height change of every stake from one reading to the other (from 1994 onward, before only the mean height change)
- the mean of all 16 height changes
- the integrated height change
- the standard deviation in space

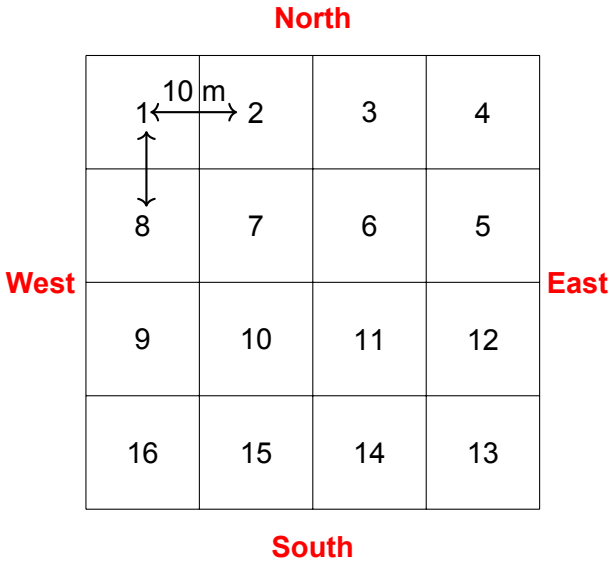

Fig. 2.2: Measuring set-up of stake farm 'Süd', stakes have a distance of 10 m in both North-South and West-East direction

- comments on the conditions of the stake farm during measurements

The Excel sheet is converted to a dataframe of purely numeric values and unique timestamps per row using Python. Comments are saved in a separate data frame.
The height differences measured at 16 stakes provide a reasonable approximation of snow accumulation. However, this measure does not reflect the complete accumulation, as the true value is slightly higher than the simple height difference. A small correction term, ΔB, must be added to account for layer thinning due to snow densification (Eisen et al. 2008). Unfortunately, ΔB can only be determined with density measurements and profiles, which are beyond the scope of this thesis. In this work, the observed height differences will be referred to as the accumulation a_i at each stake i. For precision, accumulation must also account for the time interval over which it occurred yielding accumulation rates $\dot{a}$. Measurements were taken at irregular time intervals $(t_{j,\text{irreg}})$.
Given:

- height differences a_i measured at 16 stakes i,
- 621 measurements taken on an irregular time axis $t_{j,\text{irreg}}$, ranging from date $t_{0,\text{irreg}}$ = 1990-12-29 to $t_{621,\text{irreg}}$ = 2024-03-01,

the original time series can be expressed as

$$\dot{a}_i(t_{j,irreg}). \tag{2.1}$$

Except for RQ1, we are primarily interested in the average accumulation across all 16 stakes within the stake farm:

$$\dot{a}_{v0} = \frac{\sum_i \dot{a}_i(t_{j,irreg})}{16} \tag{2.2}$$

Hereafter, I will refer to $\dot{a}_{v0}$ as version 0 (v0). A complete list of the symbols and variables used can be found in the nomenclature in the appendix.

2.2.2 Data Quality Control (QC)

At the pre-processing stage, the quality of the data is carefully evaluated. For example, if the difference between the measurements of two stakes exceeds a predefined threshold, it could indicate that one of the stakes is problematic. Homogenizing the data from an irregular to a regular time grid is not necessary at this stage, as stakes are only compared and analyzed relative to other stakes measured on the same day. Additionally, homogenizing the data into a time series of monthly accumulation rates averaged across stakes before performing quality checks on individual stakes could result in the loss of valuable information. Homogenization of the data will be addressed in section 2.2.3, where a comprehensive approach to creating a regular time grid will be outlined. In the following sections, I will assess various quality check methods, including confidence intervals and three specifically defined quality criteria, to determine their suitability, with some methods potentially being rejected based on this assessment.

Confidence Interval

Kuhns et al. (1997) proposed a method for comparing the individual snow fluxes at each stake with the estimated confidence intervals of the fluxes at the remaining stakes for a given time interval. If the flux was found to be outside the confidence interval, it was assumed that the reading was erroneous, for example, due to a misreading of the height on the stake by the field assistant. Consequently, the individual accumulation measurement was removed from the data set. In contrast to Kuhns et al. (1997), in this thesis, the confidence interval of accumulation values itself is used instead of snow fluxes.

Computing the Confidence Interval A confidence interval (CI) provides a range within which the true value of a measurement is likely to lie with a specified probability (e.g., 95%). Given the sample size ($i = 16$), a t-distribution is used to calculate the confidence intervals rather than approximating with a normal distribution, which is appropriate for larger sample sizes ($i \geq 50$). The following steps describe the calculation and application of the confidence intervals to the accumulation measurements: The mean accumulation rate $\dot{a}_{v0}$ and the spatial standard deviation $\tilde{\sigma}_{v0}$ are computed for each measurement. The standard error is then derived by dividing the standard deviation by the square root of the number of samples i, which indicates the extent of variability in the sample mean. The half-width of the confidence interval is determined using the t-distribution critical value, which depends on the desired confidence level ($\alpha = 0.999$) and the degrees of freedom ($i - 1$). The confidence interval is calculated as:

$$\text{CI} = t_{\alpha/2, i-1} \frac{\tilde{\sigma}_{v0}}{\sqrt{i}}.$$

Finally, the lower and upper bounds of the CI are computed:

$$\dot{a}_{lower/upper} = \dot{a}_{v0} \pm \text{CI}.$$

The true accumulation rate value of the measurement day lies within $[\dot{a}_{lower}, \dot{a}_{upper}]$ with a 99.9% confidence level. For each measurement, values that fall outside the calculated confidence interval bounds are set to NaN (not a number).

Applying the CI

Figure 2.3 displays the number of measurements per year that are a) available in total, b) NaNs, and c) NaNs and outside the CI. Even with a very broad CI (the chosen confidence level is 99.9%) too many data points are outside the CI. If all these values were discarded, the analysis would have lost one third of data points and 10 m of cumulative accumulation, respectively. For this reason this option of quality check has been rejected.

Defining Quality Criteria (QC)

QC1: 4σ Interval

In a first approach, outliers were defined as accumulation rates falling outside the range of $\langle \dot{a}_{v0} \rangle \pm 4\tilde{\sigma}_{\langle \dot{a}_{v0} \rangle}$. Here, $\langle \dot{a}_{v0} \rangle = 5.3$ cm Δt_j^{-1} and $\tilde{\sigma}_{\langle \dot{a}_{v0} \rangle} = 10.0$ cm Δt_j^{-1} denote the mean and standard deviation across the entire time series of individual stake accumulation rates $\dot{a}_i$, where the angled brackets $\langle \cdot \rangle$ represent a temporal average over the entire time series. The term Δt_j^{-1} refers to the irregular time intervals between measurements. Assuming a Gaussian distribution, 99.99% of the data should fall within this interval.

This method flags accumulation rates outside the range $]-34.7, 45.3[$ cm Δt^{-1} as outliers. This approach is problematic because accumulation rates can be as high as 50 cm Δt^{-1}, leading to the exclusion of valuable data from the analysis. Additionally, QC1 fails to relate the individual stakes to the others of the same measurement day. Due to these limitations, this approach is unsuitable and excluded from further quality control procedures.

QC2: Deviation from Mean Accumulation Rate

To relate individual stake measurements taken on the same day, the average accumulation rate across all stakes $\dot{a}$ is calculated and subtracted from each individual stake measurement $\dot{a}_i$. An accumulation rate $\dot{a}_i$ is considered unphysical if it falls outside the interval $[\dot{a} \pm 2\tilde{\sigma}_{\langle \dot{a}_{v0} \rangle}]$, where $2\tilde{\sigma}_{\langle \dot{a}_{v0} \rangle} = 20.0$ cm Δt_j^{-1}. Given the assumption that the spatial characteristics of accumulation remain generally similar throughout the measurement period, $\tilde{\sigma}_{\langle \dot{a}_{v0} \rangle}$ is assumed to be a reliable measure of variability within the stake farm throughout the entire measurement period. Using $\tilde{\sigma}_{\dot{a}}$, i.e. the standard deviation across the stake farm of a single measurement, can cause a single erroneous stake to have a disproportionately large impact on $\tilde{\sigma}_{\dot{a}}$, making it an unreliable and non-robust metric in time.

While QC2 generally yields good results, it has a limitation: if two or more neighboring stakes deviate significantly from the mean in the same direction, it is likely due to sastrugi in the field. Sastrugi are frequently observed to have height differences of 20 cm from their surroundings. By removing these two or more data points, valuable information is lost. Therefore, a criterion that accounts for sastrugi is necessary.

QC3: Relation of Max/Min to other stakes

To account for sastrugi, for a given measurement day, we compare the most extreme accumulation rate with the second most extreme rate and the rest of the stakes. This is done by calculating the

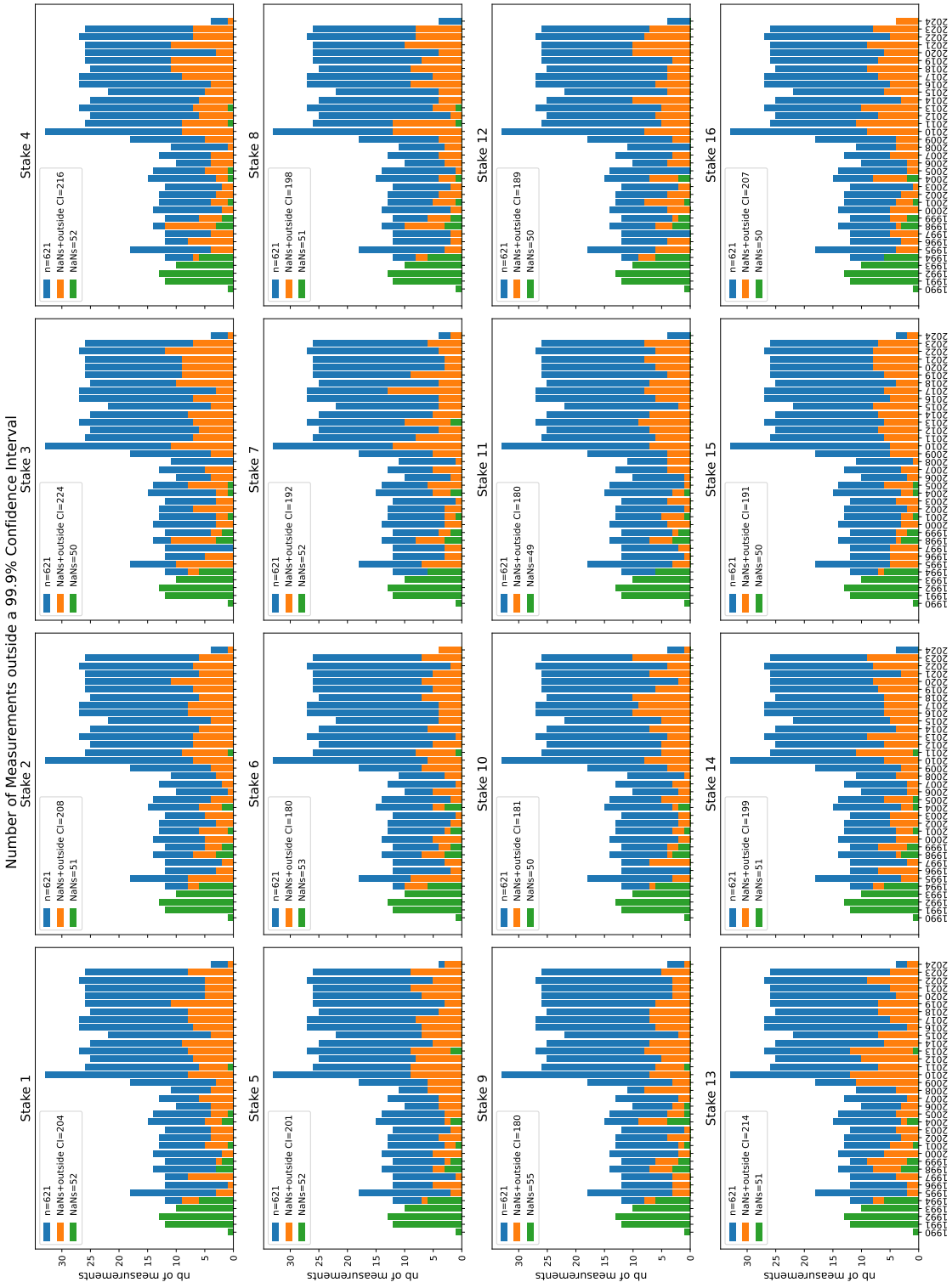

Fig. 2.3: Time series of the number of measurements from 1991 until 2024 at stake farm 'Süd'. Green bars indicate the number of missing data/NaNs per year, orange bars the sum of missing data/NaNs and data outside a 99.9% confidence interval (CI) per year, blue bars the sum of missing data/NaNs and data outside the CI and data inside the CI per year.

difference between the stake with the maximum (or minimum) accumulation rate $\dot{a}_{i,\text{max}}$ and the stake with the second-highest (or second-lowest) accumulation rate $\dot{a}_{i,\text{max2}}$. If the difference $\dot{a}_{i,\text{max}} - \dot{a}_{i,\text{max2}}$ is greater than the difference between the second-highest (or second-lowest) stake and the minimum (or maximum) stake $\dot{a}_{i,\text{max2}} - \dot{a}_{i,\text{min}}$, then the maximum (or minimum) rate $\dot{a}_{i,\text{max}}$ should be considered erroneous.

However, QC3 tends to flag too many data points in the low-accumulation range. For example, if most stakes measure around ± 1 cm and one stake measures 3 cm, this value is flagged for removal. Figure 2.4 clearly illustrates why we ultimately decided that both QC2 and QC3 must be satisfied to discard a value. QC2 performs particularly well on high-accumulation measurement days, while QC3 struggles in low-accumulation scenarios. Conversely, QC3 is effective on days with sastrugi, whereas QC2 is not. For example, in the first panel, two cells were flagged by QC2, but since they are neighboring stakes and exhibit a similar blue-ish pattern, it is likely due to sastrugi. Thus, retaining these data points is a sound decision.

On 14.05.2009, extremely high accumulation was recorded with an average accumulation of $\dot{a} = 45.7$ cm Δt_j^{-1}. It is evident that QC1 should not be used in this case, as it would result in discarding these valuable measurements. Additionally, the combination of QC1 and QC2 is not effective, as stakes 15 and 16 likely reflect the presence of sastrugi.

The combination of QC2 and QC3 proves effective, as demonstrated on 18.09.2009. On this day, nearly all stakes in the farm had red cells, except for stake 4, which was dark blue. This outlier was appropriately flagged for removal.

In total, 18 readings were discarded using the QC2 and QC3 criteria. Errors in measurements can be attributed to misreading a stake by the field assistant or erroneous data entry into the Excel table. Furthermore, stakes can break, etc., so that for 15 measurements out of 650 measurements the full set of individual 16 stake measurements is not available. The first and second moments of these 15 measurements, however, display the same distribution as the distribution of these quantities computed from the full set of stakes. The same argument is valid for the 18 additional measurements, where one or more stake readings were discarded during the quality control process (not shown). Therefore, these 33 measurements are not tracked throughout the analysis but treated equally.

2.2.3 Interpolating to a Regular Time Grid

The time intervals between consecutive measurements $t_{j-1,\text{irreg}}$ and $t_{j,\text{irreg}}$ are non-uniform ($\Delta t_j \neq$ const), which affects the accumulation rate $\dot{a}$. This effect is illustrated in Figure 2.5. For instance, an increased measurement frequency typically results in lower accumulation values per measurement. For example, if 10 cm of snow accumulates in January and is measured once, the accumulation $\dot{a}$ would be 10 cm month^{-1}. However, if two measurements are taken, the accumulation might be recorded as 2 cm Δt_j^{-1} and 8 cm Δt_{j+1}^{-1}. While this issue does not affect analyses of cumulative accumulation time series being the integral over Δt_j^{-1}, it must be addressed in other analyses by interpolating the measurements to a regular time grid. Given that measurements were taken monthly until 2009 and twice monthly thereafter, I implemented three interpolation methods (v1 – v3) to convert the data to a regular monthly time grid.

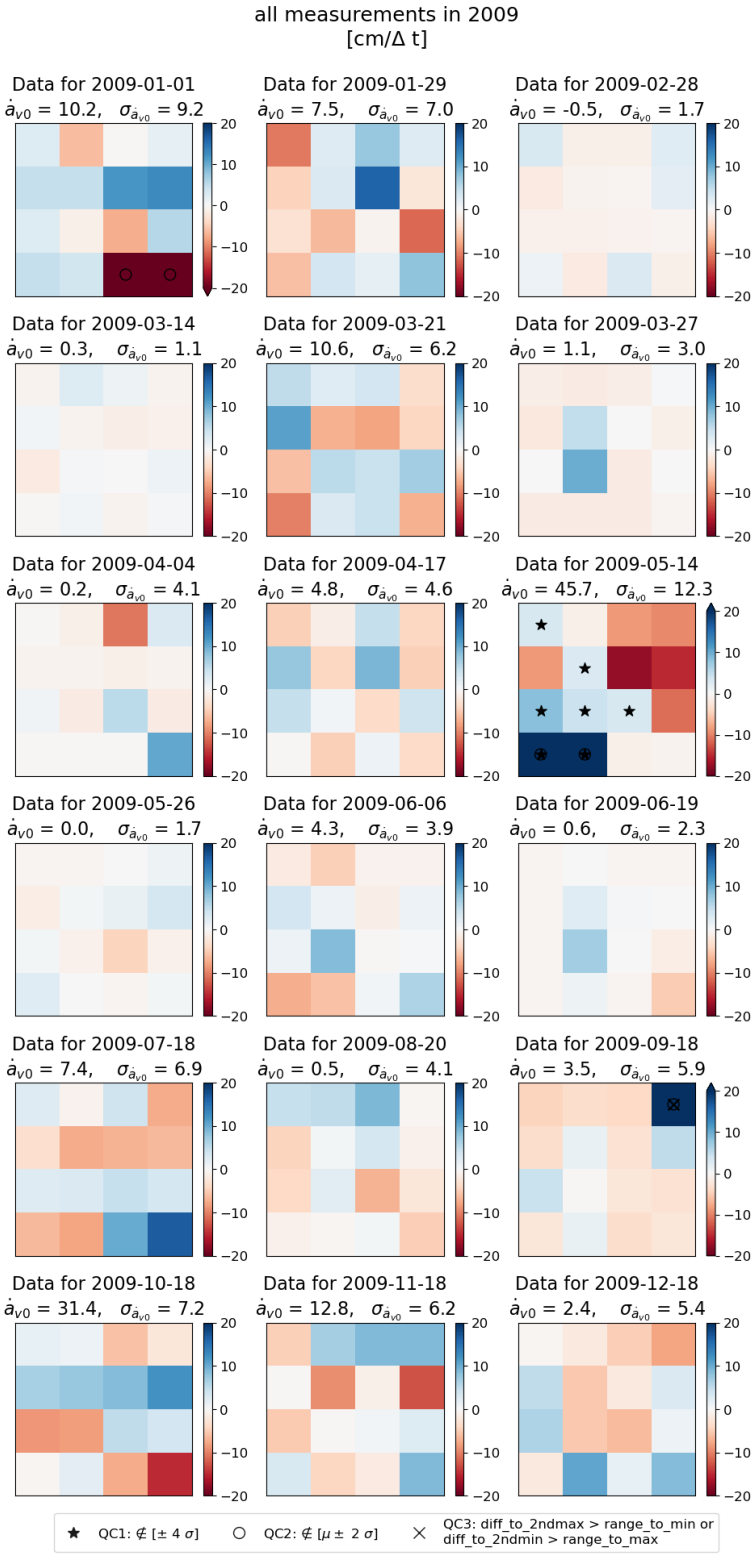

Fig. 2.4: Each panel represents the stake farm layout on a given measurement day. The top-left cell corresponds to stake 1, while the bottom-left cell represents stake 16. Colors indicate the difference between each stake's accumulation and the daily mean for the entire stake farm. Red (blue) cells mean, that the stake had less (more) accumulation than the mean.

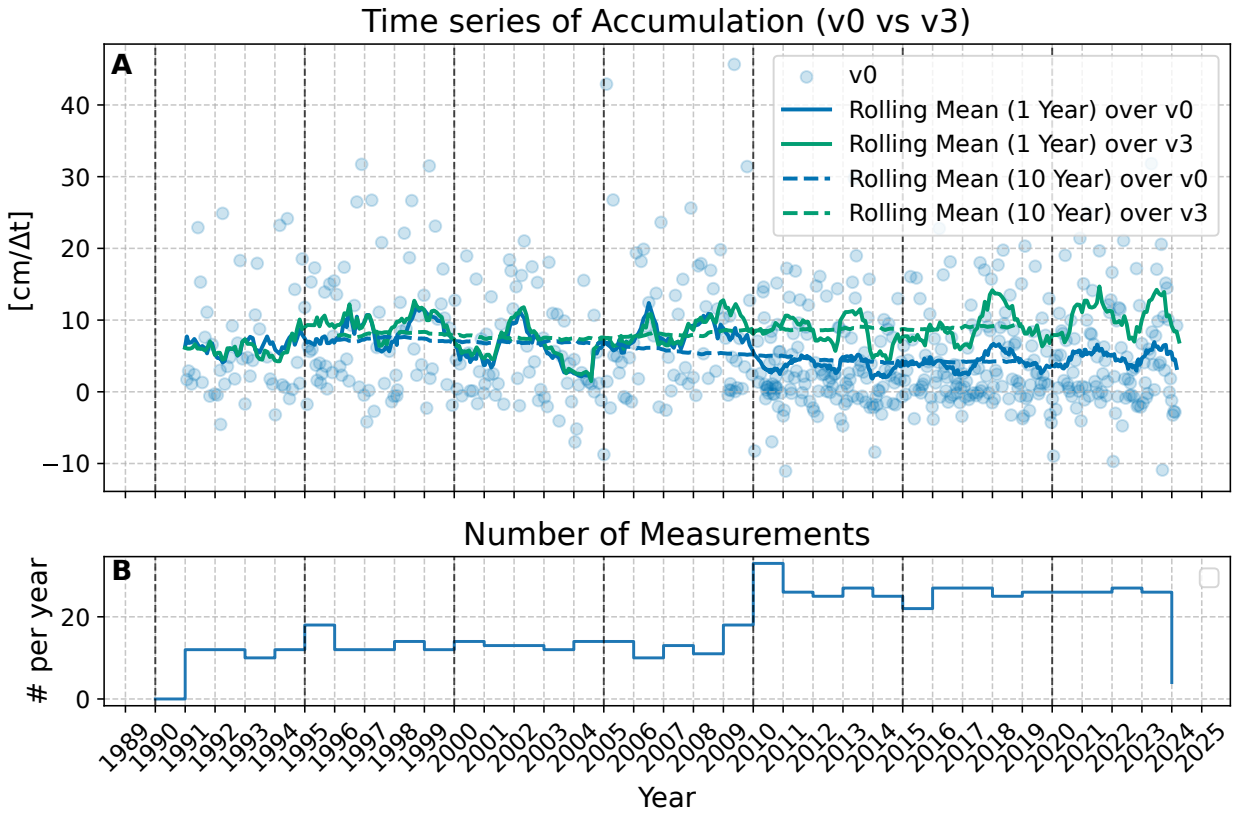

Fig. 2.5: A: Time series of the snow accumulation in cm from January 1991 til March 2024 at stake farm 'Süd'. Blue, scattered dots represent all data points, the blue (dashed) line the rolling mean over one (ten) year(s) of data version 'v0', the green (dashed) line the rolling mean over one (ten) year(s) of data version 'v3', which has been multiplied by the number of days per month for better comparison. B: Time series of the number of measurements per year.

Temporal interpolation method v1

1. Sum all measurements $\dot{a}(t_{j,\text{irreg}})$ within a given month m to obtain one value for the monthly sum. This yields monthly accumulation rates a on a regular time axis t_m. Monthly accumulation rates are referred to as a, as the dot over $\dot{a}$ is reserved for accumulation rates with units cm/day.
2. Identify all months where $a(t_m)$ is NaN (i.e., no measurements were carried out during these months).
3. Adjust the value for the preceding month m by redistributing the accumulation value $a(t_{m+1})$ over the previous and current months as follows:

$$a_{v1}(t_m) = \frac{a(t_{m+1})}{2}, \tag{2.3}$$

$$a_{v1}(t_{m+1}) = \frac{a(t_{m+1})}{2}. \tag{2.4}$$

However, if multiple measurements were taken in month $m+1$, it is more appropriate to only split the first accumulation value by 2 and apply it to the previous month m. Version 2 addresses this issue.

Temporal interpolation method v2

Steps 1 and 2 remain the same as for v1:

1. see v1
2. see v1
3. Identify all months m where $a(t_m)$ is NaN and $a(t_{m+1})$ consists of multiple measurements $\dot{a}(t_{j,\text{irreg}}), \dot{a}(t_{j+1,\text{irreg}}), \ldots$

$$a_{v2}(t_m) = \frac{\dot{a}(t_{j,irreg})}{2}, \tag{2.5}$$

$$a_{v2}(t_{m+1}) = \frac{\dot{a}(t_{j,irreg})}{2} + \dot{a}(t_{j+1,irreg}) + ... \tag{2.6}$$

However, both v1 and v2 might incorrectly assign an accumulation event to one month when it actually occurred in the previous month. For example, if an accumulation rate of 10 cm Δt_j^{-1} is measured on 20.04. and 30 cm Δt_{j+1}^{-1} on 02.05., it is more likely that most of the 30 cm snow has accumulated in the last 10 days of April rather than the first 2 days of May.

Temporal interpolation method v3

Therefore, the accumulation rate $\dot{a}(t_{j,\text{irreg}})$ is normalized by the number of days (Δt_j) between the previous measurement $t_{j-1,\text{irreg}}$ and $t_{j,\text{irreg}}$, yielding the daily accumulation rate $\dot{a}$ on the diurnally spaced time axis t_d:

$$\dot{a}(t_d) = \frac{a(t_{j,\text{irreg}})}{\Delta t_j}. \tag{2.7}$$

Daily accumulation rates are averaged onto the regular monthly grid by weighting with the number of days for which the respective daily accumulation rate is applicable (see Fig 2.6):

$$\dot{a}_{v3}(t_m) = \frac{1}{n_m} \sum_j \dot{a}(t_d) n_{m,j}, \tag{2.8}$$

where n_m is the number of days in month m, and $n_{m,j}$ is the number of days in month m up to t_j ($\sum_j n_{m,j} = n_m$). Finally, $a(t_m)$ represents the monthly accumulation rate as the sum of the monthly mean daily accumulation rate:

$$a_{v3}(t_m) = \sum_j \dot{a}(t_d) \cdot n_{m,j}. \tag{2.9}$$

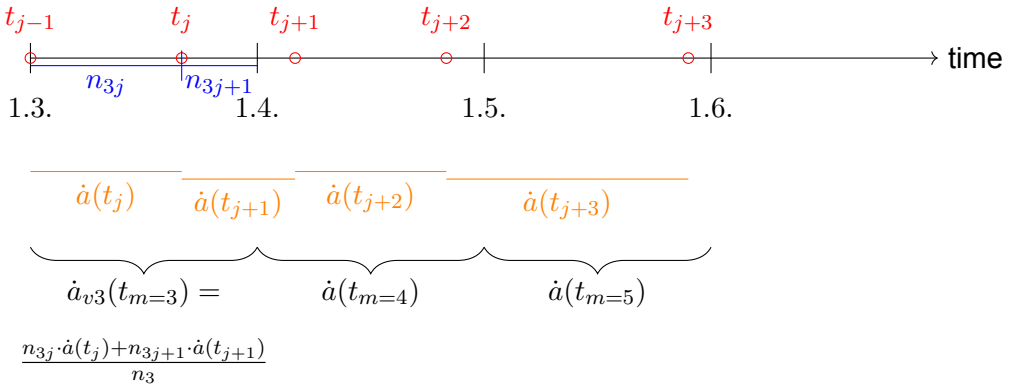

Fig. 2.6: Exemplary computation of $\dot{a}_{v3}$ for the month March

I have computed every analysis in the remaining part of this thesis with all three versions. I computed each analysis using all three versions, finding that while there were some minor differences, especially regarding trends and extrema, no major discrepancies appeared, highlighting the robustness of the results. Furthermore, differences pointed towards months, where the exact timing of the accumulation event is unknown. In these cases, accumulation rates can be shifted up to one month backward in time with v3. However, v3 captures best the probability of the timing of the accumulation event(s), in addition to the equalization of whether a month consists of 28, 29, 30, or 31 days.
Therefore, unless stated otherwise, the results presented in the remaining part of this thesis refer only to version 3 (v3).

2.3 Data Analysis

2.3.1 SAM index

The observation-based SAM index is defined as follows:

$$\text{SAM} = P^*_{40°S} - P^*_{65°S},$$

where $P^*_{40°S}$ and $P^*_{65°S}$ denote the normalized monthly zonal sea level pressure (SLP) at 40°S and 65°S, respectively. Monthly values of the SAM index from 01-1991 to 03-2024 were obtained from (NOAA Climate Prediction Center). The SAM is computed using data from six stations located near these latitudes. A comprehensive description of this methodology is provided by Marshall (2003).
A Fast Fourier Transform (FFT) was applied to the detrended SAM index time series (obtained by subtracting the mean SAM index for the entire period from each value) to identify the dominant frequencies of the SAM. This will be used later in section 4.3.2.

2.3.2 Spatial Variability of Snow Accumulation

The primary aim of this analysis is to analyze and visualize the spatial variability in snow accumulation across the stake farm. The spatial standard deviation is computed across the stakes of the stake farm. Until February 1994 only the mean height change has been recorded, for this reason, a spatial standard deviation cannot be computed for that period.
Several measures of spatial variability were computed, including standard deviation (std), interquartile range (IQR), and the standard deviation normalized by the mean accumulation, also known as the Coefficient of Variation (CV). The use of CV for analyzing spatial variability in snow accumulation rates was proposed by Goodwin (1991). These metrics were computed using the two different versions of the dataset, v0 and v3. However, the method proposed by Goodwin (1991) generates disproportionately high spatial variability values when dividing by mean accumulation with absolute values smaller than 1 cm, a commonly observed accumulation rate. Consequently, this measure is not suitable for analyzing spatial variability over short timescales with low accumulation rates.
Spatial variability can be computed for the accumulation values per stake, $a_{v0,i}$, or for the deviations of the individual stakes from the 'virtual' mean snow surface of the accumulation period. These are often very similar, as the standard deviation is calculated either with or without subtracting the mean of all 16 stakes. Since the mean represents a constant offset, subtracting it does not affect the spread of the data around the mean. The standard deviation, by definition, measures the variability of the data points relative to their mean, so centering the data by subtracting the mean simply removes any constant offset but does not change the overall variability.
Exemplarily, spatial standard deviation values computed with v3 appear to increase with the number of measurements. As shown in Figure 2.7, until 2010, the majority of values (green dots) fall within the range of 0.0 to 0.5 cm/day. Following the shift from monthly to bi-weekly measurements in 2009/2010, the values range between 0.0 and 0.75 cm/day. In 2010, which had the highest number of measurements, the data exhibited a greater spread than in other years. Consequently, spatial standard deviation computed from v3 cannot be used to reliably assess trends over time.

Instead, the spatial standard deviation is calculated for each individual measurement, without transitioning from v0 to v3. This approach offers valuable insights into the surface roughness of the snow, though it is sampled irregularly in time. However, comparing these values is challenging, as the interval between measurements affects the resulting spatial standard deviation.

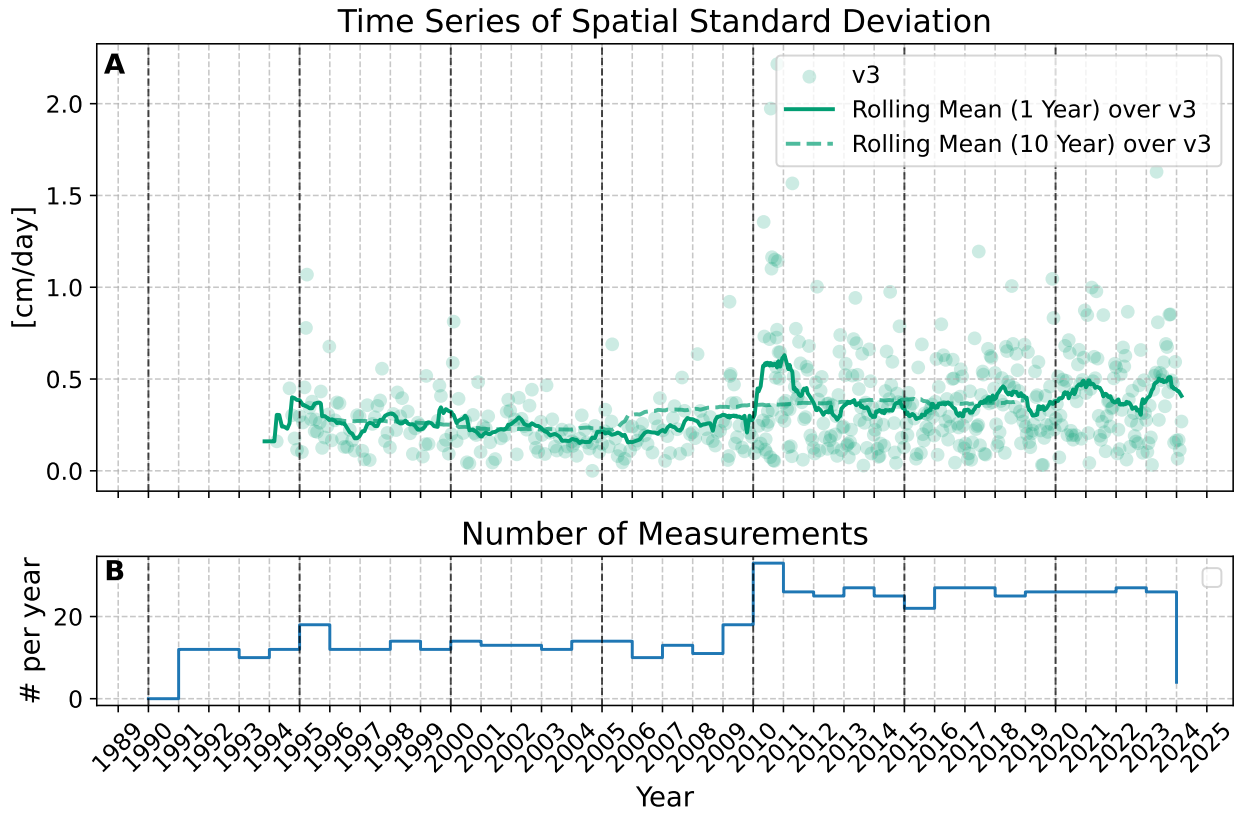

Fig. 2.7: A: Time series of the spatial standard deviation in cm/day from November 1994 to March 2024 at stake farm 'Süd'. Green scattered dots represent individual data points, while the green (dashed) line represents the rolling median over one (ten) year(s). B: Time series of the number of measurements per year.

2.3.3 Annual Snow Accumulation Trends and Variability

The long-term trend in snow accumulation is analyzed by de-trending the cumulative accumulation and examining the resulting residuals (i.e., the de-trended accumulation time series), along with the raw accumulation rates. The trend is estimated using ordinary least squares (OLS) regression. Cumulative accumulation is calculated by multiplying the monthly mean accumulation rates in cm/day by the number of days in each respective month, resulting in cumulative accumulation values expressed in cm. Accordingly, the residuals also have units of cm.

Ordinary Least Square Regression for Trend Removal

A linear regression is performed on the cumulative accumulation to remove the long-term trend from the data ('de-trending'). This is achieved by subtracting the climatological accumulation rate, defined over the period 1991-–2020, from the time series of accumulation rates, ensuring that both rates are defined over the same time interval.
The OLS method minimizes the sum of squared residuals ϵ, providing the best-fit line for the given data points. The regression model is described

$$y = \beta_0 + \beta_1 x + \epsilon$$

,
where y is the cumulative snow accumulation, x is time, β_0 is the intercept, β_1 is the slope coefficient, i.e. accumulation rates, and ϵ represents the error term.
The goal is to estimate the regression coefficients β_0 and β_1, which define the linear relationship between time and cumulative accumulation. The focus here is on understanding the relationship, not on predicting future accumulation. I acknowledge that this approach violates the following OLS assumptions: first, the variance of the residuals changes over time (heteroscedasticity), and second, the residuals are co-dependent, i.e. they are serially correlated, meaning they depend on the regressor 'time'. This correlation will be considered in further analysis. Specifically, the value of the residuals is dependent on previous values, but by analyzing the residual time series, this dependency becomes clearer and easier to interpret. Furthermore, the de-trending process acts as a low-pass filter by removing the climatological accumulation rate, which aids in frequency analysis.

Fitting Gaussian and Student-t Distributions to Histogram Data

The monthly mean accumulation rates were subset into a climate baseline (1991–2020) and recent years (2021, 2022, and 2023). Each dataset was subsequently utilized to generate histograms for visual inspection of the underlying distribution. A Gaussian function, defined as

$$G(x, \mu, \sigma) = A \exp\left(-\frac{(x-\mu)^2}{2\sigma^2}\right)$$

was fitted to the histogram data using the 'curve_fit' function from the SciPy library, which uses non-linear least squares to fit a function to the data. Initial parameter estimates for the mean μ and standard deviation σ were derived from the histogram data. The goodness of fit was assessed by calculating the sum of squares of residuals (SSR) and the total sum of squares (SST). The coefficient of determination R^2 was computed using the formula:

$$R^2 = 1 - \frac{\text{SSR}}{\text{SST}}.$$

A Student's t-distribution function was also fitted to the histogram data. The fitting process involved a similar approach to the Gaussian fitting.

Frequency Analysis

The objective of this analysis is to identify periodic patterns and dominant frequencies within the time series of the residuals and homogenized accumulation rates using a) the Fourier Transform and b) Wavelet Analysis.

Fourier Tansform

The Fourier transformation converts the time-domain residuals and accumulation rates into their frequency-domain components. This allows for the identification of dominant cycles or periodicities. Residuals and accumulation rates are transformed into the frequency domain using the Fast Fourier Transform (FFT) method, chosen for its computational efficiency in handling discrete time series, such as the monthly-resolved snow accumulation rates and residuals. The FFT returns the frequencies, amplitudes, and phases as complex numbers. The frequency calculated by the FFT indicates how often a certain component occurs in the time series per time unit (i.e., per month for a monthly resolved time series). The periods corresponding to each frequency component are calculated as the inverse of the frequency (periods = 1/frequencies), which is more interpretable in the context of periodic analysis. The amplitude indicates the strength or contribution of this frequency to the overall time series, with a high amplitude meaning that the corresponding frequency component plays a significant role. The phase indicates the shift of the sine or cosine wave relative to a reference time, which is less relevant if one is only interested in identifying predominant frequencies in the data.

Wavelet Analysis

Wavelet analysis provides a two-dimensional plot that represents the strength of variations as a function of both period and time. Unlike Fourier analysis, which characterizes the similarities between a time series and infinitely extending trigonometric functions, wavelet analysis focuses on similarities over specific segments of the time series, comparing them to waves of finite duration, known as wavelets (Wilks 2019). The Morlet wavelet is commonly used in geophysical applications due to its resemblance to patterns frequently observed in such datasets. It consists of a sinusoidal wave modulated by a Gaussian envelope that reduces its amplitude as the absolute value of its argument increases (Wilks 2019). For the wavelet analysis conducted here, I utilize the Python script provided by Torrence and Compo (1998). By default, the script uses a Morlet wavelet, where the wavelet basis is normalized to have a total energy of 1 across all scales (Figure 2.8).

The analysis applies to time series consisting of a) residuals and b) accumulation rates over a period of 33 years. In the first step, as described by Torrence and Compo (1998), the wavelet transform (the convolution of the wavelet with a vector `Y`) computes using the function:

```
wave, period, scale, coi =
    wavelet(Y, dt, dj=0.1, s0=2*dt, mother='MORLET', param=6)
```

In this context, `Y` represents the time series of residuals (accumulation rates) with monthly resolution (`dt=1`). In wavelet analysis, the scale controls the wavelet's width, determining the time window over which it detects variations. The parameter `dj` sets the spacing between discrete scales, with smaller values providing finer scale resolution. A smaller scale corresponds to a more compressed wavelet, capturing short-term fluctuations, while larger scales detect longer oscillations. The parameter `s0`

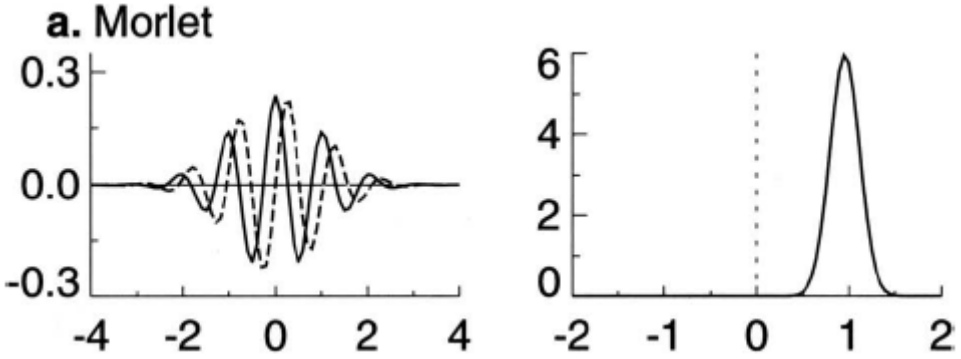

Fig. 2.8: From Torrence and Compo (1998): The plot on the left shows the real part (solid line) and the imaginary part (dashed line) of the Morlet wavelet in the time domain. The plot on the right shows the corresponding wavelets in the frequency domain. For plotting purposes, the scale is chosen to be $s = 10\delta t$.

sets the smallest scale, starting here at `s0 = 2*dt = 2` months, meaning the shortest resolvable period is two months. The mother wavelet chosen is the Morlet wavelet with a non-dimensional wavenumber $k_0 = 6$ (specified by `param=6`), which is a common default for Morlet wavelets.
The output variables are `wave`, `period`, `scale`, and `coi`. The variable `wave` represents the wavelet transform of `Y` and is an array of complex numbers. The wavelet power spectrum is obtained by squaring the absolute values of these complex numbers (`abs(wave)`^{2}), with units of σ^2 (the variance of the time series). The variable `period` provides a vector of periods (in time units) corresponding to the scales returned in `scale`. The `coi` (Cone of Influence) identifies the regions where edge effects may influence the results.
To determine whether certain features in the wavelet power spectrum are statistically significant, one needs to assess if they can be distinguished from an expected background noise spectrum, such as red noise or white noise. Red noise is characterized by higher power at low frequencies (large scales) compared to high frequencies (small scales). White noise is a random signal that contains equal intensity at different frequencies, resulting in a constant power spectral density across the entire frequency range. To establish the significance of oscillations in the wavelet power spectrum, a significance test is performed to reject the null hypothesis that these oscillations fall within the range of the expected background red (white) noise spectrum. The null hypothesis is defined based on the assumption that the time series has a mean power spectrum, which models as a red (white) noise spectrum. This assumption is evaluated later using Fourier analysis. If a peak in the wavelet power spectrum is significantly above this background spectrum, it can be considered a true feature at a 95% confidence level. To perform this significance test, the function `wave_signif` is used as follows:

```
# Assume white noise background by setting lag1 = 0.0,
# by default red noise background
signif = wave_signif(Y, dt=dt, scale=scale, mother='MORLET')
```

where `Y`, `dt`, and `scale` are the parameters from the previous function call. The output `signif` returns

the periods where the null hypothesis can be rejected at a 95% confidence level.

Interannual Variability

The aim of this analysis is to evaluate the interannual variability in snow accumulation based on annual accumulation rates. This approach provides insights into how individual years deviate from long-term trends and helps assess changes in the frequency and magnitude of positive and negative anomalies. By examining the standard deviation of annual accumulation rates, we can quantify the spread of data points within individual years.
First, the annual accumulation rates $a_{\sum}$ are calculated for each year in the dataset. For each year, the mean annual accumulation rate $\langle a_{\sum} \rangle$ over the entire dataset is subtracted from the annual rates $\sum$. This deviation represents how much each year's accumulation differs from the long-term average. The absolute value of these deviations reflects the magnitude of annual anomalies, while the sign indicates whether the anomaly is positive or negative. Interannual variability is then quantified as the standard deviation of these annual anomalies.

2.3.4 Seasonal Snow Accumulation Trends and Variability

This analysis aims to examine seasonal snow accumulation trends over the years, identifying anomalies and shifts in seasonal patterns. To focus on seasonal variations, the time series of accumulation rates, $\dot{a}$, is divided into southern hemisphere seasonal groups: Summer (December, January, February), Autumn (March, April, May), Winter (June, July, August), and Spring (September, October, November). Given that December is included in the summer season, the dataset is adjusted by shifting the December measurement to align with the following January and February. Due to autocorrelation, residuals from OLS regression are not used in this analysis.
The number of measurements per season is generally equal, with the exception of 2010, when Winter was sampled 11 times, Spring 12 times, Summer 3 times, and Autumn 6 times.
Initially, the analysis determines each season's contribution to the annual accumulation and assesses potential shifts in these contributions over the 33-year period. Monthly mean accumulation rates $\dot{a}$ are grouped by season and averaged to yield seasonal accumulation rates in cm/day ($\dot{a}_{summer}$, $\dot{a}_{autumn}$, $\dot{a}_{winter}$, $\dot{a}_{spring}$). It is important to note that $\dot{a}_{summer}$ is calculated using the accumulation rates from January and February of a given year, along with December's accumulation rate from the previous year. Additionally, annual averaged accumulation rates $\langle \dot{a}_* \rangle_{annual}$ are computed to include the previous December's accumulation, ensuring that the annual average encompasses all four seasons. The star notation indicates this adjustment.
Interannual variability is removed by subtracting $\langle \dot{a}_* \rangle_{annual}$ from each seasonal rate ($\dot{a}_{summer}$, $\dot{a}_{autumn}$, $\dot{a}_{winter}$, $\dot{a}_{spring}$).
Next, the analysis investigates whether specific seasons dominate accumulation patterns. Cumulative accumulation for each seasonal subset is computed. A regression analysis similar to that conducted for annual cumulative accumulation (2.3.3) yields climatologically balanced accumulation rates per season and year (expressed in cm/(3 months)). Additionally, deviations from the climatological mean for each season are analyzed by computing residuals from the climatologically

balanced accumulation.
Finally, these results will be visualized to facilitate interpretation and understanding of the trends and variability on a seasonal and monthly scale.

3 RESULTS

In this chapter, I present the findings of my analysis of snow accumulation variability and trends. Section 3.1 explores spatial variability in snow accumulation at the stake farm. In Section 3.2, I examine temporal trends and variability, beginning with an analysis of the long-term development of snow accumulation in Subsection 3.2.1. This subsection includes an overview of monthly and annual accumulation rates, their distributions, long-term trends derived from ordinary least squares regression, frequency analysis, and interannual variability. Subsection 3.2.2 narrows the focus to seasonal accumulation, discussing seasonal contributions to annual totals, distributions of seasonal accumulation rates, cumulative seasonal accumulation, and monthly-scale fluctuations within seasons. Finally, in Subsection 3.2.3, extreme accumulation events are identified.

3.1 Spatial Variability

The temporal evolution of spatial variability in snow accumulation is examined by analyzing the standard deviation across the stakes of the stake farm. A notable feature in this time series, shown in Figure 3.1, is the increased measurement frequency of spatial standard deviation beginning in 2010. Comparing subplot A with subplot B, the applied quality control removed 3 out of the 4 visually significant peaks from the time series. The peak, observed in 02-2008, was determined to be physical, suggesting that a spatial standard deviation of 18 cm$/\Delta t$ may serve as a reasonable threshold. Values exceeding this threshold could warrant further investigation into the quality of individual stake readings.
No discernible trend is evident in the standard deviation time series, indicating that surface roughness has remained relatively stable over the observation period. The Coefficient of Variation (CV), defined as $\frac{\langle \tilde{\sigma}_{\dot{a}_{v0}} \rangle}{\langle \dot{a}_{v0} \rangle}$, is 1.04, reflecting significant spatial variability within the stake farm throughout the measurement period.

Figure 3.2 displays the distribution of spatial standard deviation of snow accumulation measured within the stake farm. The distribution is skewed to the right, with a concentration of values between 0 and 10 cm$/\Delta t$. The distribution's skewness suggests that there are rare but significant deviations from the average surface roughness, represented by the right tail of the histogram. The most frequent standard deviation values fall between 2.5 and 7.5 cm$/\Delta t$, with a peak frequency around 5 cm$/\Delta t$. The mean standard deviation is 5.54 cm$/\Delta t$, and the standard deviation of the data (the standard deviations) itself is 3.17 cm$/\Delta t$, suggesting a substantial spread around the mean but with a predominant clustering in the lower range of values. The lack of a discernible trend in the overall

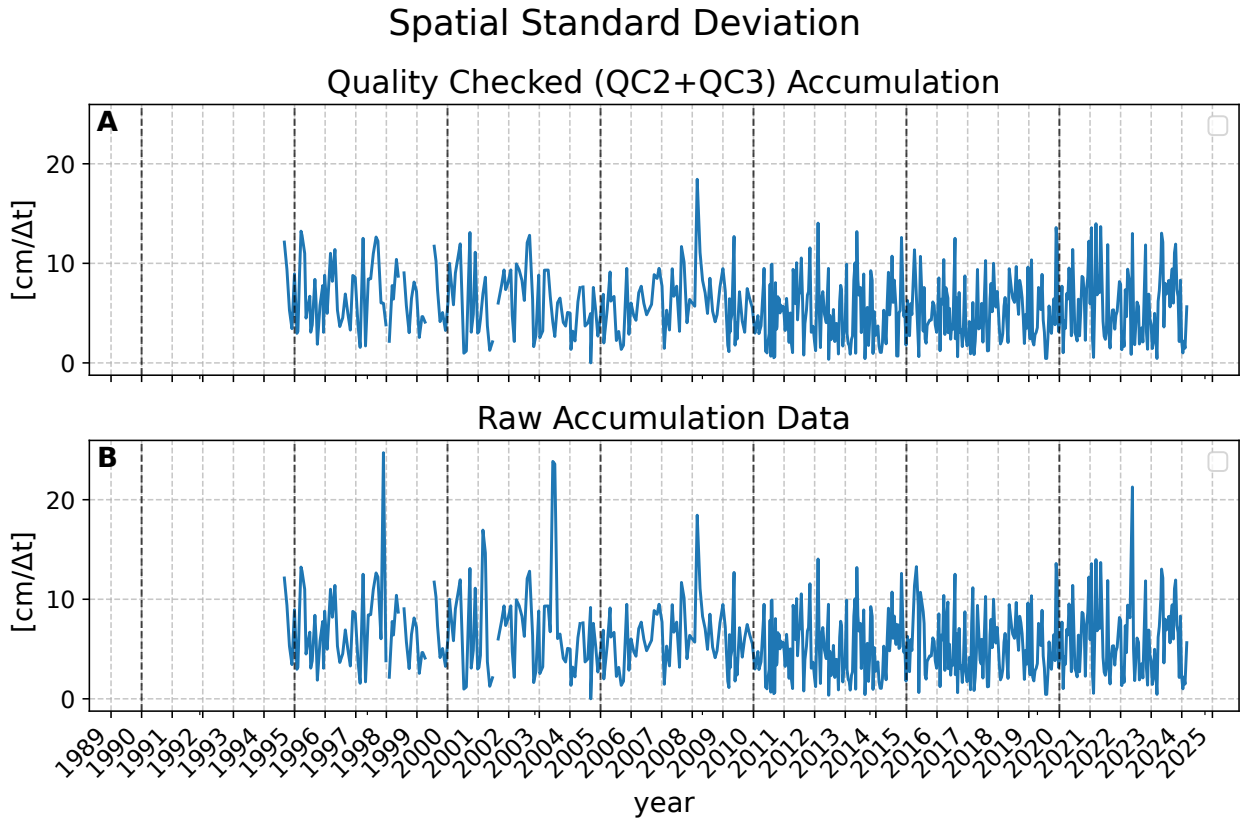

Fig. 3.1: Time series of the spatial standard deviation of the stake farm in cm$/\Delta t$ for the whole measurement period (individual stake measurements were recorded from 1994 onwards). In (A) QC-flagged stake measurements were discarded, in (B) retained.

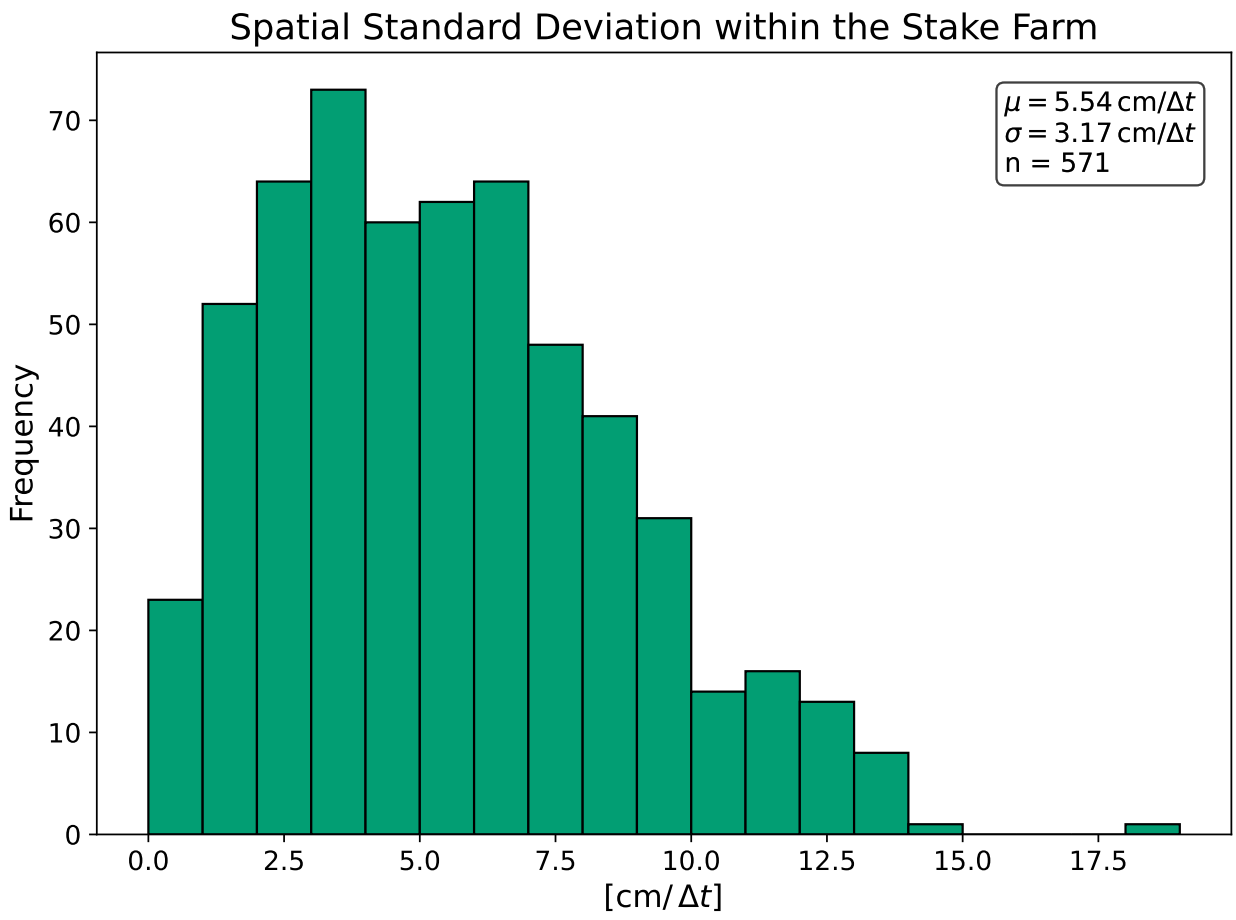

Fig. 3.2: Histogram of spatial standard deviation measured within the stake farm at 'Süd' in cm$/\Delta t$ for all measurements in the period 09-1994–03-2024

time series, paired with this distribution, suggests that the surface roughness (as expressed by the spatial standard deviation) remains largely stable, although there are occasional spikes in variability.

3.2 Temporal Snow Accumulation Trends and Variability

All results below refer to data version v3 as outlined in Chapter 2

Although the unit cm/day might imply daily snow accumulation, precipitation at NM can also occur through discrete events on specific days rather than as a continuous process. Additionally, the analysis is not based on daily measurements but on data collected once or twice per month. To ensure comparability, we introduced above the preprocessed data v3 in cm/day, which homogenizes the data. This homogenization tends to smooth out high accumulation values when measurement intervals exceed one month. When measurements are taken early in the month, the accumulation may actually reflect snowfall from the preceding month, leading to both smoothing and a 'backward' redistribution of accumulation in v3. This subsection provides an overview of the monthly and annual accumulation rates, their distributions, long-term trends obtained through ordinary least squares regression, as well as analyses of frequency patterns and interannual variability.

3.2.1 Long-Term Development

a) Time Series of Monthly Accumulation Rates

The temporal development of the accumulation rates for the total measurement period is displayed in Figure 3.3. The majority of the monthly averages scatter in a range from 0.0 to 0.75 cm/day. There is no obvious change over time. Mass loss ($\dot{a} < 0$) occurs seldomly, and more frequent are months with small-magnitude mass losses and rarely with major mass losses. In January 2011 mass loss has been strongest since the start of the measurements. More frequent positive accumulation rates ($\dot{a} > 0$) are observed with values up to 1.3 cm/day. The rolling mean computed over a window of one year reveals an interesting feature. Snow accumulation over time is characterized by several local minima and maxima, while it does not display a significant global minimum or maximum. The magnitudes of the maxima are of the same order, only a small positive trend with time is visible. The minima, in contrast, are less stable in magnitude, with an absolute minimum in 2003/04. There is a periodicity visible in these oscillations, which will later be analyzed in more detail.
A long-term change over the period 1996–2010 is not indicated by the ten-year rolling mean, which spans the period from 1996 until 2019. Accumulation rates center at a value of 0.26 cm per day (7.6 cm/month (30 days), 95 cm/year (365 days)).

b) Distribution of Monthly Accumulation Rates

The distribution of accumulation rates at 'Süd' for the climatological period 1991–2020 is shown in Figure 3.4, with additional contributions from the years 2021, 2022, and 2023. The histogram

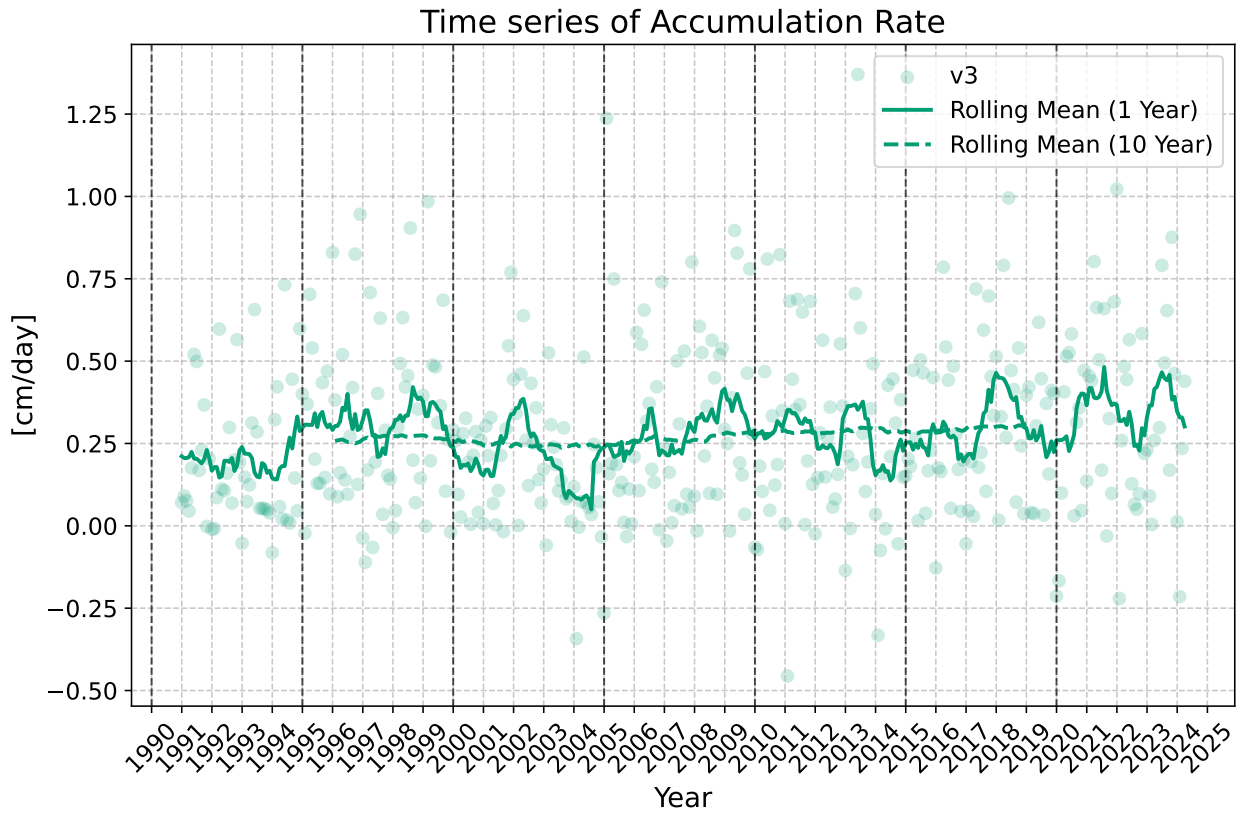

Fig. 3.3: Time series of the monthly averaged accumulation rate in cm/day as scattered dots. Every year has 12 dots representing monthly averaged accumulation rates. The (dashed) line is the running mean over one (ten) year(s).

illustrates the frequency of daily accumulation rates, alongside fitted Gaussian and Student-t distributions to the period 1991–2020. Gaussian fitting yields a mean accumulation rate $\hat{\mu} = 0.20$ cm/day and standard deviation $\hat{\sigma} = 0.22$ cm/day, and to the stacked histogram of all years (1991–2023), with $\hat{\mu} = 0.21$ cm/day and $\hat{\sigma} = 0.23$ cm/day. A Student-t distribution (red curve) was also fitted to the 1991–2020 data, with parameters $\hat{\mu} = 0.19$ cm/day, $\hat{\sigma} = 0.21$ cm/day. The fit quality by the coefficient of determination (R^2) is 0.89 for both the Gaussian and Student-t fits.

The majority of the accumulation rates are clustered in the minimal positive accumulation rates, roughly 0.5 to 1 $\sigma_{\langle \dot{a} \rangle_{clim}} = 0.25$ cm/day away from the mean value $\langle \dot{a} \rangle_{clim} = 0.28$ cm/day. The distribution is therefore skewed and unsymmetric. A gaussian fit is centered around 0.20 cm/day, with a standard deviation of 0.22 cm/day, similar to a fitted student-t distribution. Although the R^2 is quite high for both fits, we can conclude that accumulation rates are not a gaussian process, since it is clearly skewed. In detail, the histogram outline falls below the fitted distributions in the regime of net mass loss rates ($\dot{a} < 0$) and mostly above in the regime of net accumulation rates ($\dot{a} \geq 0$).

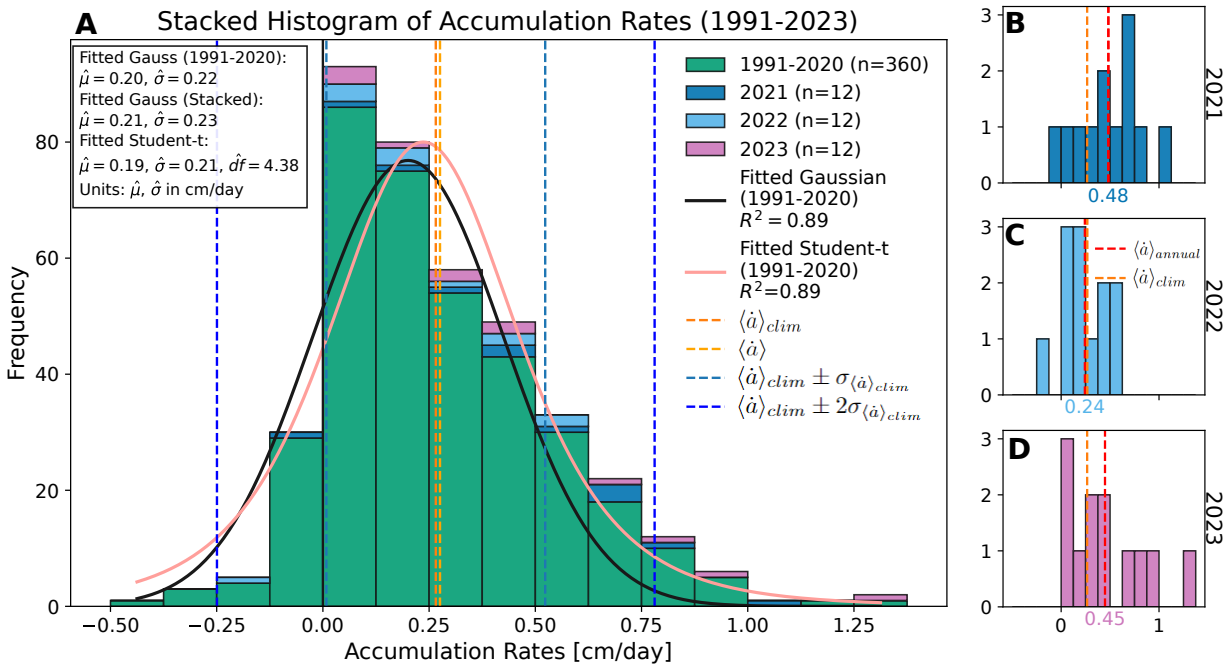

*Fig. 3.4: **A:** Stacked histogram of accumulation rates from 1991 to 2023 with green bars representing accumulation rates measured in the period 1991–2020, dark blue bars for 2021, light blue bars for 2022, and purple for 2023. Accumulation rates are given in cm/day. The dark orange line represents the average accumulation rate (1991–2020) $\langle \dot{a} \rangle_{clim}$, the lighter orange line the average over the entire period (including 2021–23) $\langle \dot{a} \rangle$. (Dark) Blue dashed vertical lines are $\langle \dot{a} \rangle_{clim} \pm (2)\sigma_{\langle \dot{a} \rangle_{clim}}$. The black and light red lines are the Gaussian and Student-t distributions fitted to the histogram with accumulation rates from 1991–2020. **B, C, D** show the histogram of the subsets 2021, 2022, and 2023 of accumulation rates in cm/day (and with frequency on the y-axis) and their annual mean $\langle \dot{a} \rangle_{annual}$ as a red dashed line. The orange dashed line represents $\langle \dot{a} \rangle_{clim}$ again.*

c) Distribution and Time Series of Annual Accumulation Rates

The annually summed accumulation is strictly positive, with a distinct minimum observed in 2004 (Figure 3.5 subplot A), which represents an anomalously low accumulation year, recording less than 25 cm of snow accumulation in total (see B in Figure 3.5), thus representing the lowest end member value. At the other extreme, 2021 and 2023 are marked by unprecedented high accumulation. The highest annual accumulation on record occurred in 2021, with 176.2 cm, followed by 2023 at 164.0 cm. Typically, annual accumulation ranges from 50 to 150 cm/year, with no discernible long-term trend apparent in the observed annual accumulation. However, 2021 and 2023 are exceptional, characterized by: a) an excess of 25 and 50 cm, respectively, relative to the highest annual accumulation of the previous 30 years, and b) an excess of 50 and 75 cm, respectively, compared to the climatological mean of 1 m per year.
Although the distribution of monthly accumulation rates is slightly skewed and therefore non-Gaussian, the distribution of annual accumulation rates, representing the sum of 12 monthly values, appears approximately Gaussian. Assuming annual accumulation rates follow a Gaussian distribution, the probability of observing values exceeding $\langle a_\Sigma \rangle_{clim} + 2\sigma_{\langle a_\Sigma \rangle_{clim}}$ for 2021 and 2023, based on the climatology of the preceding 30 years, would be approximately 2.3% each.
Interestingly, monthly accumulation rates of the last three years do not exceed maximal accumulation rates of the past climatology on the monthly basis —in contrast to the annual accumulation rates of 2021 and 2023, which both exceeded the climatological maximum. Yet, it can be stated that given the climatology it is rare that three months of a year show these high accumulation rates. This results in annual average accumulation rates of 2021 and 2023 (0.48 cm/day and 0.45 cm/day, respectively) to be almost double the annual average accumulation rate $\langle \dot{a} \rangle_{clim} = 0.28$.

d) Long-term Linear Trend

Over the entire measurement period, 33.41 m of snow has accumulated at 'Süd' (Figure 3.6). Climatologically regressed (by OLS), this results in 99.5 cm of accumulation per year or 0.27 cm per day. These values approximate the results from the previously presented averaged accumulation rates. The cumulative accumulation aligns closely with the climatological regression line. There are several periods where snow accumulation deviates from the climatological regression line, but in the long-term, it stays close to it. Only the last three years might indicate a change towards more accumulation.
In subplot B of Figure 3.6 the residuals from the climatological regression line on a monthly time scale are displayed. During the first 3 years of the measurement period, more snow accumulated than expected from the climatological regression line, followed by two years of less-than-average accumulation. A second local maximum is reached in 2000 (75 cm more than expected accumulated up to 2000). The following 5 years (2000–2005) are mostly characterized by a decrease in snow accumulation compared to the climatological regression line. This decrease introduces the absolute minimum in snow accumulation of the whole measurement period for the next 3 years (2005–2008), in which up to 1 m less than climatologically expected accumulated. Until 2014 snow accumulation gradually increases towards the climatological accumulation rate. After 4 years of below-average

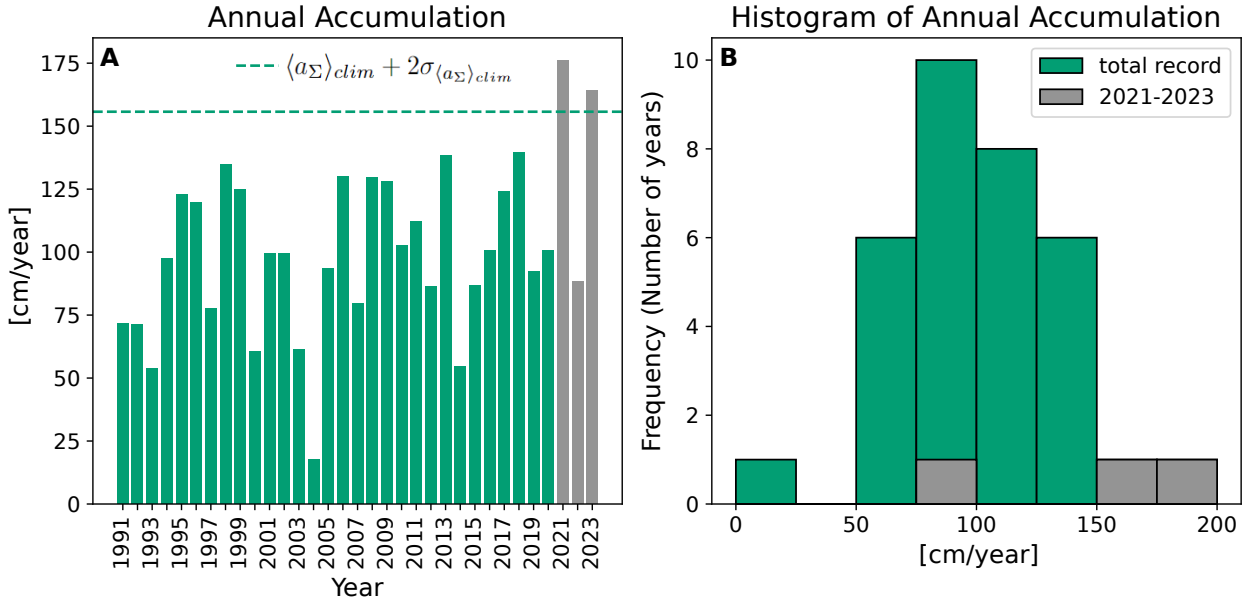

Fig. 3.5: A: Time series of the annually summed accumulation in cm at 'Süd' from 1991 until 2023. $\langle a_\Sigma \rangle_{clim} + 2\sigma_{\langle a_\Sigma \rangle_{clim}}$ *have been computed with the annual sums from 1991 until 2020. B: Histogram of the annual accumulation in cm at 'Süd' from 1991 until 2023.*

snow accumulation, the accumulation rate has risen to its absolute maximum in 2024. 150 cm more snow has accumulated than climatologically expected.

Several periodicities can be identified. From the first local minimum in 1995 to the next in 2005 it took 10 years, followed by 3 years of an absolute minimum. From 2008 to the next local minimum in 2018 it took again 10 years. A second periodicity seems close to 3.5 years. This will be further analyzed in section 3.2.1.

Smoothing intra-annual and short-term inter-annual variability, Figure 3.7 illustrates the 5-year rolling mean and median of the residuals' time series. The variability can be deduced from the shaded quartiles' range (IQR), while the curve is truncated for the first and last 2.5 years to avoid misinterpretation. The scatter points indicate that accumulation during these periods is strongly positive, with the snow surface rising up to 150 cm above the expected surface based on climatological accumulation rates. In this context, 'below-average' and 'above-average' refer to deviations from the climatological accumulation rate derived from the OLS trend, which serves as a baseline for comparison.

The slope of the curve provides key information: negative (positive) slopes indicate phases of below-average (above-average) snow accumulation rates, highlighted in red (green). Periods with nearly zero slopes, highlighted in blue, represent phases of near-climatological accumulation rates.

The first noticeable increase in the mean and median values starting around 1996 suggests a shift towards increased snow accumulation until 1999/2000 when accumulation rates return to climatological averages. Variability is low during the above-average accumulation phase, increasing when rates return to average. A phase of below-average accumulation, accompanied by high variability, occurs between 2001 and 2006. During this period, the cumulative accumulation drops by up to 1 m

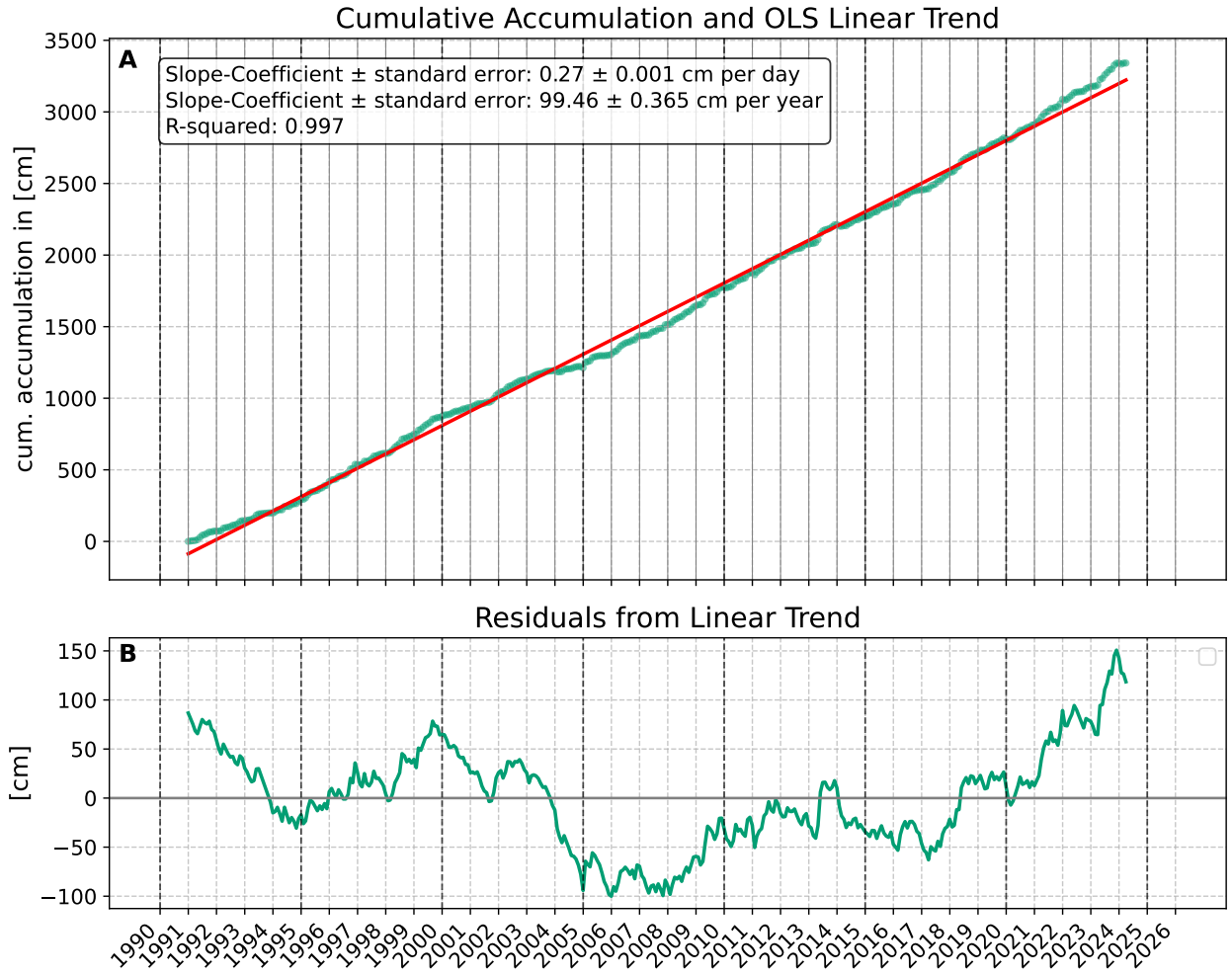

Fig. 3.6: A: Time series of the cumulative accumulation in cm at 'Süd' from 1991 until 2024 as green dots. The red line is the OLS linear regression. B: Time series of the residuals (green dots minus red line) in cm.

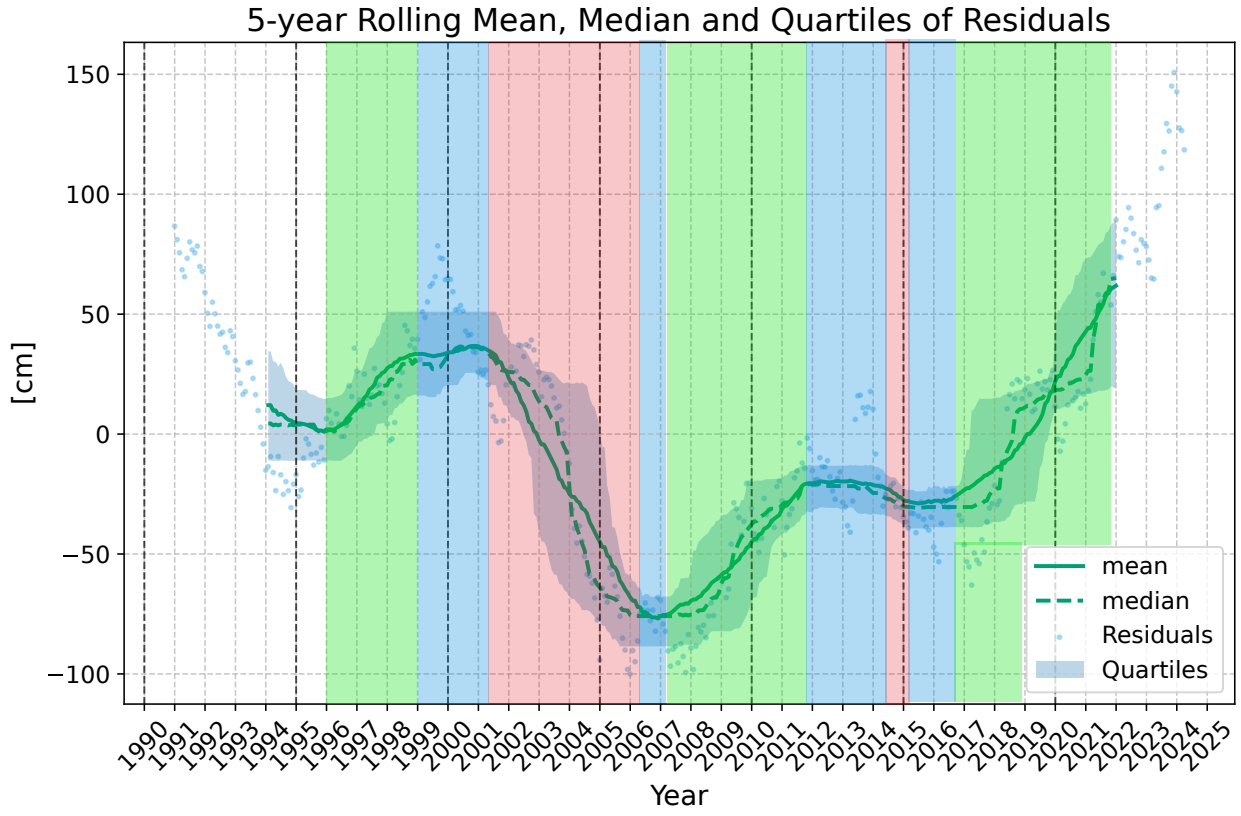

Fig. 3.7: Time series of residuals in cm (blue dots), the 5-year running mean (median) is depicted as a green (dashed) line. The blue-shaded area around the time series illustrates the range between the first and third quartile at 'Süd' 1991–2024. Phases of below-average (above-average) snow accumulation rates are highlighted in red (green). Blue highlighted periods represent phases of near-climatological accumulation rates. The curve is truncated for the first and last 2.5 years to avoid misinterpretation.

below the climatological (see Figure 3.6 B). Variability narrows as the minimum is approached, indicating reduced inter- and intra-annual fluctuations in this near-climatological phase. The following 5 years (2007–2012) are characterized by above-average accumulation with moderate variability. Afterward, a 5-year phase of near-climatological accumulation followed, interrupted by a single year of below-average accumulation in 2014. Variability during this period is especially low and stable. From 2017 onwards, accumulation rates are continuously above climatological averages with regard to the running mean, accompanied by increased variability. The running median indicates a weaker slope of above-average accumulation rates, as it gives less weight to the very high accumulation rates in 2021 but to the near-climatological accumulation rates in 2019, 2020, and 2022. The IQR narrows during this period. The analysis of the three above-average accumulation periods further reveals that the duration of these periods has increased. The first period spans 3 years, the second 5 years, and the most recent period, based on extrapolation of the rolling mean to the present day, suggests an ongoing above-average accumulation lasting for 7 years. Additionally, the slope of the current above-average period is steeper than in the previous two periods, indicating that the rate at which accumulation increases, and thus deviates from the average (climatological) accumulation, has accelerated compared to the earlier periods.

e) Spectral Characteristics of Time Series

The time series of accumulation rates and residuals both indicate temporal periodicities. In the following, these periodicities will be analyzed with the help of Fourier-Transformation and Wavelet-Analysis.

Fourier-Analysis:

Given the available dataset of 400 months, the maximum interpretable period has a length of 100 months. This is based on the criterion that at least four data points are needed to accurately represent a wave and its amplitude. Periods longer than 100 months may not be reliable, as the dataset lacks sufficient length to support them. Therefore, amplitudes corresponding to lower frequencies (higher periods) beyond 100 months should be interpreted with caution. Figure 3.8 shows the amplitude of the residuals' Fourier-transformed values across periodicities of 3.3 months to 100 months. In general, one can observe that more power lies in the low frequencies decreases as 1/f. Therefore, the time series can be categorized into the red-noise-spectrum. Peaks in the plot indicate dominant frequencies or periodicities in the residuals, with a maximum at a periodicity of 40 months (3.3 years). This finding underscores the observations from the rolling mean analysis. There is also a peak at 12–15 months, which suggests the presence of a nearly intra-annual cycle.

Analyzing the monthly average accumulation rates (Figure 3.9) in contrast yields different aspects of periodicities in the accumulation time series. The spectrum is more evenly distributed, depicting a white noise spectrum. Here maximal amplitude is found for a period of 6 months, followed by a second maximum with a period of 12 months suggesting an intra-annual cycle.

The Fourier transform of the residuals, which represent the accumulation data after removing the mean accumulation rate, reveals different characteristics compared to the raw accumulation data. By detrending the time series, the dominant periodicities on shorter, intra-annual timescales are

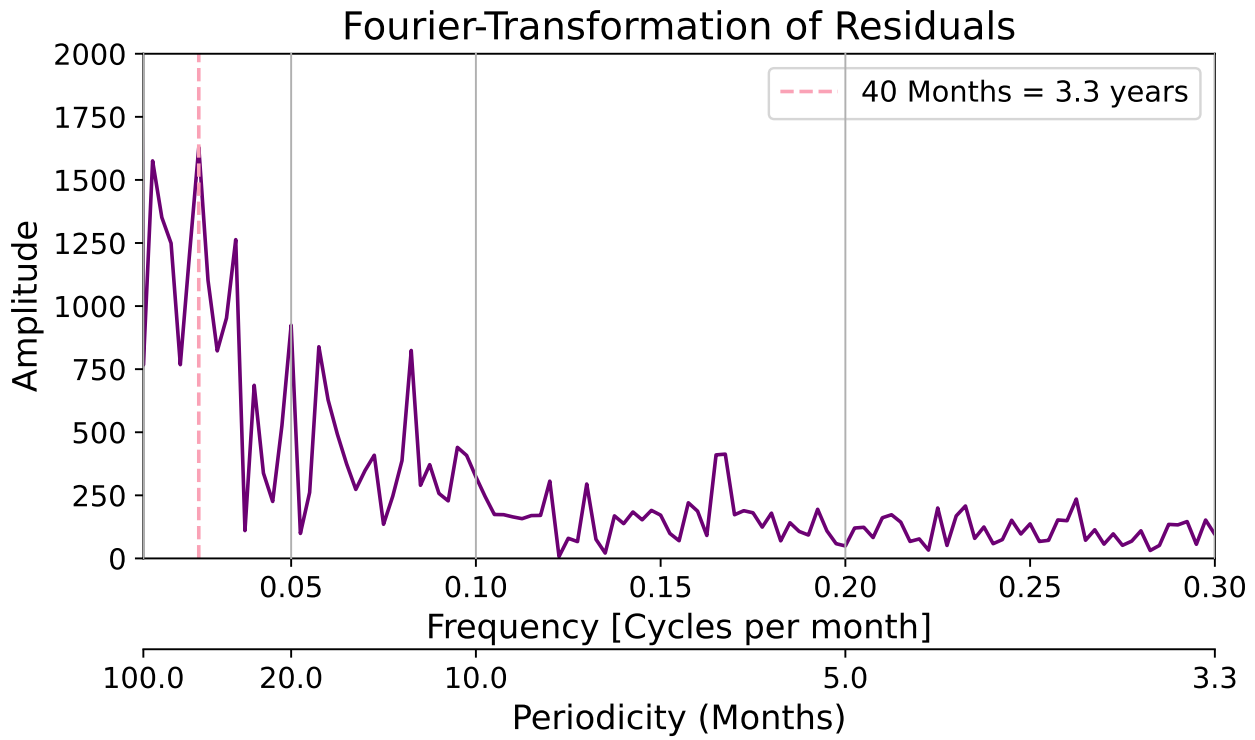

Fig. 3.8: Fourier-transformed residuals of monthly averages ('Süd', 1991–2024) for the periodicity below 100 months. Maximum amplitude is found at $x = 40$ months (red dashed line).

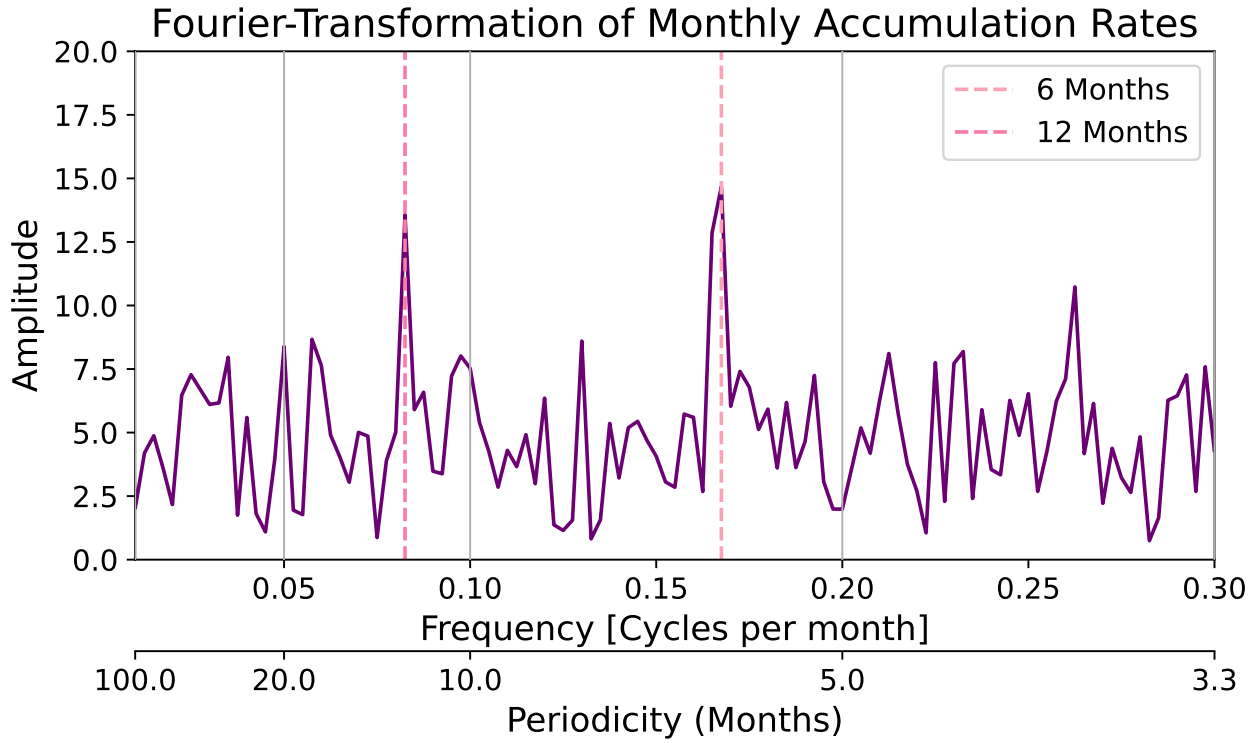

Fig. 3.9: As for Figure 3.8 but for monthly average accumulation rates [cm/day]

diminished, as they are primarily captured by the removed climatological mean. This is evident in the residuals' power spectrum, where lower frequencies corresponding to longer-term variability (e.g., 40-month cycles) become more pronounced, while shorter periods, such as monthly cycles, are less prominent. In contrast, the Fourier spectrum of the raw accumulation data reflects a more evenly distributed white noise pattern, where the energy is more uniformly spread across frequencies. This indicates that the raw accumulation rates retain significant intra-annual variability.

Wavelet Analysis:

Using a Morlet mother wave, Figure 3.10 B illustrates the similarities of this mother wave with different periodicities (y-axis) to the time series of the residuals over time (subplot A). The power of the wavelet transform is color-coded, with a lighter hue representing strong periodic components. For the 95% confidence level (blue contour), a background power spectrum equivalent to a Fourier red noise spectrum is assumed. The edge effects are represented by the Cone of Influence (COI, grey hatched area in Figure 3.10), and results outside this region should be interpreted with caution. Since we know from the Fourier analysis that more power lies in the low-frequency regime, it is obvious that the colors will become lighter towards this low-frequency / long-periodicity regime. Still, areas of interest are those, where lighter colors are surrounded by darker colors. With the help of the blue contour, we can additionally apply statistical significance, where periodicities significantly differ from the background spectrum.

Wavelet analysis of the residuals over a period from 1992 to 2024 reveals that the most significant periodic feature is again the 40-month cycle. The analysis is statistically robust within the 95% confidence niveau. Yet, this feature is not significant or present throughout the entire time. The signal ceases from 2008–2018, afterwards the power in this frequency area increases again. During the time, where the 40-month cycle is weak, shorter cycles with periodicities of 20–30 months become more dominant (lighter area starting 2012 with a periodicity of approx. 28 months). This lighter area shifts with time slightly towards the dominant 30–40 months regime.

The intra-annual cycle of approximately 12 months strengthens and becomes more continuous from 2010 onward. Prior to 2010, intra-annual cycles were infrequent and typically short-lived, occurring for no more than 2–3 consecutive years (24–36 months).

The long periodicities of 100 months (8 years and longer) have a high power, however, the time series only provides a short window where a mother wave with an extent of $>$ 100 months is unperturbed by edge effects. The observations from the time series visually suggest a periodicity of roughly 9–10 years (108–120 months), yet a longer measurement period is needed to confirm this indication.

The wavelet analysis of the accumulation rates reveals also significant periodicities throughout the time series (Figure 3.11 B). As for the residuals, a prominent 40-month cycle emerges as a strong feature, particularly between 1998 and 2006. The power of this cycle diminishes afterward. With intermittent significance from 2018 onwards a periodic signal on a slightly shorter timescale of 30–35 months emerges. This recurring pattern aligns with findings from the residuals' wavelet analysis, underscoring its persistence across the different methods.

Shorter periodicities between 10 to 20 months also become evident. The intra-annual 12-month cycle is often present throughout the measurement period, especially from 2010 onwards, where it appears with greater intensity and continuity.

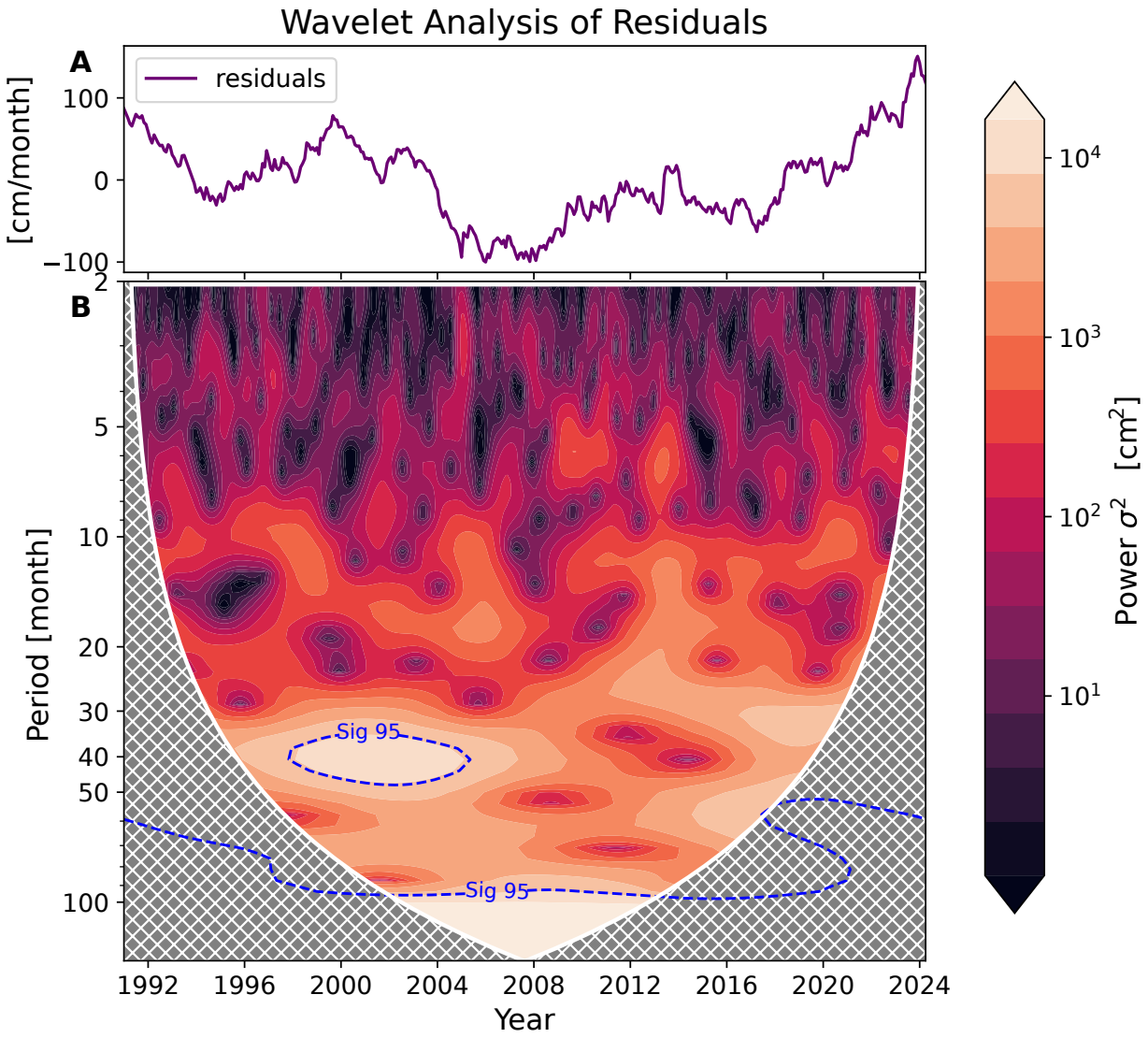

Fig. 3.10: A: Time series of residuals in cm ('Süd', 1991–2024). B: Wavelet Analysis of Residuals with the power signal color coded in units of σ^2 (cm^2). Dashed blue contour lines enclose areas, where the power surpasses a background red noise Fourier spectrum at a significance niveau of 95%. The grey hashed area depicts the cone of influence

Between 2008 and 2016, cycles with periodicities of 6 months also emerge as significant, although they also occur less significant and less continously before 2008.
Finally, periodicities exceeding 50 months (4 years and beyond), show significant power, particularly at the beginning and end of the time series. However, due to the limited data length and the presence of edge effects, the significance of these long-term cycles should be interpreted with caution. Nonetheless, the observation hints at potential long-term trends or cycles that may require a longer dataset for further verification.

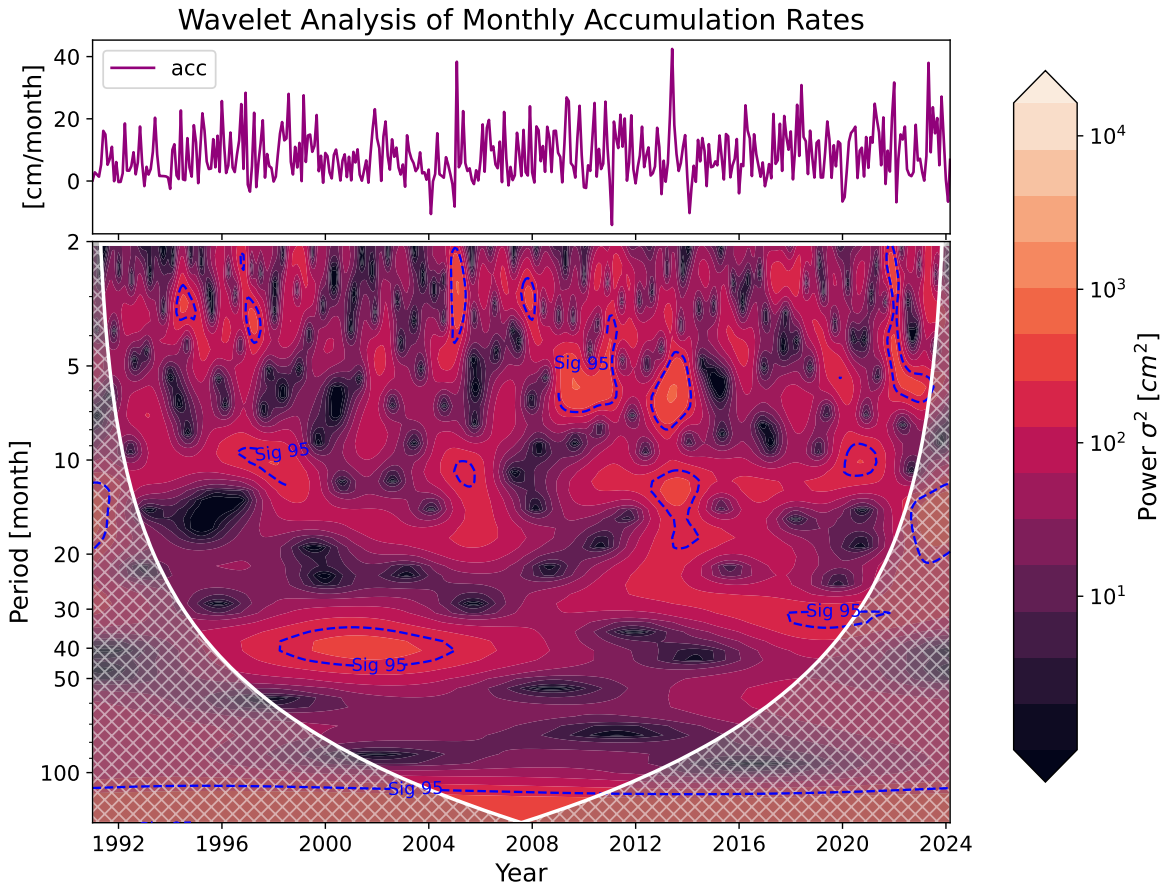

Fig. 3.11: As for Figure 3.10 but for monthly accumulation rates

f) Interannual Variability

For the analysis of interannual variability, we apply three measures: 1. interannual variability (as the standard deviation of annual accumulation rate anomalies $\overline{a}_{\sum} - a_{\sum}$), 2. the temporal standard deviation across monthly accumulation rates of a year, and 3. the absolute difference between two consecutive annual accumulation sums.
Figures 3.12 and Figure 3.13 characterize interannual variability. Subplot A of Figure 3.12 shows the

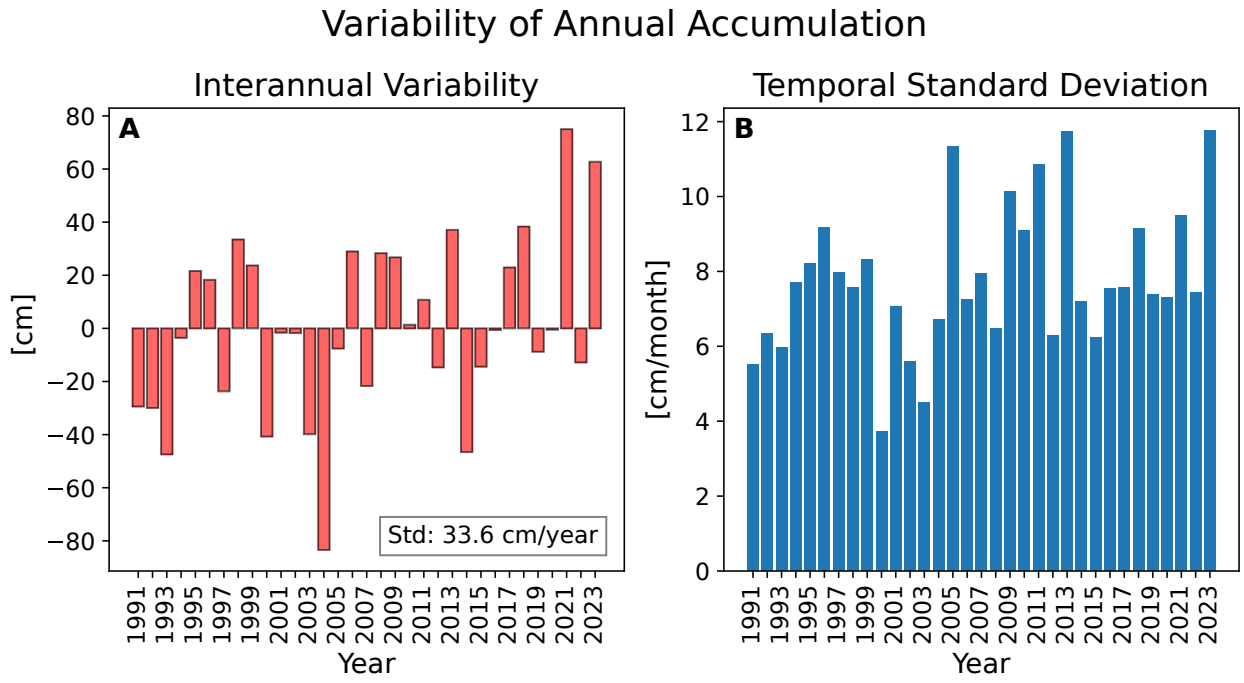

Fig. 3.12: A: Time series of annual accumulation anomalies of the accumulation in cm at 'Süd', 1991–2024. B: As for A but for the annual temporal standard deviation of the monthly accumulation rates within the year $\sigma_{\langle a \rangle_{annual}}$.

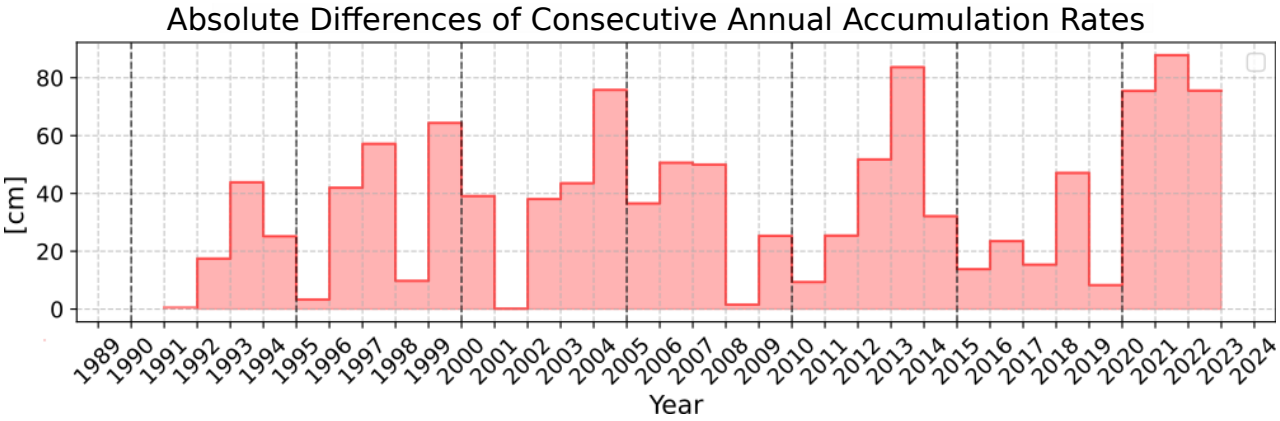

Fig. 3.13: The absolute difference in annual sums between consecutive years in cm.

fluctuation of annual accumulation rates a_Σ around the average annual accumulation rate $\langle a_\Sigma \rangle$. Positive values indicate years above average accumulation, while negative values indicate years with lower than average accumulation. The anomalies range from –80 cm to 80 cm, indicating substantial deviations from the annual mean of 1 m/year. Especially in the second half of the measurement period, the sign of the anomaly changes latest after 2 years, suggesting strong year-to-year fluctuations. Positive anomalies become more frequent over time, additionally their magnitude increases. Negative anomalies are more frequent during the first half of the measurement period. While their frequency decreases over time, their magnitude does not significantly reduce, except for the most recent years where negative anomalies show smaller amplitudes. The last four to six years are characterized by especially high interannual variability: firstly, the sign changes each year, secondly, the difference to the previous year has never been this high before (Figure 3.13). With a mean annual accumulation rate of 99.5 cm/year and a standard deviation of 33.6 cm/year, the interannual variability is considerably high, as the standard deviation accounts for approximately one-third of the annual accumulation rates.
The annual temporal standard deviation measures the variability of accumulation within the individual years. This quantity does not suggest a change over time (see subplot B of Figure 3.12). Furthermore, values vary between 4 and 12 cm between the years, such that the inter-annual change is rather small. Changes in the temporal annual standard deviation can nevertheless be very influential, as the annual standard deviation is often of the same order of magnitude as the mean.

3.2.2 Snow Accumulation at the Seasonal Scale

The following analysis aims to delve deeper by focusing on the seasonal scale. Residuals cannot be used for this analysis, as artifacts resulting from their cumulative nature would influence the results. I, therefore, focus on the analysis of monthly accumulation rates.

Seasonal contributions to the Annual Total

Figure 3.14 illustrates the seasonal differences in accumulation rates from the annual average over the period from 1991 to 2023. Summer accumulation rates are predominantly below the annual average, often correlated to autumn rates being above the annual average. Over time, negative summer anomalies have become more frequent and exhibit greater magnitudes, while positive anomalies in autumn have also increased in frequency and magnitude. In contrast to summer and autumn, which suggest a regular and stable contribution to annual accumulation (summer contributes the least and autumn the most), the contributions from winter and spring vary a lot across the years. The magnitude of contributions from winter and spring are rather close to the annual average. There is no tendency towards becoming a positive or negative anomaly or increase in magnitude. Furthermore, they do not show any correlation to the interannual course of one of the other seasons. Winter contributions can be correlated to autumn contributions from 1996–2000 and anti-correlated from 2005–2010. Spring contributions do not seem to show any (anti-)correlation to any season over years to multi-year cycles. Spring contributions can sporadically be large both in the positive and negative direction. We can deduce that usually the difference in accumulation from one season to

the next within a year is largest from the summer season to the autumn season.

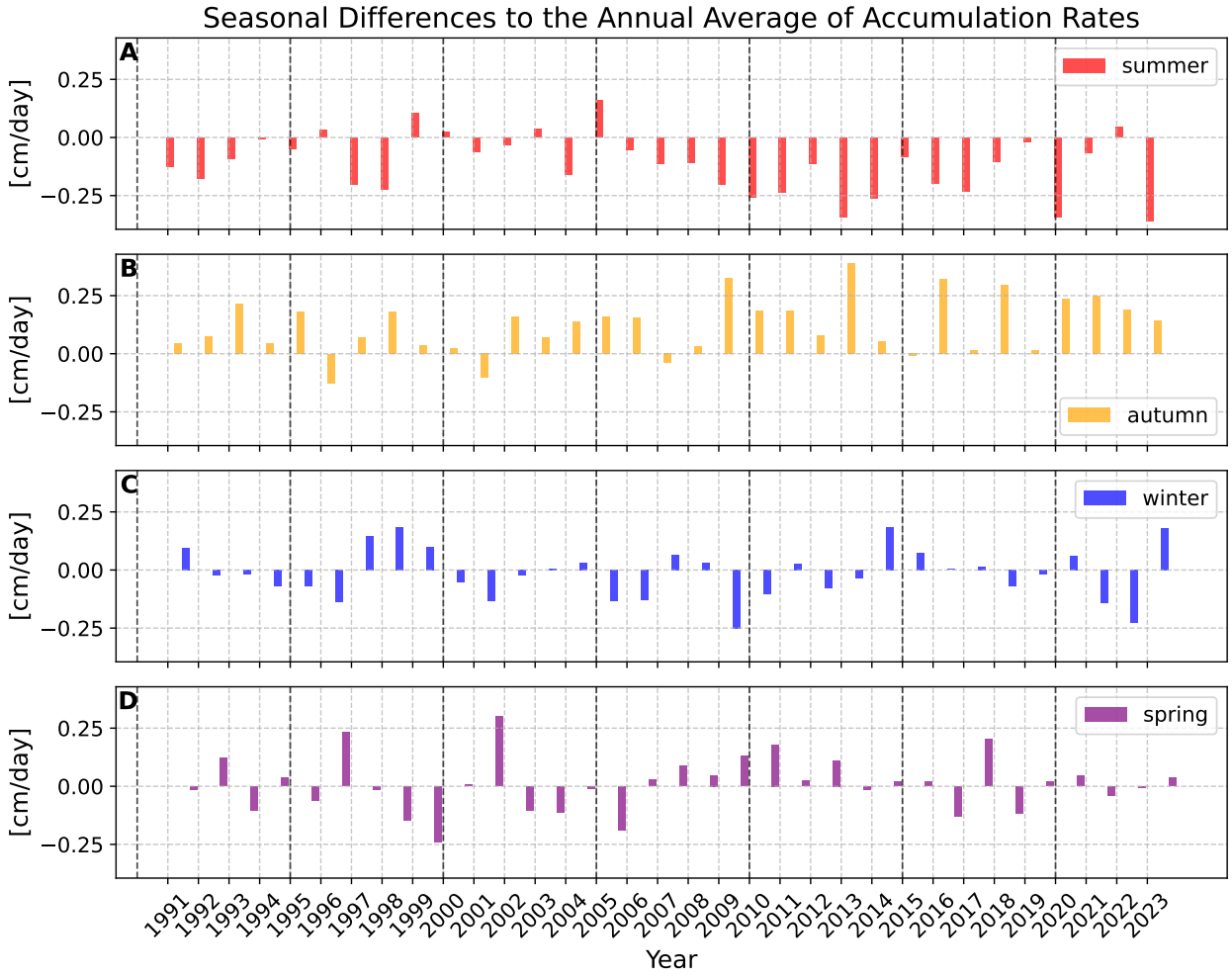

Fig. 3.14: Time series of the differences from seasonally averaged accumulation rates to annually averaged accumulation rates ('Süd', 1991–2023) for (A) summer (DJF), (B) autumn (MAM), (C) winter (JJA), and (D) spring (SON).

Figure 3.15 presents the 5-year rolling mean of the seasonal deviations from the annual mean accumulation rate, observed from 1993 to 2022 (it is truncated for the first and last two years because of the edge effects of a 5-year rolling mean). Again, the most striking feature is an inverse relationship between autumn and summer accumulation rates, which we already have seen in Figure 3.14. A trend in their dynamics can be deduced: As the system increasingly shifts towards an autumn-dominated state, the contribution from summer diminishes correspondingly. In contrast, winter and spring accumulation rates are consistently closer together, each frequently contributing their 'quarter' of the total accumulation. During the first half of the measurement period, up to approximately 2007, all four seasonal contributions are relatively close to each other. This proximity suggests a less distinct seasonal cycle, where the differences between the seasonal contributions are minor. From 2007 onwards, the divergence between autumn and summer becomes more pronounced, while winter and spring remain relatively unchanged. A seasonal cycle emerges in this period. The

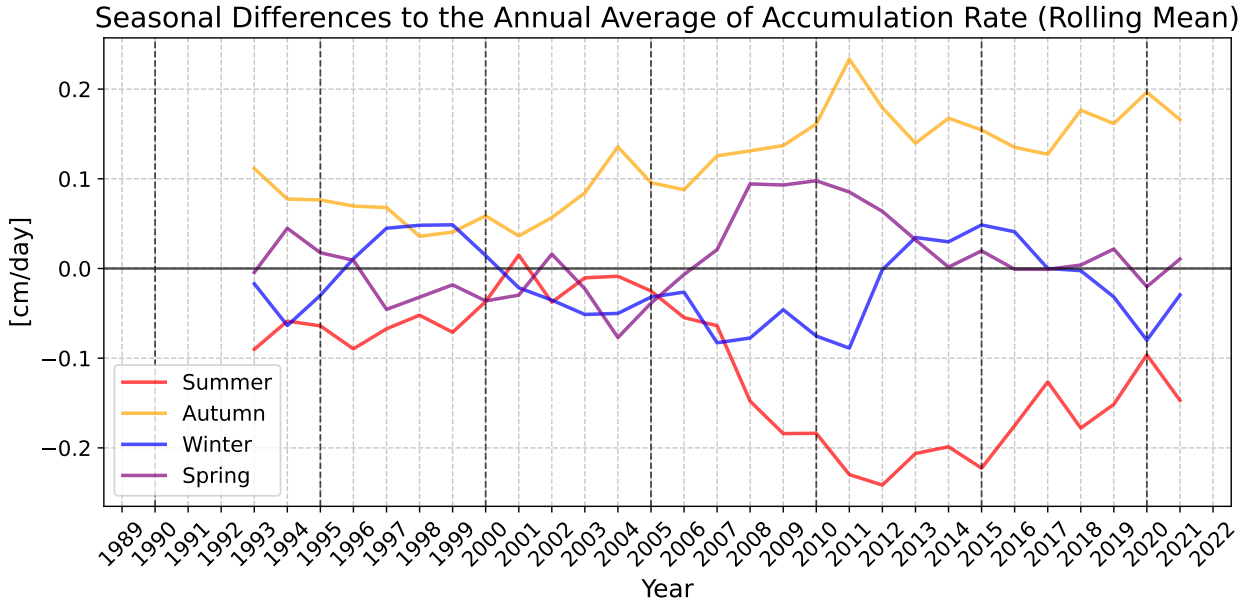

Fig. 3.15: As for 3.14 but computed with 5-year running mean.

wavelet analysis supports this observation, indicating the absence of a consistent climatological annual cycle before 2007. However, from 2009 onwards, a clearer seasonal pattern with a period of approx. 12 months becomes more prominent in the Wavelet-Figure (3.10), coinciding with the observed divergence in the contributions of autumn and summer.

Distributions of Seasonal Accumulation Rates

Figure 3.16 presents the histogram of monthly average accumulation rates by season, each season contributes three values (one for each month of the season). Panel (A) shows the accumulation rates for summer, which experiences the most significant and frequent mass loss events (accumulation < 0). The mean accumulation rate for summer is the lowest across all seasons with 0.16 cm/day. The standard deviation of 0.28 cm/day is very high in comparison to the other seasons and to the mean summer accumulation rate. This indicates a high variability in summer and/or large extrema (as seen by the the long but flat tail of the summer histogram). Panel (B) illustrates the autumn season, which has the highest mean accumulation rate of 0.40 cm/day and the equally large standard deviation of 0.28 cm/day as summer. The histogram illustrates that autumn has seen the two strongest accumulation events in addition to many medium-strong accumulation events (different amounts of accumulation occur with an equal frequency). Panels (C) and (D) represent winter and spring, respectively, with winter having a mean accumulation rate of 0.26 cm/day and a standard deviation of 0.21 cm/day, while spring shows a mean of 0.29 cm/day and a standard deviation of 0.24 cm/day. Notably, winter and spring have very similar distributions, staying both in the range of monthly mean accumulation rates from -0.13 cm/day to 1 cm/day. Mass loss on the monthly scale occurs relatively seldom in winter, spring, and autumn in small magnitudes.

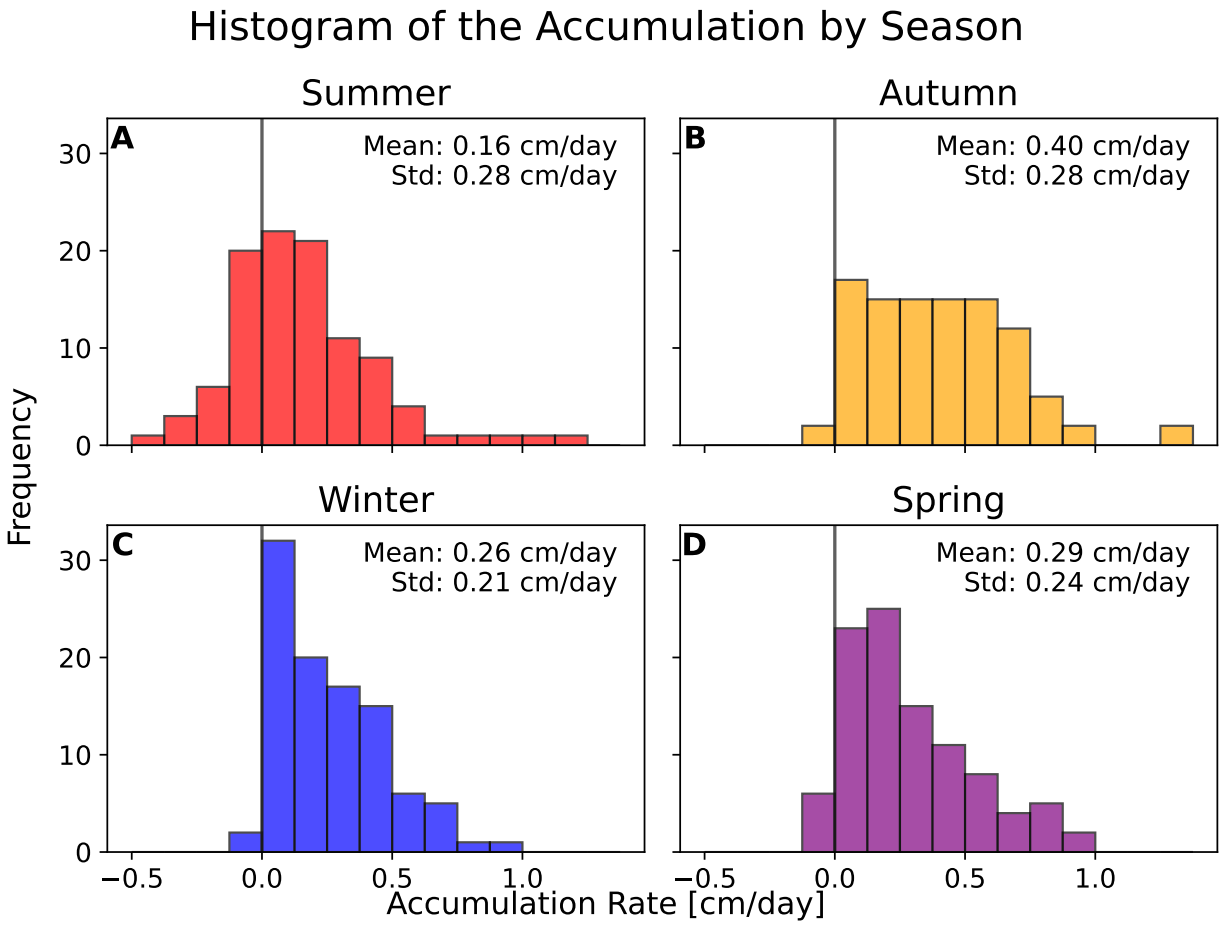

Fig. 3.16: Histogram of the accumulation rates by season ('Süd', 1991–2023) for (A) summer (DJF), (B) autumn (MAM), (C) winter (JJA), and (D) spring (SON).

Cumulative Accumulation per Season

Figure 3.17 displays the cumulative accumulation of the four seasonal subsets. Again, it becomes obvious that in autumn most accumulation occurs, followed by nearly equally strong accumulation in winter and spring, and the least accumulation in summer. Similar to the de-trending of the cumulative annual accumulation as the sum of the accumulation from the four season, each season can be de-trended individually to obtain the climatologically balanced accumulation rate per season. OLS regressing yields the climatological accumulation rate per season (Table 3.1). Their sum gives the annual accumulation rate. Their residuals sum up to the annual residuals.

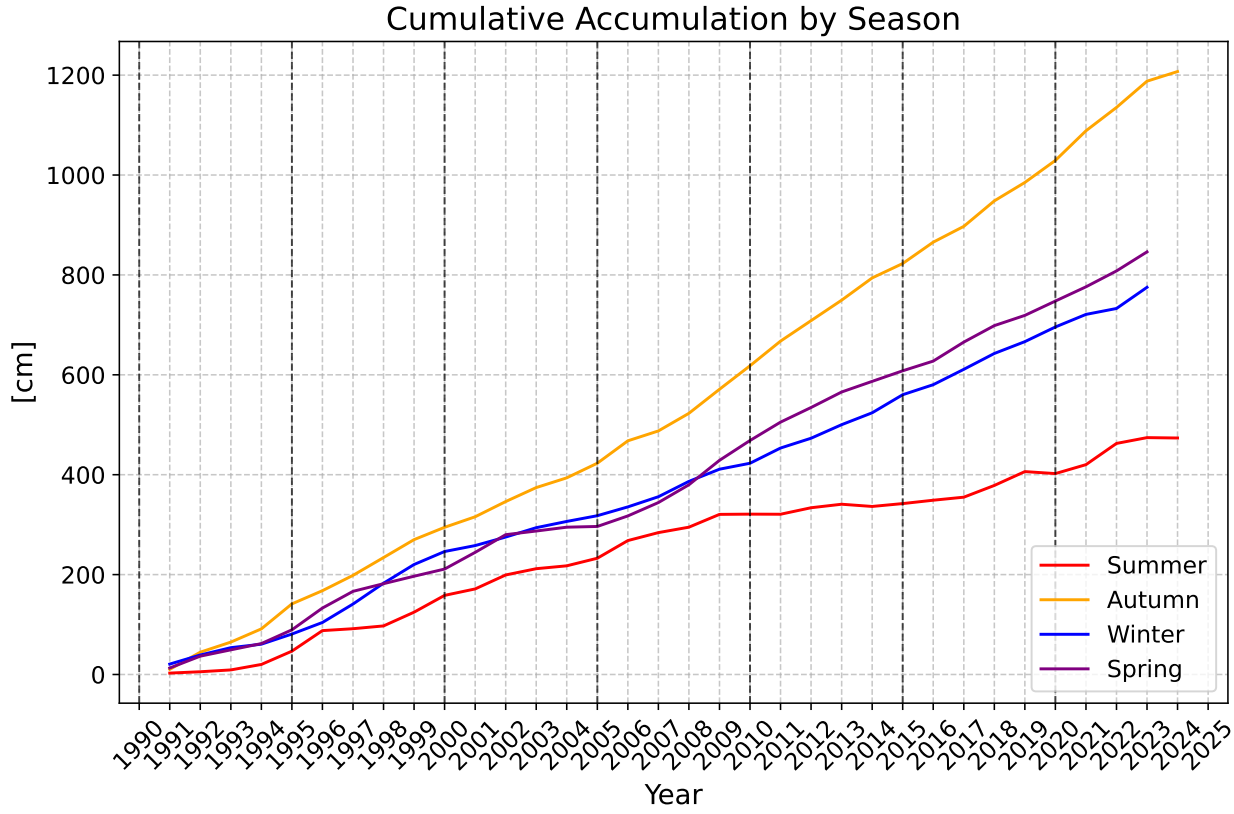

Fig. 3.17: Time series of the cumulative accumulation by season in cm ('Süd', 1991-2023).

Tab. 3.1: Average accumulation rates for each season, calculated over a three-month period.

Season	Accumulation Rate [cm/(3 months)]
summer	14.3
autumn	36.2
winter	23.3
spring	25.9

The de-trended time series for each season is shown in Figure 3.18. It appears that the residuals for autumn and summer are negatively correlated. Unlike the contributions of each season to the

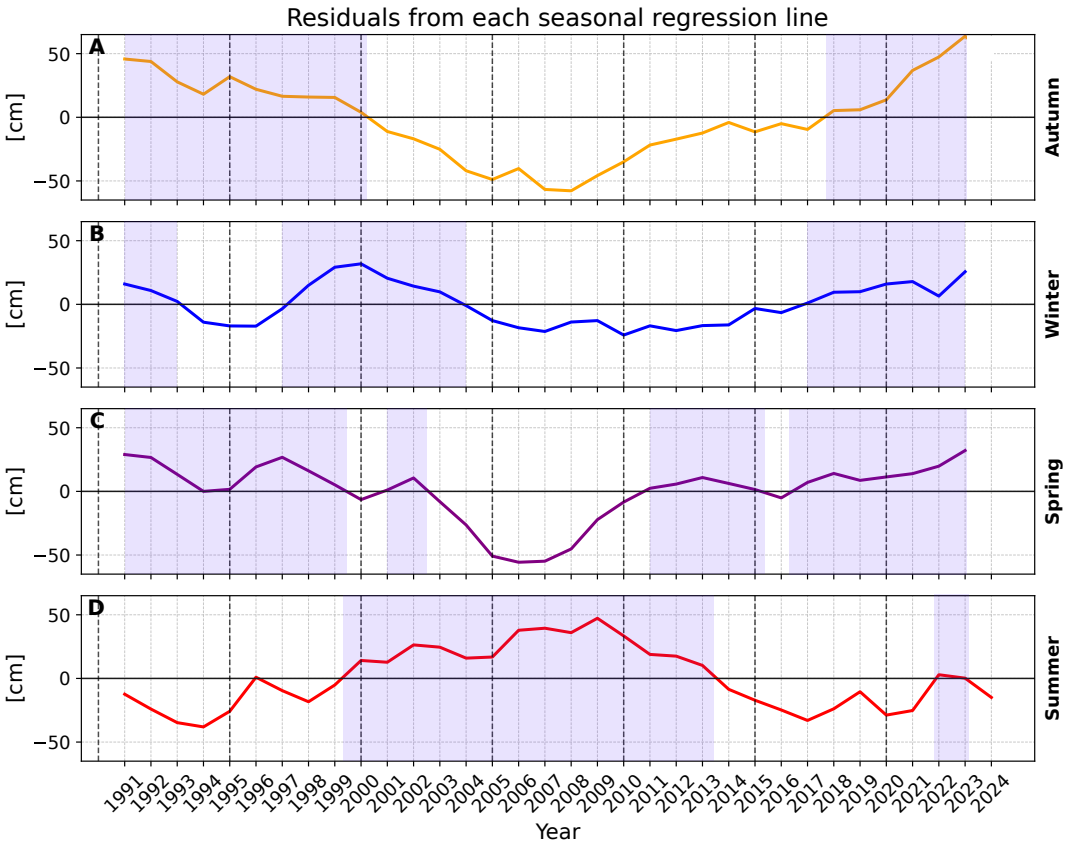

Fig. 3.18: Time series of the de-trended seasonal cumulative accumulation in cm at 'Süd', 1991-2024. Blue-shaded areas represent areas where the seasonal cumulative accumulation was above the climatological regression line. (A) summer, (B) autumn, (C) winter and (D) spring.

annual accumulation, where spring accumulation did not correlate with any other seasonal accumulation, the anomalies in their own climatological balance are closely related to the interannual course of accumulation in autumn. Both autumn and spring show above-average accumulation at the beginning and end of the measurement period (1990–1999 and 2016/17–2023). Additionally, springtime accumulation is above average in 2001/02 and 2011–2015. It is noteworthy that these two non-sequential seasons display a similar trend, suggesting that a short-term positive anomaly cannot explain the increased contributions, as winter, which separates autumn and spring, would also be affected by such an anomaly.
Winter accumulation anomalies seem to follow a similar pattern as spring and autumn accumulation. The first two years and the last six years have exhibited above-average winter accumulation. Additionally, winter accumulation is above climatological balance in 1998–2003.
Interestingly, when the de-trended cumulative accumulation of the total year is in its negative anomaly phase (from 2005–2013), all seasons except for summer are below their climatological balance. This raises the question of whether there has been a change in climate dynamics, leading to below-average accumulation but with a shift towards more accumulation in the summer months. Never before have all seasons been above their climatological balance throughout any period, except for 2022/2023 (Figure 3.18).

Snow Accumulation on the Monthly Scale

The accumulation rates at 'Süd' exhibit high variability on both interannual and intraannual scales, without a clear recurring pattern (see Figure 3.19). However, certain trends are notable: January has the most frequent and strongest ablation events, followed by December, though it also recorded the third-highest accumulation rate in January 2005. December experienced high net accumulation in both 1995 and 2021. Across all months, January and December have the lowest mean accumulation rates but the highest standard deviations (Panel C). For other months, approximately two-thirds of the net accumulation rates are positive, with a general peak in autumn (MAM), albeit with high interannual variability (Panel A), and decreased accumulation and variability in winter. October and November represent a secondary accumulation maximum.
Summer sees the most frequent net ablation months, although February, April, August, September, October, November, and December have also occasionally had ablation months. Only March, May, June, and July show no net ablation. Panel B illustrates annual mean accumulation rate fluctuations, showing no clear trend over time. The error bars indicate high intra-annual variability, with the mean accumulation rate often tied to extreme monthly events, which drive both mean accumulation and its variability.

3.2.3 Extrema

Figure 3.20 Panel A illustrates the intra-annual variability in the occurrences of minima and maxima. The data indicate that most maxima occur during the autumn months of March, April, and May. For the initial four years, maxima consistently appeared in these autumn months; however, in the subsequent years, there has been increasing year-to-year variability in the timing of maxima. Over

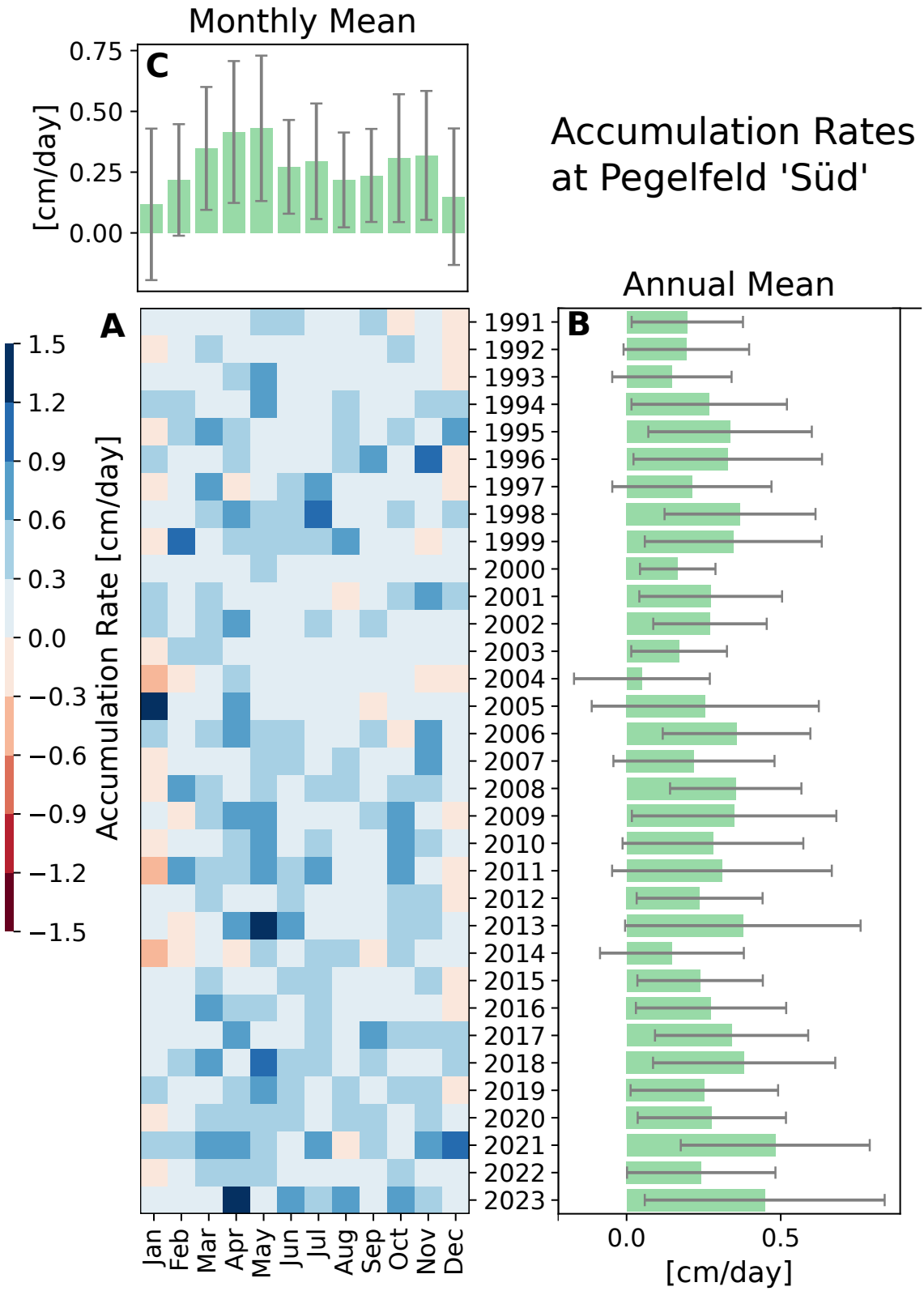

Fig. 3.19: A: Heatmap of monthly average accumulation rates (cm/day) from 1991 to 2023, where red denotes net ablation and blue net accumulation. B: Annual mean accumulation rates (cm/day) with standard deviations showing intra-annual variability. C: Monthly mean accumulation rates across years with standard deviations reflecting interannual variability.

the entire observation period, there is no indication of a trend towards more extreme maxima. Notably, 2021 recorded the highest annual accumulation rate; however, this does not correspond to significant maxima, as the monthly accumulation rates themselves were not unusually high. Minima predominantly occur in summer, with less variability in the timing of occurrence compared to maxima. In contrast, the minima show a discernible increase in magnitude over time, accompanied by a higher frequency of stronger minima. Panel B in Figure 3.20 further complements the analysis by showing that minima are significantly more extreme during summer months, whereas the magnitude of maxima exhibits minimal variability. The highest monthly accumulation rate was observed in May 2013, whereas the lowest was recorded in January 2011. Further investigation into the causes of these extreme events will be addressed in the discussion.

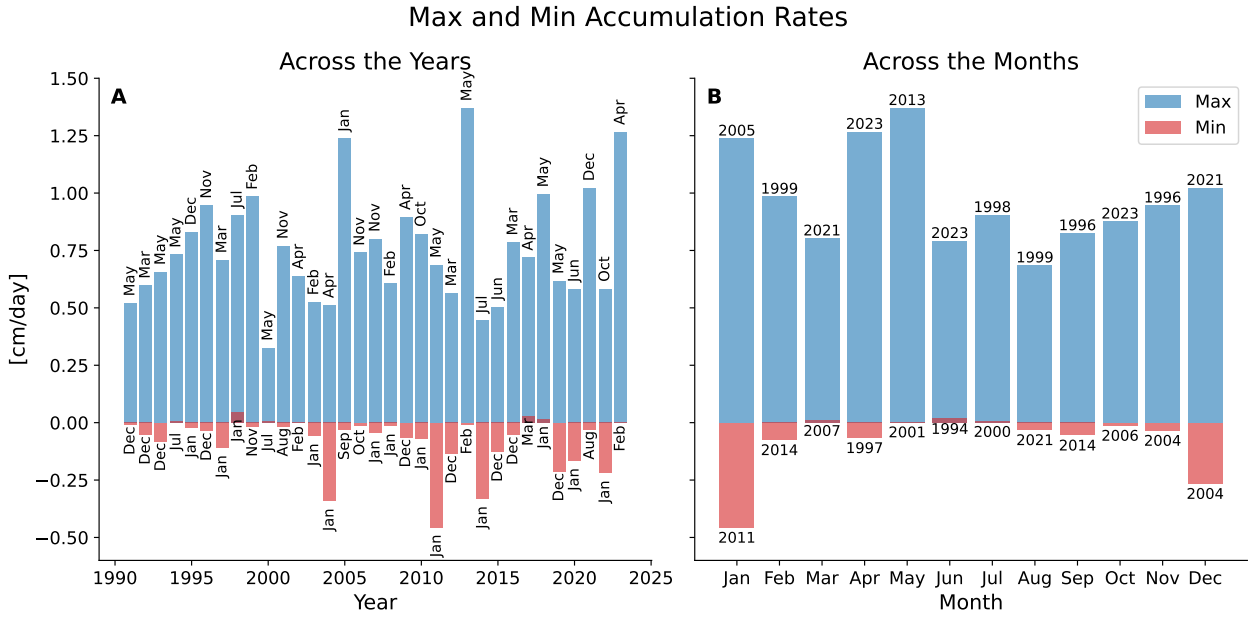

Fig. 3.20: Panel A shows the maximum (red bars) and minimum (blue bars) accumulation rates in cm/day per year across the months, panel B the maximum and minimum accumulation rates per month across the years. The bars are labeled with the corresponding month (year) of occurrence.

4 DISCUSSION

4.1 Impact of Snow Density on SMB variability

A limitation of this study is that density measurements have not been combined with height measurements to calculate SMB directly. Nevertheless, this section aims to demonstrate that changes in snow height serve as a reliable proxy for SMB variability.
The time series of annual density measurements at the stake farm 'Süd' is derived from the densities for a profile depth of $z = 1$ meter, as presented in Hecht (2022). A depth of $z = 1$ meter is chosen because, on average, 1 meter of snow accumulates annually at 'Süd'. From these values, the mean and standard deviation of annual density are computed. Additionally, the mean and standard deviation of the annual accumulation rates are computed. To estimate the contribution of density and accumulation variability to the interannual variability of SMB, the following formula is employed:

$$\left(\frac{\sigma_M}{M}\right)^2 = \left(\frac{\sigma_\rho}{\rho}\right)^2 + \left(\frac{\sigma_V}{V}\right)^2, \tag{4.1}$$

where σ_M is the standard deviation of SMB, M is the mean SMB, σ_ρ and ρ are the standard deviation and mean of density, and σ_V and V are the standard deviation and mean of accumulation (in dimensions of a volume), respectively. On the right-hand side, the first term $\left(\frac{\sigma_\rho}{\rho}\right)^2$ represents the relative contribution of density, while the second term $\left(\frac{\sigma_V}{V}\right)^2$ corresponds to the relative contribution of accumulation rate to the interannual variability of mass. This equation is appropriate because SMB is the product of density and height change (volume) over a year, and the variability of a product of independent variables can be approximated as the sum of their squared relative uncertainties. Using these relative contributions from equation 4.1, the interannual variability of SMB is primarily driven by the variability in accumulation rates, with an 8.7% contribution, while the contribution from density variability is significantly smaller, at only 0.3%. These findings align with those of Ekaykin et al. (2023), who reported that, at the Vostok stake farm, over 90% of the interannual SMB variability is explained by changes in snow height, with less than 10% due to snow density variability, although their results are based on correlation analysis, indicating a similar proportion but using a different methodological approach. This highlights the dominant role of atmospheric processes over processes within the snowpack in influencing SMB. Following this analysis, the temporal variability in snow density (from measurement to measurement) appears negligible in its contribution to SMB variability. Consequently, it may be unnecessary to account for density fluctuations at this level of frequency, and it could even be considered to discontinue monthly density measurements at NM.

4.2 Spatial Variability

RQ1: How does the spatial variability of snow accumulation within the stake farm behave?

The spatial standard deviation within the stake farm was calculated from the deviation (i.e. the difference $a_i - a$) of each stake's accumulation from the mean accumulation since the last reading, without further homogenization to v3. The spatial variability is highly sensitive to both the averaging interval and the amount of accumulation. Due to this sensitivity, I was unable to normalize spatial variability based on the time between consecutive measurements or the accumulation rate. Attempts to do so yielded unrealistic values that were either strongly dependent on accumulation amounts or the number of measurements within the interval.

A rolling time series on the irregular grid was biased by the number of measurements. For instance, before 2010, a rolling window of one year included 12 nearly monthly values, while after 2010, it included around 24 values with shorter intervals. When resampled and interpolated to a regular grid, the spatial variability exhibited a clear dependence on the number of measurements. Normalizing the standard deviation with the mean accumulation amount, as proposed by Goodwin (1991), often resulted in very high coefficients of variation (CV), particularly when accumulation rates were less than one, which distorted the variability. Normalizing the standard deviation by the number of days between measurements also showed a strong correlation with the number of measurements.

Further analysis methods need to be explored to address this issue. Normalizing the spatial standard deviation by the square root of the number of days between measurements appeared to scale the values more reasonably, though additional validation is required. For now, the standard deviations on measurement days provide an indication of the surface roughness within the stake farm, which can become significant (up to 18 cm per measurement interval).

Such high spatial variability suggests that the mean value from these measurements is representative for a localized area only. The substantial spatial variation indicates that fine-scale, localized processes influence snow accumulation, complicating the generalization of mean values to larger regions. Even temporal averages over periods as long as 10 years may only be representative for relatively small areas (a few square kilometers) (Eisen et al. 2008).

Furthermore, significant spatial variation in annual snow accumulation rates has been observed at scales as small as 10 m in Greenland (Kuhns et al. 1997). Due to time constraints, I was unable to perform a similar analysis. However, it is reasonable to assume that spatial variation within this stake farm is similarly significant.

The time series of spatial standard deviation does not indicate a long-term trend, which is consistent with the assumption that spatial variability is stable in time (Eisen et al. 2008).

4.3 Mean Accumulation from the Stake Farm

4.3.1 Intra-Annual Accumulation

RQ2: Is there an intra-annual cycle evident in the dataset of accumulation and its temporal variance?

Typical Intra-Annual Cycle

The accumulation rates do not exhibit a significant intra-annual cycle on a monthly basis. While wavelet analysis occasionally reveals a signal at a 12-month period, such patterns are not consistent. However, on a seasonal scale, climatological differences are evident over the measurement period (Figure 3.16). Analysis of the first moment, i.e., the mean accumulation, indicates that accumulation rates peak during the autumn months (March, April, and May). Winter and spring seasons show similar accumulation rates, which are lower than those in autumn. Summer accumulation rates are the lowest on a climatological scale.
In terms of the second moment, i.e., temporal variability measured by standard deviation, the autumn and summer months display the highest variability, whereas spring and winter exhibit less variability. For all seasons the variability is as high as the first moment, indicating high inter- and intra-annual variability. The high variability could stem from the fact that accumulation is largely driven by extreme precipitation events (EPEs), which are known to have significant temporal and spatial variability (Turner et al. 2019). Models estimate that 50–55% of annual precipitation originates from EPEs in coastal DML, with just 20–30 days per year accounting for 50% of total precipitation (Turner et al. 2019). Simon et al. (2023) provides a detailed regional analysis of the seasonality of extreme precipitation events (EPEs) as a percentage of total annual precipitation in DML. The study shows that at Mizuho and NM stations, seasonal peaks in EPEs contribute to intra-annual accumulation maxima. For example, at Mizuho station in eastern DML, Simon et al. (2023) identifies autumn as the season with the highest EPE contribution to the annual cycle, as shown in their Figure 3. This aligns with earlier findings by Fujii and Ohata (1982), who reported accumulation peaks in February and March at Mizuho station. Similarly, for the stake farm 'Süd', located near NM, this finding aligns well with the observed maximum accumulation occurring in autumn. The influence of EPEs on accumulation will be further discussed in section 4.3.2. However, since the analysis presented in this master thesis relies on monthly to bi-weekly stake measurements, it cannot be verified whether high accumulation rates are indeed caused by EPEs. This limitation highlights the challenges of obtaining long-term, reliable snow accumulation measurements in Antarctica. Although sonic height rangers mounted on AWSs provide high temporal resolution, they currently cover only shorter time periods (van den Broeke et al. 2004). However, regular meteorological observations at NM could be leveraged for additional analyses to supplement data from sonic height rangers.
On a seasonal scale, summer ablation becomes prominent. Ekaykin et al. (2023) suggests that the higher summer temperatures enhance snow compaction and sublimation, contributing to this seasonal pattern. According to Jakobs et al. (2019), temperatures at NM can sporadically reach the melting point in February, therefore, melt is primarily attributed to the continuous input of short-

wave radiation during the polar day. At NM, melt occurs only between November and February and amounts to 50 mm water equivalent on average but with high interannual variability (Gorodetskaya et al. 2020). Jakobs et al. (2019) used surface energy balance modeling to determine melt patterns and found high interannual variability. Similarly, my analysis reveals high variability in summer ablation, likely driven by absorbed shortwave radiation. Jakobs et al. (2019) also highlighted the importance of the snowmelt-albedo feedback, whereby fresh snow with high albedo reflects sunlight, but as melting begins, the albedo decreases, allowing for increased absorption of radiation and further melt.

Furthermore, van den Broeke et al. (2010) found that sublimation at NM is on average higher than melt. Since sublimation is primarily temperature-driven, it is almost exclusively a summer phenomenon (van den Broeke et al. 2010), though weak sublimation occurs year-round at various sites in DML (van den Broeke et al. 2004). Therefore, both sublimation and melt likely contribute to the observed summer ablation. Without density measurements or meteorological variables like dew point, temperature, and wind speed (which enhances sublimation), the primary ablation mechanism cannot be determined.

Another factor affecting summer accumulation rates is the reduced cyclonic activity during summer, meaning fewer EPEs influence accumulation in coastal areas (Turner et al. 2019). This will be further discussed in the next section.

Patterns and Shifts in Seasonal Contributions to Annual Total

Results suggest an increasing frequency and magnitude of negative summer anomalies, where summer accumulation contributes less than a quarter of the annual total. This could result from either more frequent ablation events or reduced precipitation. Modeled melt time series for NM (Jakobs et al. 2019) can only partly explain these negative anomalies. Additional processes, such as stronger sublimation, wind erosion, or compaction, could be contributing factors. For the latter, Hecht (2022) indicated a minor but insignificant increase in the density of the uppermost 15 cm of snow at 'Süd' between 2002 and 2019, which may also play a role.

Moreover, the analysis suggests a shift towards autumn-dominated accumulation at the expense of summer contributions. It can be hypothesized whether a seasonal or intra-annual cycle may develop over time as a result of an increasing gradient between summer and autumn accumulation rates.

Welker et al. (2014) found that the frequency of EPEs at Halvfarryggen, an ice ridge approx. 100 km southeast of NM, is highest in autumn and lowest in summer, a finding confirmed by Simon et al. (2023) for the entire coastal region of western DML. Additionally, Simon et al. (2023) demonstrated a significant increase in both the number and precipitation contribution of EPEs over the past 40 years. These EPEs are often accompanied by blowing snow due to high wind speeds. However, it remains unclear whether especially autumn EPEs have shown a stronger increase in recent years, which could explain the shift towards autumn-dominated accumulation.

Simon et al. (2023) and Turner et al. (2019) also demonstrate a connection between the frequency of EPE days, particularly in autumn, and the semi-annual oscillation (SAO) of mean sea level pressure. The SAO is marked by peaks in baroclinic and cyclonic activity during autumn and spring, leading

to the contraction and expansion of the circumpolar low-pressure belt twice per year and increased number of landfalling cyclones during autumn and spring. Since the mid-1970s, the weakening of the SAO has contributed to cooling in coastal Antarctica, especially during May and June (Mayewski et al. 2009).
Additionally, Simon et al. (2023) note that the SAO drives air export to lower latitudes in summer and winter, which results in fewer EPEs during these seasons. The frequency analysis of accumulation rates at 'Süd' also revealed a 6-month periodicity, potentially linked to the SAO. This suggests that the SAO could affect the seasonal accumulation measured at 'Süd', potentially influencing a shift towards autumn-dominated accumulation.
Additionally, in years where the annual de-trended cumulative accumulation is below-average, summer accumulation appears to be above-average, while accumulation during all other seasons remains below-average with respect to their seasonal averages.
Thus, it can be hypothesized that in annual below-average accumulation years, there may be a shift towards increased summer accumulation. However, summer does not become the dominant accumulation season, i.e. it does not contribute more than a quarter to the annual accumulation. This observation suggests that summer accumulation might have been, or could still be, representative of annual accumulation in certain contexts. As this phenomenon has not been linked to any established literature, further investigation is needed to identify potential relationships with atmospheric conditions or parameters.

Comparison to Modeled Seasonal Cycle of Accumulation

A comparison with results from Schlosser et al. (2002), who simulated the seasonal cycle of accumulation (precipitation minus sublimation) using the regional atmospheric model (RACMO) data near NM, shows qualitative agreement with my findings. According to the model, precipitation peaks during austral autumn (MAM), with a secondary maximum in November. Sublimation, most intense in summer, removes approximately 12% of annual precipitation. Thus, net accumulation closely follows precipitation, with the lowest values in summer due to the combination of minimum precipitation and maximum sublimation.
Both my analysis and the RACMO1 model (with updates up to 1999) indicate a minimum in accumulation during December and January, and a maximum in autumn. While my data suggest May as the peak accumulation month, Schlosser et al. (2002) identified March as the highest. Despite this discrepancy, the overall seasonal patterns align well.
Schlosser et al. (2002) validated the modeled monthly accumulation rates by comparing it to 14 years of stake farm measurements at NM, a separate site from 'Süd'. While monthly accumulation did not show significant correlation in every year, the model accurately captured most major precipitation events, indicating it effectively represents synoptic conditions. Although the model generally underestimates accumulation compared to observations, the consistency in seasonal patterns suggests that the modeled cycle provides a reasonable depiction of the temporal distribution of accumulation.

4.3.2 Long-Term Trends and Variability in Accumulation

In this section, the following key points regarding the long-term snow accumulation at NM are addressed: (1) the accumulation rates exhibit periodic fluctuations, (2) the distribution of accumulation rates, (3) the high level of interannual variability, (4) the challenges associated with detecting trends due to this high interannual variability. However, I will address the long-term trends in mean accumulation in the context of RQ 5 ”Is there evidence in the time series that corresponds to Global Climate Warming?”

RQ3: What is the temporal evolution of snow accumulation at NM over the past 33 years?

Periodic Fluctuations in Accumulation Rates

In the analysis of accumulation rates, a periodic fluctuation of 3–4 years was observed. Wavelet analysis indicated that this signal emerges as significant but can disappear at times (e.g., from 2010 to 2017). Two major modes of natural climate variability influencing the Antarctic climate are SAM and ENSO (King et al. 2023b). Notably, strong El Niño and La Niña events have coincided with both above-average and below-average accumulation rates at ’Süd’. For instance, the strong El Niño of 1997/98 occurred during a period of above-average accumulation, whereas the strong El Niño in 2015/16 coincided with the second-lowest annual accumulation rate recorded. Similarly, the strong La Niña in 1999/2000 took place during a period of average accumulation, while the La Niña events in 2007/08 and the triple-dip La Niña from 2020 to 2023 were associated with above-average accumulation rates. Based on this preliminary analysis, a clear relationship between accumulation rates and ENSO cannot be established.

According to Naik et al. (2010), SAM is known to exhibit a periodicity of approximately four years. However, the Fast Fourier Transform of the monthly resolved SAM index during the period of accumulation measurements did not reveal a dominant cycle within this timeframe (results not shown). Moreover, similar to ENSO, the SAM has experienced positive phases during both below-average and above-average accumulation periods.

Fischer et al. (2004) identified that sea salt aerosol deposition on the plateau of DML displays a 3–4 year periodicity over the last two millennia, which they attribute to the Antarctic Circumpolar Wave (ACW). The ACW is characterized by a system of coupled anomalies propagating eastward due to atmosphere-ocean interactions (White and Peterson 1996). These anomalies pertain to (sea level) pressure, wind stress, sea surface temperature, and sea ice extent. A warm sea surface temperature anomaly lags a high sea level pressure anomaly by approximately one year (around 90°) and is associated with a southward meridional wind stress anomaly onshore, as well as a negative anomaly in sea ice extent. This warm sea surface anomaly serves as a site of deep convection, leading to a positive precipitation anomaly along the fall-winter-spring sea ice edge (White et al. 2004). Fischer et al. (2004) also observed periods of a diminishing ACW cycle over their two-millennial study period. To better quantify the exact periodicity of accumulation rates, longer records of monthly resolved measurements are necessary. However, the ACW may be a plausible candidate for influ-

encing accumulation rates in coastal regions of DML. To my knowledge, no study has specifically investigated this relationship.
To further explore the influence of the ACW on accumulation rates measured at NM, a correlation analysis could be conducted between accumulation rates and detrended sea level pressure in the primary source region of air masses affecting NM. To investigate the impacts of ENSO, SAM, and ACW on accumulation rates at NM, their indices can be utilized in their original form, or they may be treated cumulatively or with lagged effects. The individual effects of these three climatic phenomena should be analyzed, potentially by isolating phases of strong individual modes. Additionally, the indices could be combined to determine whether their effects amplify or cancel each other out.

Distribution of Accumulation Rates

The distribution of accumulation rates at 'Süd' over the climatological period 1991–2020 provides valuable insights into the underlying processes affecting snow accumulation. Although the histogram of annual accumulation sums conforms to a gaussian distribution, the monthly data diverge from both student-t and gaussian distributions. This discrepancy can potentially be attributed to the central limit theorem, which posits that the sum of a large number of independent random variables tends to exhibit a normal distribution, regardless of the original distribution of the variables. In this context, the annual accumulation is the sum of monthly accumulation rates, leading to a gaussian approximation when evaluated over longer time periods.
Furthermore, the monthly accumulation rates are more strongly influenced than annual rates by several factors, including seasonal weather patterns, extreme precipitation events, and other SMB processes (including erosion, sublimation, transport, melt, deposition), which may introduce substantial variability and may be non-gaussian processes themselves. This complexity can lead to a non-gaussian distribution on a monthly basis. The findings are further supported by previous studies, such as those by Ekaykin et al. (2023) and Medley et al. (2018), which also demonstrate gaussian distributions for annual accumulation rates. On the monthly scale, however, also Ekaykin et al. (2023)'s analysis indicates a deviation from a gaussian distribution.
Furthermore, Medley et al. (2018)'s analysis is based on ice core data, whereas Ekaykin et al. (2023)'s is based on measurements taken at the stake farm at Vostok. Annual accumulation rates derived from ice cores may be less subject to or less able to capture the variability observed on smaller time scales. This suggests that the method of data collection may influence the resulting distribution patterns.

Interannual Variability in Accumulation

The interannual variability in snow accumulation rates has remained consistently high throughout the entire measurement period for both annual and seasonal accumulation rates. However, it has been particularly pronounced in the last 4–6 years, where the sign of annual anomalies relative to the climatological mean has shifted each year, and the magnitude of positive anomalies has increased significantly. Additionally, the differences in annual accumulation rates between consecutive years have reached their maximum during this time.

Turner et al. (2019) identifies EPEs as the primary factor controlling the interannual variability in accumulation for the whole continent. In line with this, the present analysis focuses on snowfall as the primary driver of this variability, given that snowfall constitutes the largest component of accumulation (Medley et al. 2018; Schlosser et al. 2010). Other processes, such as blowing snow events, can also result in substantial accumulation in localized areas. However, Turner et al. (2019) notes that these are generally isolated large SMB events, particularly in steep glacier valleys. Over the long term and in ice shelf settings, precipitation dominates as the main factor rather than redistribution. Sublimation mainly occurs during the summer, while deposition is more common in winter (van den Broeke et al. 2010). Changes in snow density and compaction explain only a minor portion of the interannual variability in SMB, as discussed in section 4.1. Therefore, it is assumed that much of the high interannual variability in accumulation is driven by variability in snowfall itself.

Turner et al. (2019) also emphasizes that Antarctic snowfall variability is driven largely by EPEs. Simon et al. (2023) identified an increase in EPEs in DML over the past 40 years, while Wille et al. (2021) reported similarly high variability in atmospheric rivers (ARs). Although AR frequency has increased in DML over the last 40 years, this trend is smaller in magnitude than the observed interannual variability in AR occurrence.

According to Turner et al. (2019), EPEs are also linked to specific phases of major climate modes that influence atmospheric circulation, such as SAM and ENSO, which are similarly characterized by interannual variability. However, Turner et al. (2019) argues that in the context of snowfall, the number of EPEs accounts for over 90% of interannual variability in coastal DML, outweighing the influence of SAM and ENSO. On decadal timescales and in terms of total ice mass, King et al. (2023b) found that SAM and ENSO primarily explain variability. However, this signal is spatially inconsistent, particularly in the vicinity of NM.

It is important to note that many studies on EPEs are limited by in-situ observations and are primarily based on model outputs (Turner et al. 2019). While the analysis presented in this thesis is able to quantify interannual variability, it cannot fully address the underlying causes or capture smaller-scale variability due to the low temporal resolution of the measurements. Both the timing and magnitude of accumulation events are critical, but this information is unavailable at the temporal scale of the current dataset.

To mitigate this limitation, I have divided the accumulation by the number of days in the measurement interval. While this approach may be misleading —since most accumulation may occur during a single event — it allowed me to incorporate the probability of event timing into the analysis. However, this method does not allow to verify or refute the dominance of EPEs in determining interannual variability, as the contribution of (non-)EPE accumulation to the total cannot be quantified.

To potentially extract more insight from the dataset, one could apply the method proposed by Schlosser et al. (2002), using SYNOP observations from NM station. SYNOP measurements are standard meteorological observations taken every three hours, including measured variables such as air temperature, pressure, wind speed, and direction. in addition to observer-recorded elements, often termed “eye observations,” such as cloud cover, visibility, snowfall, and snowdrift (Schlosser et al. 2002). If snowfall or drift is reported, those days would be considered accumulation days, while all other days would be assigned zero accumulation. The total measured accumulation could then

be divided by the number of accumulation days to better estimate the timing and amount of accumulation events. However, I decided against this approach, as NM station was relocated three times during the measurement period at the stake farm, resulting in an inconsistent time series. Moreover, the stake farm 'Süd' is not situated close enough to NM to assume that SYNOP observations from NM always apply to the conditions at 'Süd'.

4.3.3 Challenges in Trend Detection under High Interannual Variability

The required number of years (n) for the significant detection of a trend in annual accumulation rates given the interannual variability σ is calculated using the formula (Lettenmaier 1976):

$$N_T = \frac{T' n^{1/2}}{2\sigma} \tag{4.2}$$

To express this relationship in terms of n, equation 4.2 is rearranged to:

$$n = \left(\frac{N_T 2\sigma}{T'} \right)^2, \tag{4.3}$$

where N_T is defined by:

$$1 - \beta = F(N_T - t_{1-\alpha/2,\nu}). \tag{4.4}$$

Here, F denotes the cumulative distribution function of a standard Student's t-distribution.
In this context, T' represents the expected step trend, defined as $T' = |\mu_1 - \mu_2|$, where μ_1 and μ_2 are the mean values of the process for the first and second halves of the data record, respectively.
The equation must be adapted to accommodate the detection of a linear trend represented by T.
The modified formula for determining the sample size for a linear trend results as:

$$n \approx \frac{\left(N_T \sqrt{12}\sigma\right)^2}{T^2}. \tag{4.5}$$

In this analysis, σ is the known standard deviation of the annual accumulation rates, which is 33 cm/year. A significance level of $\alpha = 0.05$ was chosen, ensuring a 5% probability of erroneously rejecting the null hypothesis of no trend. Additionally, a statistical power of $1-\beta = 0.80$ was selected to maintain a high probability of detecting a true trend, should it exist. Consequently, the value of N_T is determined to be:

$$N_T = \underbrace{F^{-1}(1-\beta)}_{0.84} + \underbrace{t_{1-\alpha/2}}_{1.96} = 2.8 \tag{4.6}$$

For a step change of 1 cm/year, it is estimated that approximately 34,151 years of observations are necessary, while a linear trend requires even more than 100,000 years. This analysis highlights that

the interannual variability in snow accumulation rates is so high that the detection of small changes requires an unrealistically large number of observations. Notably, as the magnitude of the trend T increases, the required sample size decreases.
In this calculation, it has not been accounted for serial dependence and used an estimated value of σ without knowledge of the population's actual standard deviation.

4.4 Extrema

RQ4: What are the extrema observed in the snow accumulation, and what underlying causes are addressed in the literature?

The year 2021 stands out as the highest annual accumulation rate recorded, although this peak does not correspond to remarkable maxima in monthly accumulation rates. Notably, the monthly accumulation rates observed in 2021 align with the typical distribution of monthly accumulation rates derived from climatological data. This suggests that either the number of months with above-average accumulation increased in 2021 or the amount per month has exhibited a slight increase across all months. The monthly accumulation rates reached their maximum in May 2013.
A number of studies have examined the synoptic situation that led to extreme snowfall and accumulation events in DML: Schlosser et al. (2010); Boening et al. (2012); Wang et al. (2023); Gorodetskaya et al. (2014); Lenaerts et al. (2013). They all agree that a sea-saw pattern of a low- and high-pressure system was located in the South Atlantic sector. The pressure system intersected with the continent, with the high-pressure system blocking the movement of the low-pressure system. Consequently, a strong pressure gradient was established across DML together with a poleward flow along the western flank of the high. The presence of ARs, particularly when a cyclone is blocked by a high-pressure ridge, has also been documented as a key driver of extreme snowfall events (Gorodetskaya et al. 2014). Moist and warm air is transported towards the continent. As the air rises onto the ice shelf, clouds form, leading to extreme precipitation. The longer the blocking, the more snowfall occurs.
Lenaerts et al. (2013) proposed that a weaker-than-usual low-pressure system in the South Atlantic sector, combined with anomalous low pressure in the Weddell Sea, results in a southward flow of air. When subtropical and subpolar sea surface temperatures are anomalously high and these atmospheric conditions persist for several days, extreme snowfall events are likely to occur.
Boening et al. (2012) noted that the atmospheric blocking over the Atlantic sector and increased poleward moisture transport lead to significant precipitation events in 2009 and 2011. However, these reported maxima do not align with the extremes observed in this thesis. The maximal monthly accumulation rate in May 2013 needs to be examined for similar atmospheric patterns as outlined above to confirm their influence. The year 2021 as the maximum annual accumulation rate can be investigated regarding the frequency of such synoptic situations.
The lowest annual accumulation rate was recorded in 2004, while the minimum monthly accumulation rate was observed in January 2011. The existing literature on the synoptic-scale analysis of minimum accumulation events is limited. It may be worthwhile to examine whether the absence of previously described atmospheric patterns contributes to these observed minima.

Furthermore, investigating the atmospheric conditions that facilitate ablation processes—such as melting and sublimation—could yield valuable insights, particularly when establishing a climatological baseline in comparison to the conditions during January 2011. Key factors to consider include sunshine duration, cloud cover fraction, and temperature, as well as profiles of turbulent sensible and latent heat fluxes, wind speeds, and directions. Additionally, katabatic winds, which are often associated with drier conditions, may significantly influence snow transport and ablation.

4.5 Global Warming and the Recent Development of Snow Accumulation at Stake Farm 'Süd'

RQ5: Is there evidence in the time series of snow accumulation that corresponds to global climate warming?

In a warming climate, increased humidity is transported poleward, leading to enhanced precipitation over the Antarctic continent (Wille et al. 2021; Medley et al. 2018). Furthermore, Bengtsson et al. (2006) demonstrated that a warmer climate causes a poleward shift of Southern Hemispheric storm tracks, resulting in significant changes in the spatial distribution of precipitation. Model projections suggest that synoptic transport mechanisms, including cyclones and ARs, will continue to be the dominant factors driving the rise in snowfall across the entire Antarctic continent (Dalaiden et al. 2020). This increase in precipitation is expected to partially offset the dynamic mass loss of the AIS by the end of the 21st century (Dalaiden et al. 2020). Additionally, the shift of the SAM towards its positive phase, due to greenhouse gas forcing, is projected to influence future SMB trends with some degree of predictability (King et al. 2023b).

The analysis of the detrended snow accumulation time series reveals a notable departure from the climatological mean in recent years, with the snow surface rising significantly above expected levels. The most recent accumulation shows a deviation of 150 cm above the climatological norm, which is 75 cm greater than the second-largest deviation in the last 33 years. This sharp increase, primarily driven by the high annual accumulation in 2021 and 2023, might suggest a shift in snow accumulation. However, the time series also displays pronounced variability on decadal timescales. Decadal variability is difficult to assess given the limited length of the time series, which further complicates identifying long-term trends. Therefore, it is impossible (given this database only) to determine whether this deviation represents natural decadal variability or a potential onset of long-term departure from past climatology. Further monitoring is required to distinguish between these possibilities.

Recent studies have reported an increase in accumulation in DML (Medley et al. 2018; Philippe et al. 2016), which has contributed to periods of net mass gain (Wang et al. 2023). However, disentangling the influence of natural variability from long-term trends remains challenging (Medley et al. 2018; Lenaerts et al. 2013). The inherent difficulty arises from the high interannual variability in snowfall, making it hard to determine whether anomalous years reflect natural fluctuations or the beginning of a sustained trend (Lenaerts et al. 2013).

There are arguments both for and against the hypothesis that the recent anomalies signal a regime shift in snow accumulation:

- The recent increase in accumulation, while not unprecedented, is longer and steeper compared to previous increases in the time series.
- For the first time in the record, all four seasons have contributed above their respective long-term average accumulation rates in the last two years. This could point to a more systematic increase in accumulation, rather than isolated extreme events.
- Positive anomalies in accumulation rates are becoming more frequent, and their magnitude is increasing, indicating a potential change in the distribution of accumulation events. A widening and/or shifting of the distribution could signal a regime shift.
- The annual accumulation rates of 2021 and 2023 are statistically rare, exceeding 2σ from the climatological mean. While these events are exceptional, their recurrence within two years underscores the hypothesis of the onset of a new regime rather than isolated extremes. On the other hand, on a decadal scale, the snow accumulation system might currently be in an above-average phase. If this is the case, two positive anomalies of otherwise typical magnitude could push the total accumulation outside the 2-sigma threshold, without indicating a true regime shift. This would suggest that the extreme values recorded in 2021 and 2023 may simply represent an interaction between natural variability and an already elevated decadal state, rather than an unprecedented departure from past climatology. Furthermore, these fluctuations, though notable, are not significant within the context of interannual variability. Moreover, the limited length of the time series prevents any determination of decadal variability.
- Similar regime shifts have already been documented elsewhere in DML. For example, a significant shift in accumulation trends has been observed at Kohnen Station, most likely representative for the polar plateau in DML (Medley et al. 2018). However, models used by Medley et al. (2018) do not capture this shift, suggesting that they may underestimate current realities in the region.
- Philippe et al. (2016) have identified increasing SMB, particularly over the last 50 years, in an ice core drilled in a coastal region of eastern DML. This trend, though not widely observed in other ice cores until recently, supports the notion of increasing snow accumulation in DML.
- Trends in Precipitation minus Evaporation ($P-E$) were positive in the western coastal regions of DML over a 20-year period (1989–2009) compared to 1989 (Nicolas and Bromwich 2011). The study by Nicolas and Bromwich (2011), using several reanalysis products, found a clear correspondence between trends in P-E and trends in the meridional wind at 500 hPa, with stronger meridional winds toward the shore correlating with increased P-E.
- An increase in the frequency and intensity of EPEs and ARs has been documented, which is the key climatic driver of snow accumulation on the annual scale (Simon et al. 2023; Turner et al. 2019; Wille et al. 2021).

Retrospective analysis will be required to make a more informed conclusion.

5 CONCLUSIONS

In this study, snow accumulation rates from stake farm measurements over the past 33 years were analyzed. These accumulation rates, when combined with density measurements, can be used to derive SMB, one of the most critical variables for assessing the mass balance of the AIS. Understanding the (surface) mass balance is essential for quantifying the ice sheets' contribution to sea-level rise (Rignot et al. 2011). Snow accumulation can be seen as temporary storage of sea-level equivalent mass, effectively delaying its contribution to sea level rise (Medley and Thomas 2019). To accurately predict whether sea level rise will reach the levels projected by CMIP6 models (Seroussi et al. 2024), it is vital to quantify how much of this sea-level equivalent is currently stored. Glaude et al. (2024) emphasize the need to investigate SMB's response to projected climate warming, noting that SMB estimates for the Greenland Ice Sheet by 2100 vary by a factor of two. Even small changes in accumulation rates can cause significant uncertainties in projected AIS mass balance (Medley et al. 2018), underscoring the necessity of improved model guidance informed by observations.

While remote sensing methods are increasingly available, reliable estimates of SMB still heavily rely on on-site measurements. However, the remoteness and climate of Antarctica limit the availability of these direct measurements (Dahe et al. 2004). This study, which provides a statistical analysis of on-site accumulation measurements, can serve as a benchmark framework that can complement remote sensing products.

If regional climate models fail to reproduce the accumulation time series and distributions identified in this study, it could indicate that physical processes are either missing or incorrectly implemented in the models. This concern is further supported by the findings from Medley et al. (2018), which also show that the models do not accurately replicate the accumulation patterns observed at Kohnen Station. Alternatively (or additionally) the initial conditions may not be adequately captured. Wirths et al. (2024) emphasizes the importance of accurately quantifying SMB, as projected contributions to Antarctic sea level rise depend on the choice of present-day SMB baseline forcing.

Additionally, this study has shown that snow accumulation is influenced by natural climate variability, such as a 3–4-year cycle, but also by longer-term processes that are not fully captured in the limited period of measurements. To address this, the underlying processes, especially those driving the recent high accumulation years in 2021 and 2023 must be analyzed and better understood. Models must be assessed to determine whether they capture these anomalies in accumulation and their underlying processes. Once these processes are successfully represented in models, these models can be used to make future predictions. A key contribution of this analysis is its higher temporal resolution compared to other datasets used for benchmarking (e.g., ice or firn cores, which go farther back in time on the decadal to centennial-scale at annual resolution than direct observations).

Models tend to perform better on snow accumulation processes at longer timescales, making it crucial to evaluate whether they can reproduce the intra-annual dynamics of snow accumulation, such as whether monthly accumulation rates derived from climate models match the observed distribution (Medley and Thomas 2019). Another important aspect concerns the current hypothesis that the observed positive trend in the East Antarctic mass balance may not reflect ongoing increases in accumulation but could instead be a dynamic response to enhanced accumulation during the Holocene (Zwally et al. 2015). Therefore, contextualizing recent SMB trends is vital to reducing uncertainties in the ice sheet's mass balance.

This study has revealed recent positive changes in snow accumulation that deviate from climatology: annual accumulations in 2021 and 2023 exceeded the climatological mean by more than two standard deviations. Philippe et al. (2016) reported a positive SMB trend in the eastern DML plateau, and studies by Medley and Thomas (2019) and Medley et al. (2018) suggest that this trend may also extend to the western DML. The findings of this thesis indicate that the substantial positive anomalies observed in 2021 and 2023 could be early evidence of a similar trend emerging in coastal DML. This suggests a potential mitigating effect on SLR through increased snowfall across large parts of DML that is not fully captured by current climate models (Medley et al. 2018). These results underscore the central argument: robust SMB analyses are crucial for improving projections of future SLR.

The analysis of results presented in this thesis can be summarized in the following key points:

Longterm Trend

- Accumulation rates show periodic fluctuations of roughly 3.3 years with the last 3 oscillations increasing in accumulation rates (both minima and maxima are reaching higher values) (Figure 3.3)
- Frequency analysis reveals dominant periods of 6 months, 12 months, and 40 months (Figures 3.9 and 3.11)
- No long-term trends in annual accumulation rates, but 2021 and 2023 were the years with the largest annual rates of the whole record (Figure 3.5)
- The cumulative accumulation shows a climatological balance, as indicated by an OLS regression with a slope of 99.7 cm per year (Figure 3.6)
- Since 2017 surface mass balance has been in an above-average cumulative accumulation state (Figure 3.7)
- High interannual variability with positive anomalies is becoming more frequent with increasing magnitude (Figure 3.12)

Intraannual Analysis

- Mass loss mainly during summer (Figure 3.16)
- Negative summer anomalies are becoming more frequent and increasing in magnitude, meaning that summer contributes less than a quarter to the annual accumulation. These anomalies are anti-correlated with autumn accumulation rates (Figure 3.14).
- There is a systematic shift towards a more autumn-dominated accumulation pattern (Figure 3.15).
- Winter and spring accumulation rates are close to the annual average accumulation rate with no significant trend over time (Figure 3.15).
- When the total de-trended cumulative accumulation is in a below-average state, summer tends to be in an above-average state, while all other seasons are below average (Figure 3.18).
- For the first time, in two years (i.e., 2022 and 2023), all four seasons have contributed above their respective long-term average accumulation rates (Figure 3.18).
- Accumulation is characterized by high inter- and intra-annual variability; therefore, no consistent and significant intra-annual cycle is evident (Figure 3.19).
- Higher variability in summer and autumn accumulation rates than in winter and spring (Figure 3.16)

NOMENCLATURE

Accumulation Measures

$\dot{a}$ Monthly mean of daily homogenized accumulation rates [cm/day]

a Cumulative snow accumulation over one month [cm/month]

a_Σ Cumulative snow accumulation over one year [cm/year]

Spatial Averages and Standard Deviations

i Subscript: stake index $i = 1, \ldots, 16$; when a quantity is denoted without subscript i, it is averaged over all stakes

$\tilde{\sigma}$ Spatial standard deviation across all stakes, in contrast to σ, which denotes temporal standard deviation

Time Series Data

$t_{j,irreg}$ Time point at measurement index j on the irregular time axis of observations

j Temporal measurement index $j = 1, \ldots, 621$

$t_{m,reg}$ Time point at measurement index m on the regular (monthly) time axis

m Temporal index of the monthly interpolated measurements, $m = 1, \ldots, 400$

Δt_j Number of days between consecutive measurements $\dot{a}_{v0}(t_{j-1,\text{irreg}})$ and $\dot{a}_{v0}(t_{j,\text{irreg}})$

t_d Daily time axis, i.e. time axis is spaced out by a period of one day.

$\dot{a}_{v0}$ Accumulation rate time series on an irregular time axis [cm/Δt], where Δt denotes the number of days between consecutive measurements

a_{v1} Time series of monthly snow accumulation using interpolation method v1 [cm/month]

a_{v2} Time series of monthly snow accumulation using interpolation method v2 [cm/month]

a_{v3} Time series of monthly snow accumulation using interpolation method v3 [cm/month]; hereafter simplified to a (see next entry):

a Time series of monthly snow accumulation using interpolation method v3 [cm/month]

$\dot{a}_{v3}$ Monthly mean of daily snow accumulation rates using interpolation method v3 [cm/day]; hereafter simplified to $\dot{a}$ (see next entry):

$\dot{a}$ Monthly mean of daily snow accumulation rates using interpolation method v3 [cm/day]

Single Values of Time Series

$\dot{a}_{v0}(t_{j,\text{irreg}})$ j-th value of the original, irregularly spaced time series $\dot{a}_{v0}$, [cm/Δt]; for simplicity: $\dot{a}_{v0}$

$\dot{a}_{v3}(t_{m,\text{reg}})$ m-th value of the regular, monthly interpolated time series $\dot{a}$, [cm/day]; for simplicity: $\dot{a}$

Temporal Averages and Standard Deviations

$\langle \dot{a} \rangle$ Mean accumulation rate (v3) over the entire dataset [cm/day]

$\sigma_{\langle \dot{a} \rangle}$ Temporal standard deviation of the mean accumulation rate (v3) over the entire dataset [cm/day]

$\langle \dot{a} \rangle_{clim}$ Mean accumulation rate (v3) over the 30-year climatological period (1991–-2020) [cm/day]

$\sigma_{\langle \dot{a} \rangle_{clim}}$ Temporal standard deviation of the mean accumulation rate (v3) over the 30-year climatological period (1991–-2020) [cm/day]

$\langle \dot{a} \rangle_{annual}$ Mean daily accumulation rate (v3) over one year [cm/day]

$\sigma_{\langle \dot{a} \rangle_{annual}}$ Temporal standard deviation of the mean daily accumulation rate (v3) over one year [cm/day]

$\langle a \rangle_{annual}$ Mean monthly cumulative accumulation (v3) over one year [cm/month]

$\sigma_{\langle a \rangle_{annual}}$ Temporal standard deviation of the mean monthly cumulative accumulation (v3) over one year [cm/month]

DATA AVAILABILITY

The original data (v0) and the quality-checked, homogenized data (v3) will be available from the PANGAEA data portal. All additional data, figures, and the Jupyter notebook containing the complete data processing, interpolation, and analysis are accessible in the following GitLab account (accessible only to UIBK members): GitLab.

DECLARATION OF USE OF AI

In this thesis, artificial intelligence (AI) was utilized only for grammatical correction and formulation optimization. I hereby declare that I have composed this work independently and without the assistance of any other AI tools.

BIBLIOGRAPHY

Abrahamsen, E., 2012: Oceanographic conditions beneath Fimbul Ice Shelf, Antarctica. Ph.D. thesis.

Bagheri Dastgerdi, S., M. Behrens, J.-L. Bonne, M. Hörhold, G. Lohmann, E. Schlosser, and M. Werner, 2021: Continuous monitoring of surface water vapour isotopic compositions at Neumayer Station III, East Antarctica. *The Cryosphere*, **15 (10)**, 4745–4767.

Baiman, R., A. C. Winters, J. Lenaerts, and C. A. Shields, 2023: Synoptic Drivers of Atmospheric River Induced Precipitation Near Dronning Maud Land, Antarctica. *Journal of Geophysical Research: Atmospheres*, **128 (7)**, e2022JD037 859, doi:https://doi.org/10.1029/2022JD037859, URL https://agupubs.onlinelibrary.wiley.com/doi/abs/10.1029/2022JD037859, e2022JD037859 2022JD037859, https://agupubs.onlinelibrary.wiley.com/doi/pdf/10.1029/2022JD037859.

Bengtsson, L., K. I. Hodges, S. Koumoutsaris, M. Zahn, and N. Keenlyside, 2011: The changing atmospheric water cycle in Polar Regions in a warmer climate. *Tellus A: Dynamic meteorology and oceanography*, **63 (5)**, 907–920.

Bengtsson, L., K. I. Hodges, and E. Roeckner, 2006: Storm tracks and climate change. *Journal of climate*, **19 (15)**, 3518–3543.

Boening, C., M. Lebsock, F. Landerer, and G. Stephens, 2012: Snowfall-driven mass change on the East Antarctic ice sheet. *Geophysical Research Letters*, **39 (21)**.

Bromwich, D. H., 1988: Snowfall in high southern latitudes. *Reviews of Geophysics*, **26 (1)**, 149–168, doi:https://doi.org/10.1029/RG026i001p00149, URL https://agupubs.onlinelibrary.wiley.com/doi/abs/10.1029/RG026i001p00149, https://agupubs.onlinelibrary.wiley.com/doi/pdf/10.1029/RG026i001p00149.

Clark, M. P., et al., 2011: Representing spatial variability of snow water equivalent in hydrologic and land-surface models: a review. *Water Resour. Res.*, **47 (7)**, doi:10.1029/2010WR009362, URL https://doi.org/10.1029/2010WR009362.

Cuffey, K. M. and W. S. B. Paterson, 2010: *The physics of glaciers*. Academic Press.

Dahe, Q., X. Cunde, I. Allison, B. Lingen, R. Stephenson, R. Jiawen, and Y. Ming, 2004: Snow surface height variations on the Antarctic ice sheet in Princess Elizabeth Land, Antarctica: 1 year of data from an automatic weather station. *Annals of Glaciology*, **39**, 181–187, doi:10.3189/172756404781814546.

Dalaiden, Q., H. Goosse, J. T. M. Lenaerts, M. G. P. Cavitte, and N. Henderson, 2020: Future Antarctic snow accumulation trend is dominated by atmospheric synoptic-scale events. *Communications Earth & Environment*, **1 (1)**, 62, doi:10.1038/s43247-020-00062-x, URL https://doi.org/10.1038/s43247-020-00062-x.

Dufour, A., C. Charrondière, and O. Zolina, 2019: Moisture transport in observations and reanalyses as a proxy for snow accumulation in East Antarctica. *The Cryosphere*, **13 (2)**, 413–425, doi:10.5194/tc-13-413-2019, URL https://tc.copernicus.org/articles/13/413/2019/.

Eisen, O., et al., 2008: Ground-based measurements of spatial and temporal variability of snow accumulation in East Antarctica. *Reviews of Geophysics*, **46 (2)**.

Ekaykin, A. A., V. Y. Lipenkov, and N. A. Tebenkova, 2023: Fifty years of instrumental surface mass balance observations at Vostok Station, central Antarctica. *Journal of Glaciology*, 1–13, doi:10.1017/jog.2023.53, URL https://www.cambridge.org/core/product/0C5059EAAF392550C2CA577DE26D6A25.

Fischer, H., F. Traufetter, H. Oerter, R. Weller, and H. Miller, 2004: Prevalence of the Antarctic Circumpolar Wave over the last two millenia recorded in Dronning Maud Land ice. *Geophys. Res. Lett.*, **31 (8)**, doi:10.1029/2003GL019186, URL https://doi.org/10.1029/2003GL019186.

Frezzotti, M., et al., 2005: Spatial and temporal variability of snow accumulation in East Antarctica from traverse data. *Journal of Glaciology*, **51 (172)**, 113–124.

Fujii, Y. and T. Ohata, 1982: Possible causes of the variation in microparticle concentration in an ice core from Mizuho Station, Antarctica. *Annals of Glaciology*, **3**, 107–112.

Glaude, Q., et al., 2024: A Factor Two Difference in 21st-Century Greenland Ice Sheet Surface Mass Balance Projections from Three Regional Climate Models for a Strong Warming Scenario (SSP5-8.5). *Authorea Preprints*.

Goodwin, I. D., 1991: Snow-accumulation variability from seasonal surface observations and firn-core stratigraphy, eastern Wilkes Land, Antarctica. *Journal of Glaciology*, **37 (127)**, 383–387, doi:10.3189/S0022143000005815.

Gorodetskaya, I. V., T. Silva, H. Schmithüsen, and N. Hirasawa, 2020: Atmospheric River Signatures in Radiosonde Profiles and Reanalyses at the Dronning Maud Land Coast, East Antarctica. *Advances in Atmospheric Sciences*, **37 (5)**, 455–476, doi:10.1007/s00376-020-9221-8, URL https://doi.org/10.1007/s00376-020-9221-8.

Gorodetskaya, I. V., M. Tsukernik, K. Claes, M. F. Ralph, W. D. Neff, and N. P. Van Lipzig, 2014: The role of atmospheric rivers in anomalous snow accumulation in East Antarctica. *Geophysical Research Letters*, **41 (17)**, 6199–6206.

Hecht, C., 2022: Annual and Interannual Evolution of Surface Snow Densities over the Last Two Decades in the Vicinity of Neumayer Station III and their Influence on the SMB. M.S. thesis, Universität Bremen, unpublished Master Thesis.

Jakobs, C. L., C. H. Reijmer, P. Kuipers Munneke, G. König-Langlo, and M. R. van den Broeke, 2019: Quantifying the snowmelt–albedo feedback at Neumayer Station, East Antarctica. *The Cryosphere*, **13 (5)**, 1473–1485, doi:10.5194/tc-13-1473-2019, URL https://tc.copernicus.org/articles/13/1473/2019/.

King, J., K. J. Anchukaitis, K. Allen, T. Vance, and A. Hessl, 2023a: Trends and variability in the Southern Annular Mode over the Common Era. *Nature Communications*, **14 (1)**, 2324, doi:10.1038/s41467-023-37643-1, URL https://doi.org/10.1038/s41467-023-37643-1.

King, M. A. and P. Christoffersen, 2024: Major modes of climate variability dominate nonlinear Antarctic ice-sheet elevation changes 2002-2020. *Geophys Res Lett*, **51 (12)**, e2024GL108 844, doi:10.1029/2024GL108844, URL https://doi.org/10.1029/2024GL108844.

King, M. A., K. Lyu, and X. Zhang, 2023b: Climate variability a key driver of recent Antarctic ice-mass change. *Nature Geoscience*, **16 (12)**, 1128–1135, doi:10.1038/s41561-023-01317-w, URL https://doi.org/10.1038/s41561-023-01317-w.

Kuhns, H., C. Davidson, J. Dibb, C. Stearns, M. Bergin, and J.-L. Jaffrezo, 1997: Temporal and spatial variability of snow accumulation in central Greenland. *Journal of Geophysical Research: Atmospheres*, **102 (D25)**, 30 059–30 068.

König-Langlo, G., J. C. King, and P. Pettré, 1998: Climatology of the three coastal Antarctic stations Dumont d'Urville, Neumayer, and Halley. *Journal of Geophysical Research: Atmospheres*, **103 (D9)**, 10 935–10 946, doi:https://doi.org/10.1029/97JD00527, URL https://agupubs.onlinelibrary.wiley.com/doi/abs/10.1029/97JD00527, https://agupubs.onlinelibrary.wiley.com/doi/pdf/10.1029/97JD00527.

Lenaerts, J., et al., 2017: Meltwater produced by wind-albedo interaction stored in an East Antarctic ice shelf. *Nature Climate Change*, **7 (1)**, 58–62, doi:10.1038/nclimate3180, URL https://doi.org/10.1038/nclimate3180.

Lenaerts, J. T., E. van Meijgaard, M. R. van den Broeke, S. R. Ligtenberg, M. Horwath, and E. Isaksson, 2013: Recent snowfall anomalies in Dronning Maud Land, East Antarctica, in a historical and future climate perspective. *Geophysical Research Letters*, **40 (11)**, 2684–2688.

Lenaerts, J. T., M. Vizcaino, J. Fyke, L. Van Kampenhout, and M. R. van den Broeke, 2016: Present-day and future Antarctic ice sheet climate and surface mass balance in the Community Earth System Model. *Climate Dynamics*, **47**, 1367–1381.

Lenaerts, J. T. M., B. Medley, M. R. van den Broeke, and B. Wouters, 2019: Observing and modeling ice sheet surface mass balance. *Rev. Geophys.*, **57 (2)**, 376–420, doi:10.1029/2018RG000622, URL https://doi.org/10.1029/2018RG000622.

Lenaerts, J. T. M., M. R. van den Broeke, S. J. Déry, G. König-Langlo, J. Ettema, and P. K. Munneke, 2010: Modelling snowdrift sublimation on an Antarctic ice shelf. *The Cryosphere*, **4 (2)**, 179–190, doi:10.5194/tc-4-179-2010, URL https://tc.copernicus.org/articles/4/179/2010/.

Lettenmaier, D. P., 1976: Detection of trends in water quality data from records with dependent observations. *Water Resour. Res.*, **12 (5)**, 1037–1046, doi:10.1029/WR012i005p01037, URL https://doi.org/10.1029/WR012i005p01037.

Li, X., et al., 2021: Tropical teleconnection impacts on Antarctic climate changes. *Nature Reviews Earth Environment*, **2 (10)**, 680–698, doi:10.1038/s43017-021-00204-5, URL https://doi.org/10.1038/s43017-021-00204-5.

Marshall, G. J., A. Orr, and J. Turner, 2013: A predominant reversal in the relationship between the SAM and East Antarctic temperatures during the twenty-first century. *Journal of Climate*, **26 (14)**, 5196–5204, doi:10.1175/JCLI-D-12-00671.1, URL https://journals.ametsoc.org/view/journals/clim/26/14/jcli-d-12-00671.1.xml.

Mayewski, P. A., et al., 2009: State of the Antarctic and Southern Ocean climate system. *Rev. Geophys.*, **47 (1)**, doi:10.1029/2007RG000231, URL https://doi.org/10.1029/2007RG000231.

McConnell, J. R., R. C. Bales, and D. R. Davis, 1997: Recent intra-annual snow accumulation at South Pole: Implications for ice core interpretation. *Journal of Geophysical Research: Atmospheres*, **102 (D18)**, 21 947–21 954.

Medley, B., J. R. McConnell, T. Neumann, C. Reijmer, N. Chellman, M. Sigl, and S. Kipfstuhl, 2018: Temperature and snowfall in western Queen Maud Land increasing faster than climate model projections. *Geophysical Research Letters*, **45 (3)**, 1472–1480.

Medley, B. and E. R. Thomas, 2019: Increased snowfall over the Antarctic Ice Sheet mitigated twentieth-century sea-level rise. *Nature Climate Change*, **9 (1)**, 34–39, doi:10.1038/s41558-018-0356-x, URL https://doi.org/10.1038/s41558-018-0356-x.

Naik, S. S., M. Thamban, C. M. Laluraj, B. L. Redkar, and A. Chaturvedi, 2010: A century of climate variability in central Dronning Maud Land, East Antarctica, and its relation to Southern Annular Mode and El Niño-Southern Oscillation. *J. Geophys. Res.*, **115 (D16)**, doi:10.1029/2009JD013268, URL https://doi.org/10.1029/2009JD013268.

Nicolas, J. P. and D. H. Bromwich, 2011: Precipitation changes in high southern latitudes from global reanalyses: A cautionary tale. *Surveys in geophysics*, **32**, 475–494.

on Climate Change, I. P., 2023: *Climate Change 2023: Synthesis Report*. IPCC, Geneva, Switzerland, 35–115 pp., doi:10.59327/IPCC/AR6-9789291691647.

Philippe, M., et al., 2016: Ice core evidence for a 20th century increase in surface mass balance in coastal Dronning Maud Land, East Antarctica. *The Cryosphere*, **10 (5)**, 2501–2516, doi:10.5194/tc-10-2501-2016, URL https://tc.copernicus.org/articles/10/2501/2016/.

Reijmer, C. H. and M. R. v. d. Broeke, 2003: Temporal and spatial variability of the surface mass balance in Dronning Maud Land, Antarctica, as derived from automatic weather stations. *Journal of Glaciology*, **49 (167)**, 512–520, doi:10.3189/172756503781830494.

Rignot, E., I. Velicogna, M. R. van den Broeke, A. Monaghan, and J. T. M. Lenaerts, 2011: Acceleration of the contribution of the Greenland and Antarctic ice sheets to sea level rise. *Geophys. Res. Lett.*, **38 (5)**, doi:10.1029/2011GL046583, URL https://doi.org/10.1029/2011GL046583.

Rotschky, G., 2007: Spatial distribution of snow accumulation and snowpack properties in Dronning Maud Land, Antarctica : observational techniques and methods for surface mass-balance assessments of polar ice sheets = Räumliche Verteilung von Schneeakkumulation und Schneedeckeneigenschaften in Droning Maud Land, Antarktis : Observationstechniken und Methoden der Netto-Massenbilanzbestimmung polarer Eisschilde. Alfred Wegener Institute for Polar and Marine Research, Bremerhaven, doi:10.2312/BzPM_0552_2007.

Schlosser, E., 1999: Effects of seasonal variability of accumulation on yearly mean δ18O values in Antarctic snow. *Journal of Glaciology*, **45 (151)**, 463–468.

Schlosser, E., M. G. Duda, J. G. Powers, and K. W. Manning, 2008: Precipitation regime of Dronning Maud Land, Antarctica, derived from Antarctic Mesoscale Prediction System (AMPS) archive data. *Journal of Geophysical Research: Atmospheres*, **113 (D24)**, doi:https://doi.org/10.1029/2008JD009968, URL https://agupubs.onlinelibrary.wiley.com/doi/abs/10.1029/2008JD009968, https://agupubs.onlinelibrary.wiley.com/doi/pdf/10.1029/2008JD009968.

Schlosser, E., K. W. Manning, J. G. Powers, M. G. Duda, G. Birnbaum, and K. Fujita, 2010: Characteristics of high-precipitation events in Dronning Maud Land, Antarctica. *Journal of Geophysical Research: Atmospheres*, **115 (D14)**, doi:https://doi.org/10.1029/2009JD013410, URL https://agupubs.onlinelibrary.wiley.com/doi/abs/10.1029/2009JD013410, https://agupubs.onlinelibrary.wiley.com/doi/pdf/10.1029/2009JD013410.

Schlosser, E. and H. Oerter, 2002: Shallow firn cores from Neumayer, Ekströmisen, Antarctica: a comparison of accumulation rates and stable-isotope ratios. *Annals of Glaciology*, **35**, 91–96.

Schlosser, E., N. Van Lipzig, and H. Oerter, 2002: Temporal variability of accumulation at Neumayer station, Antarctica, from stake array measurements and a regional atmospheric model. *Journal of Glaciology*, **48 (160)**, 87–94.

Seroussi, H., et al., 2024: Evolution of the Antarctic Ice Sheet Over the Next Three Centuries From an ISMIP6 Model Ensemble. *Earth's Future*, **12 (9)**, e2024EF004 561, doi:10.1029/2024EF004561, URL https://doi.org/10.1029/2024EF004561.

Simon, S., J. Turner, M. Thamban, J. Wille, and P. Deb, 2023: Spatiotemporal variability of extreme precipitation events and associated atmospheric processes over Dronning Maud Land, East Antarctica. *Authorea Preprints*.

Sundsbø, P.-A., 1998: Numerical simulations of wind deflection fins to control snow accumulation in building steps. *Journal of Wind Engineering and Industrial Aerodynamics*, **74-76**, 543–552, doi:10.1016/S0167-6105(98)00049-X, URL https://www.sciencedirect.com/science/article/pii/S016761059800049X.

Torrence, C. and G. P. Compo, 1998: A Practical Guide to Wavelet Analysis. *Bulletin of the American Meteorological Society*, **79 (1)**, 61–78, URL https://journals.ametsoc.org/view/journals/bams/79/1/1520-0477_1998_079_0061_apgtwa_2_0_co_2.xml.

Trenberth, K. E., 1997: The definition of El Niño. *Bulletin of the American Meteorological Society*, **78 (12)**, 2771–2778, URL https://journals.ametsoc.org/view/journals/bams/78/12/1520-0477_1997_078_2771_tdoeno_2_0_co_2.xml.

Turner, J., et al., 2019: The Dominant Role of Extreme Precipitation Events in Antarctic Snowfall Variability. *Geophysical Research Letters*, **46 (6)**, 3502–3511, doi:https://doi.org/10.1029/2018GL081517, URL https://agupubs.onlinelibrary.wiley.com/doi/abs/10.1029/2018GL081517, https://agupubs.onlinelibrary.wiley.com/doi/pdf/10.1029/2018GL081517.

van den Broeke, M. and R. Giesen, 2021: Mass balance. *Glaciers and Ice Sheets in the Climate System: The Karthaus Summer School Lecture Notes*, A. Fowler and F. Ng, Eds., Springer International Publishing, Cham, 161–184, doi:10.1007/978-3-030-42584-5_7, URL https://doi.org/10.1007/978-3-030-42584-5_7.

van den Broeke, M., G. König-Langlo, G. Picard, P. Kuipers Munneke, and J. Lenaerts, 2010: Surface energy balance, melt and sublimation at Neumayer Station, East Antarctica. *Antarctic Science*, **22 (1)**, 87–96, doi:10.1017/S0954102009990538, URL https://www.cambridge.org/core/product/BB501698464647112 40FD0E1997C6644.

van den Broeke, M. R., C. H. Reijmer, and R. S. van de Wal, 2004: A study of the surface mass balance in Dronning Maud Land, Antarctica, using automatic weather stations. *Journal of Glaciology*, **50 (171)**, 565–582, doi:10.3189/172756504781829756.

Velicogna, I., et al., 2020: Continuity of Ice Sheet Mass Loss in Greenland and Antarctica From the GRACE and GRACE Follow-On Missions. *Geophys. Res. Lett.*, **47 (8)**, e2020GL087 291, doi:10.1029/2020GL087291, URL https://doi.org/10.1029/2020GL087291.

Voordendag, A., B. Goger, R. Prinz, T. Sauter, T. Mölg, M. Saigger, and G. Kaser, 2024: A novel framework to investigate wind-driven snow redistribution over an Alpine glacier: combination of high-resolution terrestrial laser scans and large-eddy simulations. *The Cryosphere*, **18 (2)**, 849–868, doi:10.5194/tc-18-849-2024, URL https://tc.copernicus.org/articles/18/849/2024/.

Wahr, J., D. Wingham, and C. Bentley, 2000: A method of combining ICESat and GRACE satellite data to constrain Antarctic mass balance. *Journal of Geophysical Research: Solid Earth*, **105 (B7)**, 16 279–16 294.

Wallace, J. M. and P. V. Hobbs, 2006: *Atmospheric science: an introductory survey*, Vol. 92. Elsevier, pp. 432 ff.

Wang, W., Y. Shen, Q. Chen, and F. Wang, 2023: Unprecedented mass gain over the Antarctic ice sheet between 2021 and 2022 caused by large precipitation anomalies. *Environmental Research Letters*, **18 (12)**, 124 012, doi:10.1088/1748-9326/ad0863, URL https://dx.doi.org/10.1088/1748-9326/ad0863.

Wang, Y., et al., 2017: Snow accumulation variability over the West Antarctic Ice Sheet since 1900: A comparison of ice core records with ERA-20C reanalysis. *Geophysical Research Letters*, **44 (22)**, 11–482.

Weinhart, A. H., J. Freitag, M. Hörhold, S. Kipfstuhl, and O. Eisen, 2020: Representative surface snow density on the east antarctic plateau. *The Cryosphere*, **14 (11)**, 3663–3685, doi:10.5194/tc-14-3663-2020, URL https://tc.copernicus.org/articles/14/3663/2020/.

Welker, C., O. Martius, P. Froidevaux, C. H. Reijmer, and H. Fischer, 2014: A climatological analysis of high-precipitation events in Dronning Maud Land, Antarctica, and associated large-scale atmospheric conditions. *Journal of Geophysical Research: Atmospheres*, **119 (21)**, 11,932–11,954, doi:https://doi.org/10.1002/2014JD022259, URL https://agupubs.onlinelibrary.wiley.com/doi/abs/10.1002/2014JD022259, https://agupubs.onlinelibrary.wiley.com/doi/pdf/10.1002/2014JD022259.

White, W. B., P. Gloersen, and I. Simmonds, 2004: Tropospheric Response in the Antarctic Circumpolar Wave along the Sea Ice Edge around Antarctica. *Journal of Climate*, **17 (14)**, 2765–2779, URL https://journals.ametsoc.org/view/journals/clim/17/14/1520-0442_2004_017_2765_tritac_2.0.co_2.xml.

White, W. B. and R. G. Peterson, 1996: An Antarctic circumpolar wave in surface pressure, wind, temperature and sea-ice extent. *Nature*, **380 (6576)**, 699–702, doi:10.1038/380699a0, URL https://doi.org/10.1038/380699a0.

Wilks, D. S., 2019: *Statistical methods in the atmospheric sciences*. Academic press.

Wille, J. D., et al., 2021: Antarctic Atmospheric River Climatology and Precipitation Impacts. *Journal of Geophysical Research: Atmospheres*, **126 (8)**, e2020JD033 788, doi:https://doi.org/10.1029/2020JD033788, URL https://agupubs.onlinelibrary.wiley.com/doi/abs/10.1029/2020JD033788, e2020JD033788 2020JD033788, https://agupubs.onlinelibrary.wiley.com/doi/pdf/10.1029/2020JD033788.

Wirths, C., T. F. Stocker, and J. C. R. Sutter, 2024: The influence of present-day regional surface mass balance uncertainties on the future evolution of the Antarctic Ice Sheet. *The Cryosphere*, **18 (9)**, 4435–4462, doi:10.5194/tc-18-4435-2024, URL https://tc.copernicus.org/articles/18/4435/2024/.

Zwally, H. J., J. Li, J. W. Robbins, J. L. Saba, D. Yi, and A. C. Brenner, 2015: Mass gains of the antarctic ice sheet exceed losses. *Journal of Glaciology*, **61 (230)**, 1019–1036, doi:10.3189/2015JoG15J071, URL https://www.cambridge.org/core/product/983F196E23C3A6E7908E5FB32EB42268.

Die **Berichte zur Polar- und Meeresforschung** (ISSN 1866-3192) werden beginnend mit dem Band 569 (2008) als Open-Access-Publikation herausgegeben. Ein Verzeichnis aller Bände einschließlich der Druckausgaben (ISSN 1618-3193, Band 377-568, von 2000 bis 2008) sowie der früheren **Berichte zur Polarforschung** (ISSN 0176-5027, Band 1–376, von 1981 bis 2000) befindet sich im electronic Publication Information Center **(ePIC)** des Alfred-Wegener-Instituts, Helmholtz-Zentrum für Polar- und Meeresforschung (AWI); see https://epic.awi.de. Durch Auswahl "Reports on Polar- and Marine Research" (via "browse"/"type") wird eine Liste der Publikationen, sortiert nach Bandnummer, innerhalb der absteigenden chronologischen Reihenfolge der Jahrgänge mit Verweis auf das jeweilige pdf-Symbol zum Herunterladen angezeigt.

The **Reports on Polar and Marine Research** (ISSN 1866-3192) are available as open access publications since 2008. A table of all volumes including the printed issues (ISSN 1618-3193, Vol. 377-568, from 2000 until 2008), as well as the earlier **Reports on Polar Research** (ISSN 0176-5027, Vol. 1–376, from 1981 until 2000) is provided by the electronic Publication Information Center **(ePIC)** of the Alfred Wegener Institute, Helmholtz Centre for Polar and Marine Research (AWI); see URL https://epic.awi.de. To generate a list of all Reports, use the URL http://epic.awi.de and select "browse"/"type" to browse "Reports on Polar and Marine Research". A chronological list in declining order will be presented, and pdf-icons displayed for downloading.

Zuletzt erschienene Ausgaben:

Recently published issues:

792 (2025) Climate Signals from Neumayer, coastal Dronning Maud Land, Antarctica: A 33-Year statistical Analysis of Snow Accumulation in a Stake Farm, by Valerie Reppert

791 (2025) TIDAL–HX01: Trialing Innovative Data Acquisition from a Platform of Opportunity – the HX Vessel MS FRIDTJOF NANSEN, edited by Andreas Herber, Laura Köhler, Verena Meraldi, Katja Metfies, Melf Paulsen, Daniel Pröfrock, Tobias Steinhoff and Hongyan Xi with contributions of the participants

790 (2024) The Expedition PS140 of the Research Vessel POLARSTERN to the Cooperation Sea and Davis Sea in 2023 / 2024, edited by Marcus Gutjahr and Oliver Esper with contributions of the participants

789 (2024) The Expedition PS142 of the Research Vessel POLARSTERN to the Atlantic Ocean in 2024, edited by Simon Dreutter with contributions of the participants

788 (2024) The Expedition PS138 of the Research Vessel POLARSTERN to the Arctic Ocean in 2024 edited by Antje Boetius and Christina Bienhold with contributions of the participants

786 (2024) The MOSES Sternfahrt Expeditions of the Research Vessels ALBIS, LITTORINA, LUDWIG PRANDTL and MYA II to the Elbe River, Elbe Estuary and German Bight in 2023 edited by Ingeborg Bussmann, Martin Krauss, Holger Brix, Norbert Kamjunke, Björn Raupers and Tina Sanders with contributions of the participants

785 (2024) The Expeditions PS139 / 1 and PS139 / 2 of the Research Vessel POLARSTERN to the Atlantic Ocean in 2023, edited by Simon Dreutter and Claudia Hanfland with contributions of the participants

784 (2024) Expeditions to Antarctica: ANT-Land 2022/23 NEUMAYER STATION III, Kohnen Station, Flight Operations and Field Campaigns. Edited by Julia Regnery, Thomas Matz, Peter Köhler and Christine Wesche with contributions of the participants

ALFRED-WEGENER-INSTITUT
HELMHOLTZ-ZENTRUM FÜR POLAR-
UND MEERESFORSCHUNG

BREMERHAVEN

Am Handelshafen 12
27570 Bremerhaven
Telefon 0471 4831-0
Telefax 0471 4831-1149
www.awi.de

HELMHOLTZ